MODELING OF RAINDROP SIZE DISTRIBUTION AND CRITICAL DIAMETERS FOR RAINFALL ATTENUATION OVER MICROWAVE LINKS IN SOUTHERN AFRICA

By

Oluwumi Adetan

Submitted in fulfillment of the academic requirements for the degree of Doctor of Philosophy in Electronic Engineering,

University of KwaZulu-Natal, South Africa

JANUARY 2014

MODELING OF RAINDROP SIZE DISTRIBUTION AND CRITICAL DIAMETERS FOR RAINFALL ATTENUATION OVER MICROWAVE LINKS IN SOUTHERN AFRICA

SUBMITTED BY

Oluwumi Adetan

IN FULFILLMENT OF THE DEGREE OF

Doctor of Philosophy in Electronic Engineering from the University of KwaZulu-Natal, Durban, South Africa

DATE OF SUBMISSION

JANUARY 2014

SUPERVISED BY

Professor Thomas Joachim Odhiambo Afullo

As the candidate's supervisor, I agree to the submission of this thesis

Signed: ----------

Name: ---------- Date: ----------

DECLARATION

I, **OLUWUMI ADETAN**, declare that:

i. The research reported in this thesis, except where otherwise indicated, is my original work.

ii. This thesis has not been submitted for any degree or examination at any other university.

iii. This thesis does not contain any other person's data, pictures, graphs or other information, unless specifically acknowledged as being sourced from other persons.

iv. This thesis does not contain any other person's writings, unless specifically acknowledged as being sourced from other researchers. Where other sources have been quoted, then:

   a. Their words have been re-written but the general information attributed to them has been referenced.

   b. Where their exact words have been used, then their writings have been placed in italics and inside quotation marks, and referenced.

v. Where I have reproduced a publication of which I am an author, co-author or editor, I have indicated in detail which part of the publication was actually written by myself alone and have fully referenced such publication.

vi. This thesis does not contain text, graphics or tables copied and pasted from the internet, unless specifically acknowledged, and the source being detailed in the thesis and in the References sections.

DEDICATION

To Taiwo Temitayo, my wife, sweetheart and best friend

PREFACE

The research presented in this thesis was carried out by Oluwumi Adetan, under the supervision of Professor Thomas Joachim Odhiambo Afullo in the School of Engineering, Discipline of Electrical, Electronic and Computer Engineering at the University of KwaZulu-Natal, South Africa. This work has been partially supported by Telkom South Africa through the Center of Excellence (CoE) programme in the school. Certain aspects of the thesis has been presented and published by the author at various fora: the Southern Africa Telecommunication Networks and Applications Conference (SATNAC) in 2012 and 2013; the IASTED International Conference on Modeling and Simulation (AfricaMS) at Gaborone, Botswana in 2012; IEEE AFRICON Conference, Mauritius in 2013. Part of this work has also been published in Progress in Electromagnetics Research B (PIERS) in 2013; International Journal of Scientific and Engineering Research (IJSER) in 2013; the South Africa Institute of Electrical Engineers (SAIEE) Africa Research Journal and the Annals of Telecommunications – Annals des Télécommunications in 2014. The entire work, unless otherwise indicated, is the author's work and has not been submitted in part, or in whole, to any other University for degree purpose.

ACKNOWLEDGEMENTS

My profound gratitude goes to the LORD GOD ALMIGHTY who was, is and is to come. I can boldly say that "*If it had not been the LORD who was on my side, where would I have been today……" Psalm 124:1*. I give God all the glory, honor, adoration and praise for the successful completion of this PhD research program.

I am sincerely grateful to my supervisor, Professor Thomas Joachim Odhiambo Afullo, whose guidance, encouragement, teaching and fatherly roles has been useful towards the completion of my PhD research program. Your statements like, "*Life is not a straight line!*"; "*Life is real ALUTA!*" and "*You cannot earn this degree through osmosis!*" have provided me with the strength and fortitude to finish this work. Sir, may you continue to enjoy the grace of God all the days of your life. Thank you!

I am grateful to Professor Moses Oludare Ajewole of the Center for Space Research and Applications (CESRA), Akure, Nigeria who made available for me some of the research journals/materials used in this work. Sir, the advice and encouragement from you is highly appreciated. I appreciate the very first words of encouragement received from Professor Jules-Raymond Tapamo on my first day in the University. He said: "*See everything as a challenge, prove them wrong."* This statement was so precious to me throughout my study, though he might not remember this.

I am grateful to Professor Stanley Mneney, the Head of School who would always ask me about this work. Although he was not my supervisor, he was so much interested in me and the work. Thank you Prof. I would like to gratefully acknowledge the financial support~~s~~ received from the Telkom Centre of Excellence (CoE) and the Centre for Engineering and Postgraduate Studies (CEPS) in the School of Engineering, University of KwaZulu-Natal, South Africa. In addition, the financial supports received from the Tertiary Education Trust Fund (TETFUND) and the Management of the Ekiti State University, Nigeria, is greatly appreciated. I would like to acknowledge my members at the GCC, Ado Ekiti and CoC, Queen Mary Church, Durban. Thanks for your prayers and love. I appreciate the supports of the staff and students of the Faculty of Engineering, Ekiti State University, Nigeria. God bless you.

To all the academic, technical and supporting staffs in the School of Electrical, Electronic and Computer Engineering, I say thank you for accepting me to work with you. I am indebted to Mr. Roland Koch (Safety Manager, School of Engineering). Thank you very much for your love and offering me a lift every day to campus. I would also like to acknowledge Dr. Felix Akorli of the National University of Rwanda for providing part of the disdrometer data used in this study from Butare, Rwanda. Fruitful discussions with Dr Joseph Ojo of the Federal University of Technology, Akure, Nigeria are appreciated.

To all my postgraduate friends and associates on this journey: Dr. Oluwafemi Ilesanmi, Chrispin Mulangu, Peter Akuon, Akintunde Alonge, Remmy Musumpuka, John Msumba, Burnet Mkandawire,

Rambiz Yazdi, Olayinka Adewumi, Gbenga Ogidan, Obiseye Obiyemi, Lucky Asuelime, Lanre Wojuola, Gbolahan Aiyetoro, Mike Asiyo, Sunday Fadugba, Gbenga Imole, Abraham Nyete, Maria Sefumba, Adeola Adisa, Fulatsa Zwane, Sithembiso Gamma- You guys are fantastic! Remember this: ***"When you feel like quitting: Think about why you started".***

I appreciate my wonderful parents, in-laws, family members and siblings for their prayers and encouragements towards the completion of this research program. I am particularly grateful to Barrister and Deaconess Dele Agbede. You are all wonderful people. I would also like to specially appreciate my very good friend Olusegun Adewumi for always being there for me. You have been so wonderful. Words alone cannot express my appreciation to you. The good Lord will increase His Grace to you more and more in Jesus' name (Amen).

Lastly, my special thanks to my wife, *Taiwo Temitayo* who gave me her unalloyed and tremendous support throughout my research program. She was always there at the time I was far away from home, bearing all the emotional and physical difficulties created by an absentee husband. I appreciate your patience, love, endurance, care and for holding fort throughout the period of the PhD work. To my three boys that God of Heaven has granted us - *Victor, David* and *Emmanuel* ("The *Segullahs*") - I am eternally grateful for your understanding as you waited patiently for daddy to finish the program. You shall be greater than me in Jesus name (Amen). God bless you.

I love you ALL!

ABSTRACT

The inability of service providers to constantly meet the design target of 99.99 % availability of the line-of-sight (LOS) microwave links has caused concern among both the operators and consumers. The non-availability of the links is predominantly due to propagation impairments along the propagation link. These propagation effects include cloud, snow, fog, gas attenuation, rain and atmospheric scintillation. Various studies have shown high vulnerability of radio communication systems operating at microwave (3-30 GHz) and millimeter wave (30-300 GHz) to rainfall attenuation especially in the tropical regions characterized by heavy rainfall and relatively large rain drops when compared to the temperate regions. In order to understand the effects of attenuation due to rain on communication systems in any locality (region), a good knowledge of the raindrop size distribution (DSD) and the rainfall rate estimates is necessary for accurate prediction and estimation of the rainfall attenuation.

For this study, experimental raindrop size measurements gathered over a period of three years, using the Joss-Waldvogel RD-80 disdrometer installed at the roof top of the Electrical, Electronic and Computer Engineering building, University of Kwa-Zulu Natal, Durban, a subtropical location in South Africa, is analysed. Disdrometer measurements, sampled at one-minute rate over a period of nine months from Butare, an equatorial site in Rwanda, is also analysed for the purpose of comparison. The estimated $R_{0.01}$ values for Durban and Butare are employed for the purpose of analysis. Based on the statistical analysis of the measured data samples, DSD parameters are proposed from the negative exponential, modified gamma, Weibull and the lognormal models. The DSD models are compared to models from other countries within and outside the region. The Mie scattering approximation at temperature of 20^{o}C for spherical raindrop shape is adopted for the estimation of the scattering functions. The study further investigates the influence of critical raindrop diameters on the specific rain attenuation for the annual, seasonal and various rainfall regimes in southern Africa. This is achieved analytically by integrating the total rainfall attenuation over all the raindrop sizes and observing the differential change in the attenuation over a given range of drop size diameters. The peak diameter at which the specific rainfall attenuation is maxima is determined for different rainfall regimes. Finally, the cross-polarisation discrimination (XPD) due to rain over Durban is computed at two elevation angles. The results of this study will be helpful for the proper design and allocation of adequate fade margins to achieve the expected quality of service (QoS) in a radio communication system operating in the Southern Africa region.

TABLE OF CONTENTS

LIST OF FIGURES

Chapter Two

Chapter Three

Chapter Four

Chapter Five

Chapter Six

LIST OF TABLES

Chapter Two

Chapter Three

Chapter Four

Chapter Five

Chapter Six

LIST OF ABBREVIATIONS

The followings are the notations and abbreviations used in this report.

CDF	Cumulative Distribution Function
CPA	Co-Polar Attenuation
DA	Differential Attenuation
DPS	Differential Phase Shift
DSD	Drop Size Distribution
EHF	Extra High Frequency
EMW	Electromagnetic Waves
EXP	Exponential
FSS	Fixed Satellite Service
G-M	Gamma Model
HF	High Frequency
IEEE	Institute of Electrical and Electronic Engineering
ITU-R	International Telecommunications Union Recommendation
JD	Joss- Drizzle
JT	Joss- Thunderstorm
JW	Joss- Widespread
JWD	Joss Waldvogel Disdrometer
LF	Low Frequency
LGM	Lognormal Model
L-M	Lognormal Model
LOS	Line-of-Sight
LP	Laws and Parsons
LWC	Liquid Water Content
MGM	Modified Gamma Model
MLE	Maximum Likelihood Estimation
MoM	Method of Moments
MP	Marshall Palmer
MPM	Marshall Palmer Model
PDF	Probability Density Function
QoS	Quality of Service
RDSD	Raindrop Size Distribution
RF	Radio Frequency
RMS	Root Mean Square

RMSE	Root Mean Square Error
SHF	Super High Frequency
VHF	Very High Frequency
WBM	Weibull Model
XPD	Cross Polarisation Discrimination
Z	Reflectivity

LIST OF NOTATIONS AND MATHEMATICAL SYMBOLS

μ	Distribution shape parameter
λ	Wavelength
Γ	Gamma function
A	Specific attenuation
κ	Power law coefficient of A-R relationship
c_i, n_i	Disdrometer channel(bin) number
σ	Standard deviation
D	Raindrop diameter
N_t	Number of drops in a given volume
Λ	Parameter of the gamma DSD
f	Frequency
$\in_0$	Permittivity of free-space
μ_0	Permeability of free-space
K_1, K_2	Scattering amplitude and polarisation state of scattered wave
α	Linear fit coefficient of attenuation-rain rate
$d\gamma$	Change in specific rain attenuation
$v(D)$	Raindrop fall velocity of raindrop diameter D
T	Temperature
t	Time
Q_{ext}	Extinction cross-sections
C_θ	Elevation angle
C_σ	Canting angle
C_τ	Polarisation improvement factor
R	Rainfall rate

CHAPTER ONE

GENERAL INTRODUCTION

1.1 Introduction

The transmission, reception, and processing of information with the use of electronic circuits is generally known as communications [*Tomasi*, 1987]. The basic concepts involved in electronic communication have not changed significantly since their inception, although the methods through which these concepts are implemented have undergone dramatic changes. Communication systems comprises of three (3) main sections: a source (transmitter), transmission medium (a pair of wires, coaxial cable, fiber link, or free space) and a destination (receiver). The information that is propagated through a communication system can be categorized as either analog (which may be voice, video or picture information, music) or digital (such as binary-coded numbers, alpha/numeric codes, graphic symbols, microprocessor op-codes, or data-base information). In some digital communication systems, analogue signals are coded (source coding) before being transmitted. For free space transmission of information, use is made of an appropriate interface - an antenna. It should be noted that not all communication systems require antennas (e.g. optic-based and sound-based communication systems). Once the information has been transformed to the desired form, it has to be placed onto a carrier before transmission to the destination. This transformation can be done through the use of sampling and quantization. Sampling and quantization techniques are often referred to as formatting and source coding [*Proakis et al.,* 1994]. In some cases, channel coding, symbol mapping, and maybe carrier modulation are required before the information is transmitted to the destination.

All media of wireless communication systems (radio communication system in particular) are characterized by attenuation, which is the progressive decrease of signal power with increasing distance and, in some instances, may be as a result of insertion loss in the signal. The amount of attenuation is a function of distance. In some situations, the attenuation can be quite considerable as it plays a very important role in the selection of the transmission media and, thus, of additional equipment required to restore it to an intelligible form. The receiver performs the function of extracting and reconditioning the received signal from the transmission channel and converts it to a form which can be interpreted by the output transducer. The antenna, which is a device that couples the transmitter or receiver network to space, is also used at the reception. The ideal antenna is the one that radiates all the power delivered to it in the desired direction and with the desired polarization. The received signal may be weak due to attenuation in which case several stages of amplification may be embedded into the receiver to boost the received signal. The key function performed by the receiver is demodulation (detection) and signal conditioning. As a result of the significant

developments in the technology industry, the media has evolved over low frequency (LF), high frequency (HF), extremely high frequency (EHF) radio, to microwave (3-30 *GHz*) and millimetric (30-300 *GHz*) transmission, to optical fiber, to name a few – each having its distinct properties, advantages and disadvantages [*Tomasi*, 1987; *Proakis et al.*, 1994].

The availability of wider bandwidths for carrying communications system at the microwave and millimetric wave spectrum is of major interest to both service operators and systems designers. Such wide bandwidths (30-300 *GHz*) are useful for applications such as improved anti-jam performance for secure communications applications, video distribution, high speed data transmission and smaller component sizes [*Marcus and Pattan*, 2005]. These advantages can however be offset very easily due to increased propagation problems as the frequency of operation increases.

Several propagation mechanisms affect the earth-space and terrestrial communications performances and constitute a major concern to system planners and designers. These mechanisms include ice depolarization, gaseous attenuation; sky noise, cloud and fog attenuation; rain attenuation and amplitude scintillation. However, attenuation due to rain is the most severe [*Crane*, 1996; *Roddy*, 2001]. Rain-caused attenuation has for a long time been identified as a major inhibitor in radar and communication systems operating at millimetric and microwave frequencies. The attenuation of microwave line-of-sight signals due to precipitation (rainfall, in particular) limits the propagation path length of line-of-sight communication systems. To understand how this attenuation is influenced by rain parameters, a detailed understanding of the inherent raindrop size distributions (DSD) and the corresponding scattering mechanisms at an operating frequency is essential. The DSD is fundamental in the evaluation of microwave rainfall techniques. The drop size distribution is often made of temporal and spatial variability that influences microwave measurements and ground validation [*Rincon and Lang*, 2002]. Drop size distribution is highly sensitive to rainfall estimation techniques exploring attenuation, phase shift of microwave signals and reflectivity. Most ground validation schemes depending on disdrometer measurements and rain gauges are influenced by the drop size distribution variability.

This work seeks to determine and model the regional raindrop size distribution, as well as the corresponding specific attenuation due to rain in southern Africa. The Mie scattering approximation at temperature of 20^{o}C for spherical raindrop shapes is adopted for the estimation of the scattering functions. The Mie scattering theory is applied under the assumption that each spherical raindrop illuminated by a plane wave is uniformly distributed in a rain filled medium. Similarly, it is assumed that the distance between each drop is large enough to avoid any interaction between them. A comparison with countries within similar region is also investigated. The study investigates the influence of critical raindrop diameters on the specific rain attenuation for the annual, seasonal and various regimes of rainfall in southern Africa. The peak diameter at which maximum specific attenuation due to rain occurs is also determined analytically. The estimation of cross polarisation discrimination due to rainfall over the southern Africa is also studied.

1.2 Research Motivation

In the works of *Mulangu* and *Afullo* [2009] and *Odedina* and *Afullo* [2010], while analyzing the attenuation due to signal scattering by raindrops, the raindrop size distributions (DSD) assumed in the models have been largely due to ITU-R Recommendation [*ITU-R P.838-3,* 2005].The ITU-R model however, is not universal. Thus it is paramount to model the raindrop size distribution for south-eastern region of Africa through measurements. This study therefore aims at determining the regional raindrop size distribution, as well as the corresponding specific attenuation due to rain. In addition, it is pertinent to mention that no work has been done to determine the particular raindrop channels (or diameters) at which the rain attenuation is affected significantly in the southern Africa region. This study seeks to investigate these critical and peak diameters that produce a major contribution to the total specific attenuation due to rain in the South Africa region. Thus, Durban and Butare are considered as initial targets in this study, with special focus on Durban, South Africa.

1.3 Aims and Objectives

The specific objectives of this study are to:

- Determine the raindrop size distribution for southern Africa using the disdrometer measurements. The models to be tested include the exponential model, the lognormal model, the gamma model, and the Weibull model;
- Investigate the critical raindrop diameters (as determined through disdrometer measurements) that affect the measured rainfall rate and examine their contribution to the attenuation on millimetric signals;
- Determine the peak diameters at which the rainfall attenuation is maximum using an analytical approach for various rainfall regimes in the southern Africa region;
- Compare the raindrop size models, the critical diameters, and the attenuation due to rain for subtropical southern Africa regions and equatorial regions of Africa;
- Use the Mie scattering coefficients to evaluate the effect of the developed models on rain attenuation calculations at microwave and millimetric wave frequencies in the southern Africa region; and
- Estimate and investigate the effects of the elevation angles, rain rate and frequency on cross polarisation discrimination due to rainfall in south eastern coast of Africa.

1.4 Organization of the Thesis

This thesis is presented in seven (7) chapters. Chapter one gives the general introduction to this work. The specific aims and objectives of the study are itemized. The original contributions to knowledge and the results presented in conferences and learned journals are also stated in this chapter. A theoretical background (literature review) on propagation theory and the effects of scattering and absorption of millimeter waves during propagation through precipitation are discussed in chapter two. Elements of the atmosphere (the troposphere) that affect the drop size distribution and possibly contribute to attenuation on propagation links are also discussed. Different rainfall attenuation models such as the Crane models, the Moupfouma models and the globally known ITU-R attenuation model are presented. A relationship between rainfall attenuation and rain depolarisation is also discussed. A review of the different raindrop size distribution models (i.e. the negative exponential, lognormal, modified gamma and Weibull models) and specific rainfall attenuation are also discussed. Previous work done on critical raindrop diameters as it affects rain attenuation is also reviewed in chapter two.

Chapter three presents a description of the experimental set up, data collection, sorting and analysis used for the investigation of the DSD and its relationship with the rain rate for a given rain event. A comparative analysis of the two commonly used methods for the estimation of the input parameters required for the modeling of drop size distribution is discussed. These methods are the maximum likelihood estimation and the method of moments. Different drop size distribution models using the estimated input parameters for Durban, South Africa are also proposed.

Chapter four provides an analytical approach to raindrop diameters in drop size distribution and its effect on specific rain attenuation. Two classes of diameters are analysed in chapter four: the peak diameter and the critical diameters. The range of diameters producing maximum attenuation defines the *critical* diameters, whereas the single diameter at which the peak attenuation is obtained is called the *peak* diameter. There are four (4) distinct seasons associated with South Africa rainfall, namely: winter, summer, autumn and spring. The critical raindrop diameters for rainfall attenuation in southern Africa based on these seasons is proposed. Similarly, the influence of the disdrometer channels (bins) on specific rain attenuation over microwave links in South Africa is also analyzed. On the basis of the different rainfall regimes, the role of drop diameters on rain attenuation in Durban is also investigated.

Chapter five gives a comparative analysis of the raindrop size distribution models and critical diameters in Durban, a subtropical location in South Africa and Butare, an equatorial site in Rwanda. In chapter six, the cross polarisation discrimination (XPD) due to rain in Durban is computed at two elevation angles. The variations of the XPD with rainfall rate, frequency and elevation angles are discussed. Lastly, chapter seven gives a brief summary of the contributions of the work presented in this thesis as well as a statement regarding some suggestions for future work.

1.5 Contributions to Knowledge

In this work, a comparative analysis of the methods used for the estimation of input parameters required for the modeling of raindrop size distribution in southern Africa is discussed. The methods are the maximum likelihood estimation (MLE) and the method of moments (MoM). The MLE technique gives a larger deviation error from the measured data while the MoM gives a better agreement with the measured data [*Adetan* and *Afullo*, 2012]. The method of moment is proposed for the estimation of the input parameters necessary for the modeling of DSD in South Africa. Based on the statistical analysis of the measured data samples, DSD parameters are developed from the negative exponential, modified gamma, Weibull and the lognormal models, by employing the method of moment (MoM) technique. The lognormal model is proposed for South Africa as it gives the best fit to the measured data with least error when compared to other DSD models. However, the gamma model can also be used to model the DSD in South Africa as the error rates is quite close to the lognormal model. The two models are used for the purpose of analysis in the two locations (Durban, South Africa and Butare, Rwanda) considered in this study. Furthermore, the DSD models are compared against models from other countries within and outside the region. The Mie scattering approximation at temperature of 20^{o}C for spherical raindrop shape is adopted for the estimation of the scattering functions.

Investigation of the influence of critical raindrop diameters on the specific rain attenuation in southern Africa is analyzed. The total rainfall attenuation is evaluated by integrating over all the raindrop sizes and the differential change in the attenuation is observed over a given range of drop size diameters. It is proposed that the larger diameters do not contribute significantly to rain attenuation and therefore can be ignored. The major contribution to the specific attenuation for the drop size distribution (DSD) models considered is created by the raindrop diameters not exceeding 2 mm especially at higher frequencies. A formula for the determination of the peak diameter at which the specific rain attenuation is highest for different rainfall regimes is proposed.

In this study, analysis of the critical diameters influencing optimum attenuation in South Africa and Rwanda are also studied. The percentage of time rain rate is exceeded, $R_{0.01}$ values for Durban, South Africa and Butare, Rwanda have been estimated for the purpose of this comparative analysis. Cross polarisation discrimination was computed for Durban, South Africa at two elevation angles and at operating frequencies of 10 to 35 GHz.

1.6 Publications in Journals and Conference Proceedings

In the course of this work, the following papers have been published in refereed journals and conference proceedings:

1. **O. Adetan** and T.J. Afullo, "Comparison of Two Methods to Evaluate the Lognormal Raindrop Size Distribution Model in Durban," *In the Proceedings of the Southern Africa Telecommunications Networks Applications Conference, (SATNAC 2012),* Fancourt, George, South Africa, ISBN 978-0-620-53713-1, September 2012.
2. **O. Adetan** and T.J. Afullo, "Three-Parameter Raindrop Size Distribution Modeling for Microwave Propagation in South Africa," *In the Proceedings of The International Association of Science and Technology for Development (IASTED), International Conference on Modeling and Simulation (Africa MS 2012),* Gaborone, Botswana, DOI:10-2316/P.2012.761-027, pp. 155-160, 2012.
3. **O. Adetan** and T.J. Afullo, "The Critical Diameters for Rainfall Attenuation in Southern Africa," *Progress In Electromagnetics Research (PIER) B,* Vol. 46, pp. 275-297, 2013 **[*Journal Article*]**.
4. **O. Adetan** and T.J. Afullo, : "Attenuation-Rain Rate Power-Law Relation and Critical Diameters from Drop Size Distribution Measurements in Durban," *Proceedings of IEEE AFRICON Conference,* ISBN: 978-1-4673—5940-5, ISSN: 2153-0025, Mauritius, pp.242-247, 9th to 12th September 2013.
5. **O. Adetan** and T.J. Afullo, "The Role of Raindrop Diameters on Attenuation Due to Rain in Durban, South Africa," *In the Proceedings of Southern Africa Telecommunications Networks Applications Conference, (SATNAC 2013),* ISBN: 978-0-620-57883-7, Stellenbosch, Western Cape, South Africa. pp. 21-25, 1st to 4th September 2013.
6. **O. Adetan** and T.J. Afullo, "Computation of Cross-Polarisation due to Rain over Durban, South Africa," *International Journal of Scientific and Engineering Research (IJSER)*, volume 4, Issue 10, ISSN 2229-5518, pp. 1169-1175, October 2013 **[*Journal Article*]**.
7. **O. Adetan** and T.J. Afullo "Raindrop Size Distribution and Rainfall Attenuation Modeling in Equatorial and Subtropical Africa: The Critical Diameters," *Annals of Telecommunications-Annals des Télécommunications*, DOI: 10.1007/s12243-013-0418-z, ISSN: 0003-4347 January, 2014 **[*Journal Article*].**
8. **O. Adetan** and T.J. Afullo: "The Influence of Disdrometer Channels on Specific Attenuation Due to Rain over Microwave Links in Southern Africa," *South African Institute on Electrical Engineers (SAIEE) Africa Research Journal* **[*Accepted Journal Article*].**

CHAPTER TWO

LITERATURE REVIEW

2.1 Introduction

In this section, the theoretical background of electromagnetic wave (EMW) propagation with particular emphasis on effects of scattering and absorption on radio wave propagation and propagation losses in communication systems is discussed. The effects of the atmosphere and gaseous components on signal transmission as the frequency increases are also discussed. The chapter defines and classifies the different types of precipitation. The South Africa weather and climate characteristics are also discussed. The contributions of various researchers to rainfall attenuation vis-à-vis the commonly known rain attenuation models, raindrop shapes, sizes and drop size distribution modeling, is presented. The chapter concludes with a brief review of previous investigation of critical diameters on rainfall attenuation in some countries across the globe.

2.2 Microwave Propagation Theory

The propagation characteristics of the atmosphere that most strongly influence the fixed satellite service (FSS) systems are associated with rain. Rain on a satellite radio path causes fading, or rain attenuation. It is therefore necessary to understand the nature of the atmosphere through which propagation of radio wave takes place. Rain propagation research for satellite applications until recently focused on developing techniques for predicting fading which might occur 0.01 to 0.001 percent of the time, since these values corresponded to the reliabilities that a telephone system had to deliver. Predicting the statistics of rain attenuation from local rain rate statistics is fairly well understood. The rain rate statistics are themselves reasonably well characterized for most of Europe, North America, and Japan, less so for the tropical/equatorial regions. Small-scale terrain effects, localized climates, and the normal year-to-year fluctuations in rainfall all combine to introduce some irreducible variability in the phenomena [*Edelson et al*., 1993]. More recent research efforts have focused on determining attenuation statistics at higher percentages of time, say 10 to 0.1 percent since these correspond to the reliabilities and the 1 to 3 dB fade margins that very small aperture terminal (VSAT) systems and other low margin services provide.

2.2.1 Propagation in Free Space

Free space is a region characterized with isotropic, homogenous and loss free properties and which is remote from regions of differing properties. The permittivity and permeability of such a region have the constant values of $\in_0$, the permittivity of free-space and μ_0,the permeability of free-

space, respectively, and the ray paths are straight lines normal to the wave front [*Mathews*, 1965]. Transmission takes place only along the direct ray path from the transmitter to the receiver. Let P_T be the transmitter radiating output power from an isotropic antenna (an antenna that radiates equally in all directions). If the receiver is situated at a distance r (meters) from the transmitter, the power flux density P_{av} is given as:

$$P_{av} = \frac{P_T}{4\pi r^2} \qquad (watts/m^2) \tag{2.1}$$

The received power P_R over an effective aperture of area A_R (m^2) is at distance r is:

$$P_R = \frac{P_T A_R}{4\pi r^2}\ , \quad (watts) \tag{2.2}$$

For an isotropic antenna, the effective area A_R is given as $\lambda^2/4\pi$, where λ is the wavelength of the incident radiation field. If the gain of the transmitting antenna is G_T, the received power in equation (2.2) will be:

$$P_R = \frac{P_T G_T A_R}{4\pi r^2} \qquad (watts) \tag{2.3}$$

The gain of the transmitting antenna in relation with the effective aperture is $4\pi A_R/\lambda^2$ hence equation (2.3) becomes:

$$P_R = \frac{P_T G_T G_R \lambda^2}{16\pi^2 r^2} \tag{2.4}$$

The effective aperture determines the amount of power that the receiving antenna extracts from the RF power density of the field [*Ishimaru*, 1997]. The transmission loss between transmit and receive antennas is given by:

$$L_{dB} = 10\log_{10}\frac{P_T}{P_R} \tag{2.5}$$

2.2.2 Effects of the Atmosphere

The atmosphere consists of gases and water vapor. The proportion of the gases, temperature and humidity vary with height. The troposphere is the lowest portion of the Earth's atmosphere containing

approximately 75% of the atmosphere's mass, 99% of water vapor (or moisture) and aerosols, 78% of nitrogen, 21% oxygen and small concentrations of other trace gases. The troposphere region is the part of the atmosphere where most of the effects of weather affecting radio propagation occur. Such propagation effect includes cloud formation, precipitation, wind blow, variation of humidity etc. The height of the troposphere with respect to sea level ranges from 7 km around the poles to about 20 km in tropical regions, with an approximate average of 17 km. The atmosphere is separated from the stratosphere by a narrow region of ionized temperature called the tropopause. The ionosphere is the region of ionized gases that starts to affect radio propagation at a height of about 60 km [*Mathews*, 1965]. The atmosphere is divided into layers. The lowest of these is the troposphere, which extends up to about 11 kilometers, depending upon the geographical latitude. In the tropics it may extend up to 15 kilometers, due to the updrafts produced by massive tropical rain bearing cumulonimbus clouds. The troposphere is the warmest, most dense and wettest layer of the atmosphere. Virtually all of the difficulties encountered in microwave transmission, be it between terrestrial transceivers, or satellite ground stations, originate from the physical properties of the troposphere. The effects of the troposphere are the most important, although propagation can occur between points on the earth by ionospheric refraction at the lower VHF and HF frequencies.

Transmission losses occur when millimeter waves travelling through the atmosphere are absorbed by molecules oxygen, water vapor and other atmospheric constituents. These losses are greater at certain frequencies, coinciding with mechanical resonant frequencies of gas molecules [*Marcus* and *Pattan,* 2005]. Other gases display resonant lines as well, such as N_2O, SO_2, O_3, NO_2 and NH_3 but because of their low density in the atmosphere; they have negligible effect on propagation [*Ishimaru*, 1997]. According to Crane [*Crane,* 2003], the most dominant gaseous components in the atmosphere that often produce attenuation include water vapor, O_2 and Co_2. These gaseous components produce atmospheric loss affecting signal transmission especially at frequencies between 2 GHz and 100 GHz. The contribution of different atmospheric influences at different frequencies is shown in Figure 2-1. The gaseous attenuation ($A_{gaseous}$) due to the gaseous components in the atmosphere is directly proportional to the specific attenuation, γ_a and computed for the terrestrial link using the *ITU-R P.530-13* [2009] recommendation as given in equations (2.6) and (2.7).

$$A_{gaseous} = \gamma_a \times d \quad \left(\frac{dB}{km}\right) \tag{2.6}$$

$$\gamma_a = \gamma_o + \gamma_w \tag{2.7}$$

where the specific attenuation in the atmosphere is denoted by γ_a in dB/km, d is the line-of-sight distance in km, γ_o and γ_w represent the specific attenuation for oxygen and water vapor respectively.

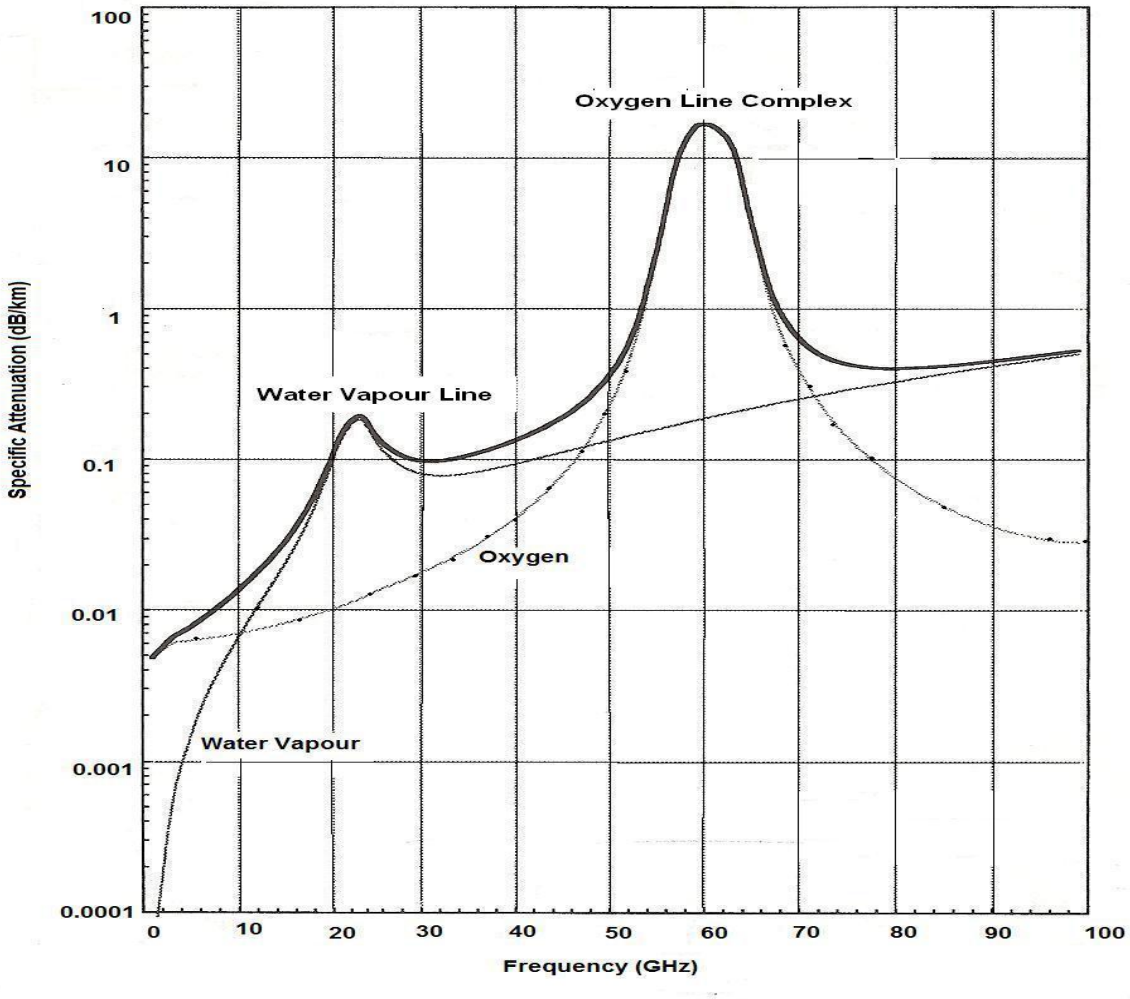

Figure 2-1: Specific attenuation caused by oxygen and water vapor at microwave and millimeter wave frequencies [*Source: Crane*, 1996]

Whether the propagation is a terrestrial link or a satellite link, the effects of the atmosphere frequently dominate losses in propagation. Microwave wave designers should therefore consider the effect of the atmosphere in the link design, as ignoring it would be at their own peril.

2.3 The Physics of Rain

Various definitions have been given to rain by different researchers. Precipitation is said to occur when particles in the cloud develop in high complexity (such as condensation and aggregation), reaching a size where their falling velocity is greater than the upward wind speed in the air. It is often referred to as rain when these particles become liquid water on reaching the ground surface. In addition, rain is essentially a propagation of falling drops interacting with each other, causing collisions and breakups with their environment [see

http://www.newton.dep.anl.gov/askasci/wea00.htm]. A form of precipitation in which water falls back to the earth as a liquid may be defined as rain. Rain may also occur in a solid form as snow or hail. Rainfall on the other hand means the amount of rain that falls in a particular area during a particular period of time [*Ajewole,* 1997]. Precipitation is dependent on several factors such as location relative to the general global circulation, elevation, latitude and proximity to certain geological features, which can be mountains and oceans. Therefore, a rain event occurring in a given location or area is not constant. It is important to mention that rain does not distribute evenly in a region experiencing precipitation, hence there is the need to find rain cell size distribution to account for the non-uniformity of rain for larger distances. This is especially important in tropical regions than in the temperate regions [*Khamis,* 2005].

Due to the variability of rain in space, time and frequency of occurrence, it is often difficult to classify rain [*Matricciani et al.,* 2000]. Meteorologists have categorized rain into two broad groups, namely: the stratiform and the convective groups [*Green,* 2004; *Ajayi et al.,* 1996; *Houze,* 1994]. The radio communication engineers however classified rain as drizzle, widespread, shower and thunderstorm [*Joss et al.,* 1968; *Adimula and Ajayi,* 1996]. These four classes are subsets of the stratiform and convective types of rain. According to *Atlas et al.,* [*Atlas et al.,* 1999] rain events are further classified as convective, transition and stratiform types. They identified rain events as initially convective, if rain rises sharply to peak in excess of about 10-15 mm/h while D_o (mass weighted mean diameter) does not vary greatly. When the mass weighted mean drop diameter and the rain rate decrease simultaneously following convective period, the rain is classified as transition. Stratiform rain is identified by approximately steady rain rate, $R \leq 10$ mm/h and often with larger values of mean diameter, D_o *(*mm*).* Stratiform rain cells cover large geographical areas typically exceeding 100 *km* and are associated with rain rates less than 25 mm/h. The rain rate is mostly uniform across the entire cell for long durations, often exceeding one hour. In communication systems, where stratiform rain dominates, these sizeable durations often warrant the usage of an appropriate link margin to negate the resulting attenuation.

Tropical rainfall occurs from various types of rain systems and the classification of the rain into regimes is useful for a variety of applications, such as the determination of the vertical distribution of latent heat, [*Houze,* 1989; *Tokay and Short,* 1996] and from improving quantitative rain retrieval schemes by way of remote sensing from ground-based and spaceborne instruments [e.g. *Rosenfeld et al.,* 1995*; Simpson et al.*1988]. The stratiform rain type originates from nimbostratus clouds which by definition are stably stratified [*Houze,* 1994]. The vertical air velocity within clouds plays a crucial role in distinguishing between the stratiform and convective rain types [*Tokay and Short,* 1996]. In stratiform rain cloud, the vertical air velocity is less than the terminal velocity of ice crystals and snow (1-3 m/s), whereas in convective rain clouds, the vertical air velocity is greater than the terminal velocity. The growth of ice crystals in the upper portion of the stratiform clouds is due primarily to vapor deposition where vertical air motion does not exceed a few tens of centimeters per second

[*Tokay and Short*, 1996]. Stratiform rains are formed from small ice particles in the upper tropospheric layers, which join together to form bigger nuclei as they fall. As these growing nuclei pass through the melting layer they become unstable and turn into raindrops that fall down to the earth surface [*Green*, 2004; *Ajayi et al.*, 1996]. Raindrop growth in stratiform clouds is slow, so its rain consists of small drops. This normally results in light rain and drizzle. Drizzle refers to very light widespread rain, with rain rates generally below 1 to 2 mm/h. It is characterized by a large concentration in raindrops with small diameters. Widespread rain generally refers to the higher rain rates up to 25 mm/h and is characterized by raindrops with small to medium diameters.

Convective rain originates from cumulonimbus clouds, large towering clouds that extend the entire troposphere. They are stirred up by strong movement of the air masses caused by tropospheric pressure difference. This type of rain results when masses of relatively warm air rise to higher levels in the troposphere. Upon reaching these upper levels, these air masses are cooled and return to the lower levels producing heavy showers and thunderstorm. In this process, water drops are formed and they grow in size until they are precipitated by gravity [*Green*, 2004; *Houze*, 1994]. Showers generally refer to rain rates below 40-50 mm/h and are characterized by raindrops with medium to large diameters. Thunderstorm refers to very heavy rainfall with rain rates up to 200 mm/h [*Ajayi et al.*, 1996]. Convective rain cells generally extend for a few kilometers and are embedded within larger stratiform rain cells and thunderstorms. Due to the localized nature of these cells, they generally pass over the communication link within a few minutes; nevertheless, they cause severe attenuation and the required fade margin is often too large to be implemented and uneconomical since it is required for only a short duration of time. They are also characterized by sharper spatial and temporal intensity gradients than stratiform rain. The time required for the growth of precipitation particles in convective clouds is much less than that in stratiform clouds. Hence, the precipitation particles originate and grow not far from the cloud base [*Tokay and Short*, 1996]. Rain in the tropics, in most cases, occurs in the forms of cells which are a complex mixture of stratiform and convective rains with the convective rain accounting for about 70% or more of the total rain in most cases [*Timothy et al.*, 2002; *Ajayi*, 1990; *Houze*, 1997].

2.4 Absorption and Scattering of Radio Waves

The major sources of microwave band, and especially millimetric wave band transmission losses in the lower atmosphere are absorption and scattering [*Ivanovs* and *Serdega*, 2006]. These two phenomena are of major concern to system designers. The primary source of absorption losses at all altitudes is an effect called gaseous absorption, resulting from the quantum physical behavior of atmospheric gas molecules. These gas molecule, such as nitrogen, oxygen, carbon dioxide or water vapor often experience resonance effects. Of major interest for the microwave engineer is that these resonances produce electromagnetic effects. If such a molecule is placed inside a microwave beam,

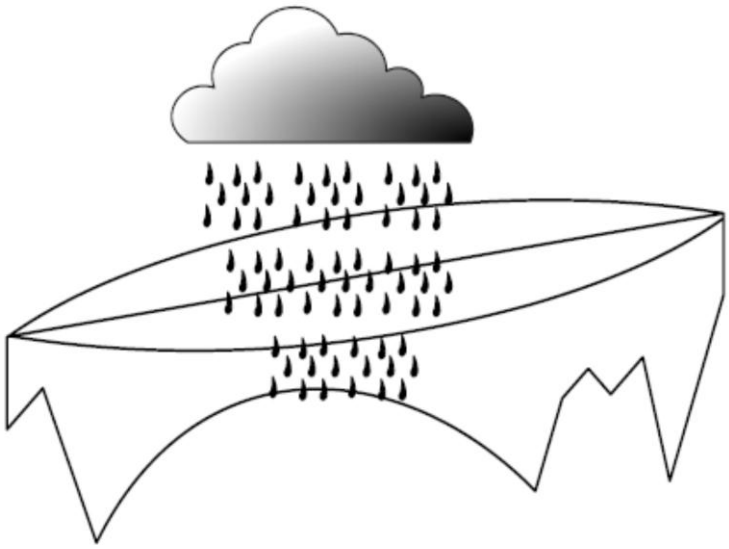

Figure 2-2: Rain shower [source: *Ivanovs* and *Serdega*, 2006]

and if the frequency of the beam is close enough to the resonance frequency of the molecule, the molecule will draw energy from the beam as it is excited. An appreciable amount of power is lost if enough molecules are put into the beam.

Transmission of microwave signals above 10 GHz is vulnerable to precipitation. Hydrometeors such as rain, snow, sleet, ice particles and hail may attenuate and scatter microwave signals and thus result in reduced availability from a system point of view. Figure 2-2 shows a radio relay path where the Fresnel zone is partially filled with rain droplets from a shower. Each particular raindrop will contribute to the attenuation of the wanted signal. The actual amount of fading is dependent on the frequency of the signal and the size of the raindrop. As earlier mentioned, the two major causes of attenuation due to rain are scattering and absorption. When the wavelength is fairly large relative to the raindrop size, scattering is predominant. Conversely, when the wavelength is small compared to the raindrop size, absorption tends to dominate [*Ivanovs* and *Serdega*, 2006].

Scattering losses constitute a source of problems in microwave propagation, be it point to point links or satellite links. They vary significantly with local weather conditions and cannot be avoided in most parts of the world. A scattering loss will arise when the microwave beam encounters droplets or particles in the atmosphere. If these particles are smaller than a wavelength, an effect called Rayleigh scattering occurs, whereby the droplet or particle reflects a small proportion of the impinging energy. The amount of energy scattered that never reaches the receiver depends upon the size of the scatterers relative to the wavelength, their density per volume of the atmosphere, the path length through the scattering environment, and the dielectric properties of the scatterers. A common source of scattering losses is the cloud. Low density clouds like stratus and stratocumulus clouds introduce some losses,

increasing with frequency, but are almost insignificant in comparison with dense water-laden rain clouds, and especially the cumulonimbus thunderstorm cloud.

2.5 Raindrop Size and Shapes

Rain drops in free fall are not spheroids (except for the smallest drops). The true shape of raindrops is an oblate spheroid with a flattened base. As the drop size increases above 4 mm, the base actually becomes concave [*Barclay*, 2003]. The shape of raindrops was initially studied from a meteorological point of view in the 20th century, since it was relevant to various subjects in meteorology, such as fall velocity and drop breakup. The size of raindrops can vary from the smallest drops of diameter D ≈ 0.1 mm to relatively large drops with D ≈ 7.0 mm. Raindrops bigger than 7 mm are hydrodynamically unstable and thus break up very easily when they fall towards the ground. Many investigators have made photographic measurements of the drop shape. Some measurements were made while the drops were suspended in the air stream of a vertical wind tunnel, and some were made when the drops attained their terminal velocity after falling from a sufficient height (≈12 m) in stagnant air. These measurements revealed that water drops larger than about 1.0 mm in radius were of oblate spheroidal shape with a flattened base.

Generally, the shapes of raindrops are believed to largely vary with respect to the rainfall rate, the type of rainfall, the closeness of the cloud to the ground, the ambient temperature, the terminal velocity etc. [*Pruppacher* and *Pitter* , 1971; *Jiang et al.*,1997, and *Li et al.*, 2000]. Three different shapes have been suggested by various workers which are the spherical, spheroidal and oblate spheroidal [*Pruppacher* and *Pitter*, 1971; *Oguchi*, 1973; *Oguchi*, 1977, *Nader*, 1998*; Li et al.*, 2000]. The spherical and spheroidal [*Oguchi*, 1977] raindrop shapes are axisymmetrical about the horizontal axis while the oblate spheroidal [*Pruppacher* and *Pitter*, 1971] are distorted, but more realistic than the first two earlier mentioned [*Nader*, 1998].

Other investigators have theoretically studied the drop shape, by solving an equation describing the balance of internal and external pressure at the surface of a drop. Because it has been difficult to solve this equation rigorously, several assumptions or approximations have had to be introduced. In 1971, *Pruppache*r and *Pitter* introduced some assumptions into the aerodynamic pressure around the surface of a water sphere, and numerically solved the pressure-balance equation [*Pruppacher* and *Pitter*, 1971]. Recent measurements of drop shapes by two-dimensional video disdrometer under calm-air conditions seem to indicate that the *Pruppacher–Pitter* model slightly overestimates real drop deformation; no concave deformation of the bottom of large drops has yet been found [*Thurai* and *Bringi*, 2005; *Thurai et al.*, 2005, and *Thurai et al.*, 2009]. The shapes of the raindrops of given sizes are shown in Figure 2-3.

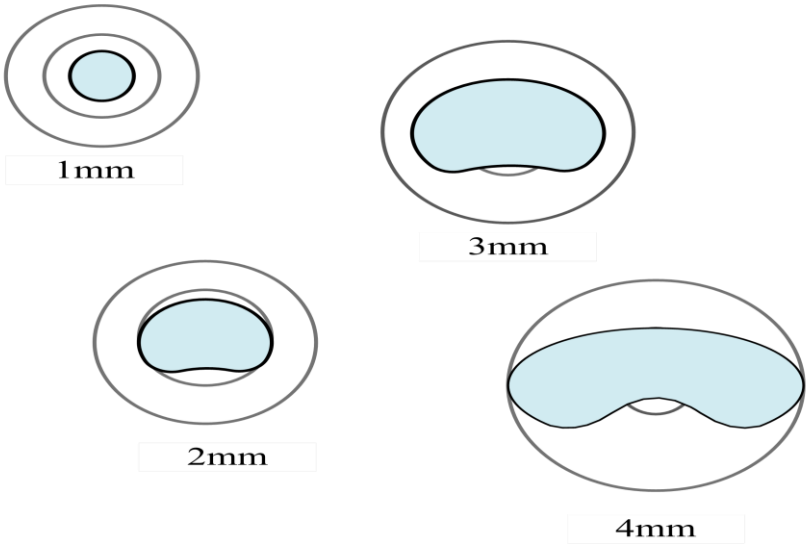

Figure 2-3: Raindrop shapes at radius: 1 mm, 2 mm, 3 mm and 4 mm
[*Pruppacher and Pitter*, 1971]

2.6 Rainfall Attenuation Prediction Models

The attenuation on any given path depends on the value of the specific attenuation, frequency of transmission, polarization, ambient temperature, propagation path length and latitude [*Kanellopoulos et al*, 1990]. Several empirical and semi-empirical rainfall attenuation prediction models have been proposed and published by a number of researchers for global applications. A power law empirical relation between the specific attenuation and the rainfall rate as established by *Olsen* [1978] has been found to be a good approximation for the estimation of the rainfall attenuation for a given precipitation [*Olsen*, 1978]. The path attenuation was first computed directly by *Lin* [1977] using the *Oguchi* [1960] perturbation method. Later, Crane, [*Crane*, 1980] proposed a power law relation between the line rate and point rain rate from which he evaluated the instantaneous rain profile [*Nader*, 1998]. In general, the two principal requirements for accurate prediction of rainfall attenuation are: firstly, the estimation of a surface rain rate distribution; and, secondly, the prediction of the radio wave attenuation distribution, from the given by the rain rate distribution [*Ojo et al., 2008; Pontes et al., 2005*]. It should be mentioned that most of the studies related to rainfall attenuation are based on data obtained from the temperate regions. The models do not give an accurate prediction of rain attenuation in the tropical, sub-tropical and equatorial regions characterized by heavy rainfall. Although the ITU-R model [*ITU-R P.530-12, 2007*] and the Crane [*Crane, 1980*] model are the most widely used, yet they underestimate the cumulative distribution of rainfall attenuation when applied to links located in tropical regions, leading to poor prediction [*Silva Mello et al.,*]. The commonly known rain attenuation models are discussed in the next section.

2.6.1 The ITU-R Rain Attenuation Model

The ITU-R has stated a step- by- step technique for computing the long time statistics of rain attenuation on terrestrial line of sight in [*ITU-R P.530-12, 2007*]. The rain attenuation exceeded at 0.01 % of time is computed from the rainfall rate data, and an extrapolation formula is used to calculate the attenuation exceeded at other percentages of time between 1 and 0.001 percent. The improved ITU-R model avoided the extrapolation procedure by calculating the attenuation distribution using the full rainfall rate distribution in an equiprobable basis. The rain attenuation exceeded during *p%* of the time is then given as:

$$A_p(dB) = \kappa R^{\alpha}(p)\left(\frac{dB}{km}\right) r(p) d(p) \tag{2.8}$$

where $R_{(p)}$ is the point rainfall rate exceeded at *p*% of the time, d is the link distance (km), κ and α are parameters that depend on the operating frequency and polarization [*ITU-R* 838-3, 2005]. The multiplying factor *r(p)* accounts for the non-uniform distribution of rain along the propagation path.

$$r = \frac{1}{(1 + \frac{d}{d_0})} \tag{2.9}$$

and

$$d_0 = 35e^{-0.015R} \quad [km] \tag{2.10}$$

d_0 is the effective path length and r is the path reduction factor. A more detailed description of the ITU-R model is found in Appendix A-1. A number of workers have reported that the ITU-R model does not give a correct prediction of attenuation in the tropical regions because it is based on data obtained from the temperate regions [*Ojo et al.*, 2008*; Mandeep et al.*, 2008]. The underestimation of the attenuation statistics can be overcome using a larger experimental database and adopting a path correction factor greater than unity [*Abdurrahman et al*., 2011].

2.6.2 The Crane Rain Attenuation Models

The Crane models are commonly used for both satellite and terrestrial links. These models were developed to provide a statistical relationship between the rain rate and path attenuation predictions for use on Earth-Space links or on terrestrial paths [*Crane*, 1996]. The three forms of Crane models were proposed at different times [*Crane*, 1980, 1982, *Crane and Shieh*, 1989]. The Two-Component (T-C) rain attenuation model (*Crane*, 1982] determines the probability of exceeding a given attenuation threshold. The model's name relates to the fact that two distinctive types of rain events are addressed: the convective cells (called "volume" cell by Crane) and the widespread "debris" [*Crane,*

1982]. The T-C model was formulated in such a way that it might later be extended to site diversity systems, rain scatter interference and attenuation duration statistics [*Crane,* 1982]. The global Crane attenuation model was based on the ITU-R rain attenuation model earlier discussed. The model was for attenuation on a horizontal or terrestrial link. A summary of the Global Crane rain attenuation model is given below [*Crane,* 1980, 1996]:

$$A(R_p, D) = \alpha {R_p}^{\beta} \left[\frac{e^{u\beta d} - 1}{u\beta} - \frac{b^{\beta} e^{c\beta d}}{c\beta} + \frac{b^{\beta} e^{c\beta D}}{c\beta} \right], \quad d \le D \le 22.5\ km \tag{2.11}$$

$$A(R_p, D) = \alpha {R_p}^{\beta} \left[\frac{e^{u\beta d} - 1}{u\beta} \right], \quad 0 < D \le d\ \ km \tag{2.12}$$

where:

A = horizontal path attenuation in dB

R_p = Rain rate in mm/h

D = path length in km

αR^{β} = the specific attenuation in dB/km [*Olsen et al,*].

where *b*, *c* and *d* are the empirical constants of the piecewise exponential model given as:

$$u = \frac{\ln[\, b\, e^{cd}]}{d}\ , d \text{ in km} \tag{2.13}$$

$$b = 2.3 {R_p}^{-0.17}, \quad R_p \text{ in mm/h} \tag{2.13b}$$

$$c = 0.026 - 0.03 \ln(R_p) \tag{2.13c}$$

$$d = 3.8 - 0.6 \ln(R_p) \tag{2.13d}$$

For propagation paths longer than 22.5 km, the attenuation is computed for a 22.5 km path, and the resulting attenuation is multiplied by a factor of *D/22.5* km. This global Crane model provides a prediction of the attenuation for path integrated rain rate given the equiprobable value of rain rate [*Crane,* 1996].

2.6.3 The Moupfouma Rain Attenuation Model

The experimental data gathered by Moupfouma [*Moupfouma,* 1984] in thirty (30) different terrestrial radio links operating in the frequency range 7-38 *GHz* band and path length ranging

from1.3 to 58 *km* located in Africa, Japan, United States and Europe was used to propose this model, generally known as the Moupfouma rain attenuation model. He proposed an empirical model for estimating rain-induced attenuation on terrestrial paths using effective path length. Moupfouma's work was found to be in agreement with the ITU-R model. The rain induced attenuation on a line-of-sight path can be expressed as:

$$\gamma(dB) = \kappa R^{\alpha} L_{eff} \tag{2.14}$$

$$L_{eff} = r \times l \tag{2.15}$$

The actual path length *l*, and effective path length L_{eff}, in kilometers, are related to the path reduction factor coefficient *r*, which is generally expressed in the form:

$$r = \frac{1}{1 + Cl^{m}} \tag{2.16}$$

with κ and α obtained from the power law regression coefficients which depend on the operating frequency and polarisation. With these parameters, the rain-induced attenuation $\gamma(dB)$ can be predicted. The parameters *C* and *m* in equation (2.16) above are estimated using the experimental data obtained from radio links. It was observed that *C* is dependent on the probability level, *P* (percent) of interest for which data are available as *m* depends on the radio link path length and the operating frequency in *GHz*. Therefore, the overall path length reduction formula in equation (2.16) becomes:

$$r = \frac{1}{1 + 0.03\left\{\frac{P}{0.01}\right\}^{-\beta} l^{m}} \tag{2.17}$$

with

$$m(F, l) = 1 + \Psi(F) \log_e l \tag{2.18}$$

$$\Psi(f) = 1.4 \times 10^{-4} F^{1.76} \tag{2.19}$$

The β coefficient in equation (2.17) is expressed as a result of best fit by:

$$for\ l < 50\ km$$

$$\beta = 0.45 \quad for\ 0.001 \leq P\ (percent) \leq 0.01 \tag{2.20}$$

$$\beta = 0.6 \qquad for\ 0.01 \leq P\ (percent) \leq 0.1$$

$$for\ l \geq 50\ km$$

$$\beta = 0.36 \qquad for\ 0.001 \leq P\ (percent) \leq 0.01 \tag{2.21}$$

$$\beta = 0.6 \qquad for\ 0.01 \leq P\ (percent) \leq 0.1$$

According to *Moupfouma*, the effective path length reflects the effect of the spatial inhomogeneity in rain along the radio link paths [*Moupfouma*, 1984].

2.6.4 The Modified Moupfouma Rain Attenuation Model

The modified (new) Moupfouma attenuation model has been globally adapted in some tropical countries in Africa and Latin America. The new Moupfouma model was developed due to the inadequacies in the earlier model. This model employs the power law empirical relationship developed by *Olsen et al.*, [1978] for the prediction of rain rate provided the $R_{0.01}$ in mm/h values exceeded 0.01 percent of the time is known [*Ajayi et al.*, 1996]. The related specific rain attenuation $\gamma_{R_{0.01}}$ on the microwave link of interest can then be expressed by:

$$\gamma_{R_{0.01}} = \kappa R^{\alpha}{}_{0.01} \tag{2.22}$$

where κ and α are parameters that depend on the operating frequency on the radio link and polarization. The non-uniformity of rain structure along the propagation path during a given rain event necessitated the use of the equivalent propagation path length, L_{eq} on which the rain structure is assumed to be uniform, rather than the entire path length [*Moupfouma*, 2009]. This equivalent path length is usually less than the total length of propagation along the radio link. The attenuation exceeded at 0.01% of the time along a terrestrial line-of-sight link is therefore given as the product of the specific rain attenuation and the equivalent or effective path length given in equation (2.23) as:

$$A_{0.01} = \kappa R^{\alpha}{}_{0.01} \times L_{eq} \tag{2.23}$$

To determine the effective path length, an adjustment factor δ that compensates for the non-uniformity of the rain structure along the propagation path is defined as:

$$L_{eq} = \delta \times L \tag{2.24}$$

The adjustment factor δ with respect to the $R_{0.01}$ and propagation length using data from a given terrestrial link is:

$$\delta(\mathrm{R}_{0.01}, \mathrm{L}) = \exp\left[\frac{-R_{0.01}}{1 + \xi(L) \times R_{0.01}}\right] \tag{2.25}$$

Substituting equation (2.25) into equation (2.24) yields:

$$\mathrm{L_{eq}}(\mathrm{R_{0.01}}, \mathrm{L}) = \mathrm{L} \times \exp\left[\frac{-R_{0.01}}{1 + \xi(L) \times R_{0.01}}\right] \tag{2.26}$$

Equation (2.26) is a function of two parameters, namely: the actual or total path length of the terrestrial link, L, and the rain rate observed for 0.01% of the time on the radio link. The parameter, $\xi(L)$ when $R_{0.01} \to +0$, is:

$$\mathrm{L_{eq}}(\mathrm{R_{0.01}}, \mathrm{L}) \approx L \tag{2.27}$$

Equation (2.26) implies that when it stops raining on a terrestrial radio link, the equivalent path length is the same as the terrestrial radio link path. However, when $R_{0.01} \to +\infty$, then;

$$\mathrm{L_{eq}}(\mathrm{R_{0.01}}, \mathrm{L}) = \mathrm{L} \times \exp\left(-\frac{1}{\xi}\right) \begin{cases} > L \; when \; \xi(\mathrm{L}) < 0 \\ \text{or} \\ \leq \mathrm{L} \;\; \text{when} \; \xi(\mathrm{L}) > 0 \end{cases} \tag{2.28}$$

According to Moupfouma [*Moupfouma*, 2009], for convective rainfall (very high rain rates), two scenarios are possible. The first is a situation where the rain covers the entire terrestrial path length and over (i.e.$\xi(L) < 0$). The second scenario is when the rain covers less than the actual path length of the terrestrial link. This implies that the reduction factor may be greater than, less than, or equal to unity, depending on some parameters (i.e.$\xi(L) > 0$). The parameter $\xi(L)$ is determined by the magnitudes of the actual path length of about 34 terrestrial radio links in Africa, Europe, Japan and United States. Therefore, for terrestrial link of propagation length L, such that $\mathrm{L} \leq 7$ km then,

$$\xi(L) = -100 \tag{2.29}$$

while for path lengths longer than 7 km, $\mathrm{L} > 7\ km$,

$$\xi(L) = \left(\frac{44.2}{L}\right)^{0.78} \tag{2.30}$$

In summary, the rain attenuation for terrestrial line-of-sight link can be predicted with the following expressions as given by Moupfouma [*Moupfouma*, 2009]:

$$\gamma_{0.01} = \kappa {\mathrm{R_{0.01}}}^{\alpha} \times \mathrm{L} \times \exp\left[\frac{-\mathrm{R_{0.01}}}{1 + \xi(\mathrm{L}) \times \mathrm{R_{0.01}}}\right] \quad \text{with} \quad \xi(\mathrm{L}) = -100 \tag{2.31}$$

for any terrestrial link of length $L \leq 7$ km and ,

$$\gamma_{0.01} = \kappa R_{0.01}{}^{\alpha} \times L \times \exp\left[\frac{-R_{0.01}}{1 + \xi(L) \times R_{0.01}}\right] \quad \text{with} \quad \xi(L) = \left(\frac{44.2}{L}\right)^{0.78} \tag{2.32}$$

whenever propagation path length $L > 7\ km$. This model can also be used to predict the rain rate at a given percentage of time for line-of-sight SHF and EHF radio communication links. As earlier mentioned, this new model makes use of $R_{0.01}$ value exceeded for 0.01percent of time in the locality of interest, and does not require all rain rate spectra for all time percentages [*Moupfouma*, 2009].

2.7 Rainfall Rate

The measure of the intensity of rainfall at a given time is referred to as the rainfall rate. It is a natural time varying phenomenon. Rainfall rate is obtained by calculating the amount of rain that falls on the earth surface per unit area per unit time [*Ajewole*, 1997]. Rainfall intensity and duration of rainfall are usually inversely related, that is, high rainstorms tends to be concentrated in short periods of time, and low intensity rainstorms are associated with long duration of occurrence. Rainfall intensity is classified according to the rate of precipitation as stratiform or convective. The stratiform type is further classified into drizzle and widespread, and the convective type into shower and thunderstorm for the purpose of application in radio communication [*Adimula and Ajayi*, 1996; *Ajewole*, 1997]. According to Crane, [*Crane*, 2003], rain rate is one principal factor in estimating the amount of attenuation likely to be experienced by any microwave link. The rain rate in millimeter per hour is computed from the disdrometer measurements using equation (2.33) as given by [*Bartholomew*, 2009]:

$$R = \sum_{i=1}^{20} \frac{\pi}{6} {D_i}^3 n_i \frac{3600}{S.T} \qquad \left[\frac{mm}{h}\right] \tag{2.33}$$

The precipitation rate, *R (*mm/h*)* can be determined from the measured DSD data as:

$$\left.\begin{aligned} R &= \frac{1}{6.A.T} \pi \sum_{j=1}^{20} n_j {D_j}^3 \\ &= 6.28318536 \times 10^{-3} \sum_{j=1}^{20} {D_j}^3 n_j \end{aligned}\right\} \left[\frac{mm}{h}\right] \tag{2.34}$$

A well-known integral equation of the rain rate *R* as computed from the drop size distribution model, *N (D)*, is given by *Gun* and *Kinzer* [1949] as:

$$\left.\begin{aligned} R &= 6\pi \times 10^{-4} \int_0^{\infty} {D_j}^3 . V(D_j) . N(D_j) dD_j \ \ [mm/h] \\ &= \ 1.88496 \times 10^{-3} \sum_{j=1}^{20} {D_j}^3 \, . V(D_j) . N(D_j) dD_j \end{aligned}\right\} \tag{2.35}$$

Equations (2.34) and (2.35) must not be violated by any drop size distribution.

2.8 Rain Attenuation and Depolarization

A proper knowledge of the depolarization properties of the transmission medium is important in planning frequency reuse by employing orthogonal polarizations in a radio communication system [*Chu*, 1974]. Depolarization is due to the lack of spherical symmetry of raindrops (the top and bottom are flattened) along with their tendency to have a preferred orientation. The effects of a medium filled with rain on a wave propagating through it are functions of the orientation of the electric field vector with respect to the preferred drop orientation. As the incident signal is scattered by the oblate spheroid raindrops, part of the scattered signal becomes polarized in a plane which is orthogonal to the direction of the plane of polarization of the transmitted signal [*Marcus and Pattan*, 2005]. Generally, raindrops and ice crystal depolarization is caused by the differential phase shift (DPS) and differential attenuation (DA) of the components of the electromagnetic wave along two major (horizontal) and minor (vertical) axes of hydrometeors [*Brussaard and Watson*, 1995]. In most cases, the rain effects are predominant in C-band (6/4 GHz) while the ice effects become more considerable in Ku-band (14/11 GHz) and sometimes quite significant in Ka-band (30/20 *GHz*) [*Dennis*, 2001; *Crane*, 1996; *Marcus* and *Pattan*, 2005].

Modeling of rain depolarization can be achieved by using the same principles as applied to rain attenuation. The main difference is that while considering depolarization, the raindrops are assumed to be oblate spheroids [*Ippolito et al.*, 1981]. The amount of orthogonal polarization depends on the rain rate, the shape and the size of the raindrops, the rain cell size and the distribution of canting angles that the raindrops acquire during their descent to the ground [*Laws and Parsons*, 1943; *Chu*, 1974].
Depolarisation often results in cross talk between two orthogonal polarized channels, transmitted on the same path and frequency band [*Oguchi, 1983; Ajayi, 1990; Brussaard and Watson,* 1995*; Ajewole, 1997; Van de Kamp, 2001; Barclay, 2003*]. As a result of this, radiowaves propagating through such paths suffer differential attenuation and phase shift. This may also constitute a problem in communication systems using polarisation orthogonality to maintain isolation between channels. Below 18 GHz, differential attenuation and phase shift increase with frequency for a given rain event, while they decrease for a given fade depth [*Barclay*, 2003]. This is partly because the less deformed smaller drops make a greater relative contribution to the total attenuation as frequency is increased. Polarisation can be linear or circular (elliptical).The most general case of polarisation is the elliptical

or circular polarisation. The electric field vector **E** (*t*), as expressed by *Brussaard and Watson* [*Brussaard and Watson*, 1995] in (1) composed of two sinusoidal components, having different amplitudes $|E_x|$ and $|E_y|$ and a phase difference $arg\left(\frac{E_y}{E_x}\right)$:

$$\boldsymbol{E}(t) = \mathrm{R_e}\mathrm{E}e^{jwt} = \mathrm{R_e}\left[\left(u_x E_x + u_y E_y\right)e^{jwt}\right] \tag{2.36}$$

$$\boldsymbol{E}(t) = u_x|E_x|\cos(wt) + u_y|E_y|\cos(wt + \phi) \tag{2.37}$$

where u_x, and u_y are the unit vectors in the x- and y- directions respectively; ω is the angular frequency, ϕ is the phase angle and *t* is the time. The phase is taken relative to the phase of E_x. As observed in equation (2.32), the polarisation may be frequency dependent and time varying as the hydrometeors change. Oftentimes, EM waves transmitted along the principal planes will arrive unchanged (magnitude) but, experience differential attenuation and phase shifts. Consequently, any transmitted polarisation that is not one of the link's principal planes will be cross polarized on reception [*Brussaard and Watson, 1995; Barclay,* 2003]. It is important to mention that the relative contribution of differential attenuation and phase shift is different at different frequencies. Differential phase shift appears to be the dominant factor in rain induced depolarisation at frequencies below 10 GHz and differential attenuation becomes increasingly significant at higher frequencies. A reliable estimate of the depolarizing properties of tropical rainfall for terrestrial and earth space links therefore requires among other parameters, the investigation of the differential attenuation, differential phase shift, cross polarisation discrimination (*XPD*) in the orthogonal channels, and the co-polar attenuation (*CPA*).

2.9 Review of Raindrop Size Distribution Models

Rain drops are known to grow and eventually break up as their diameters approach 8*mm.*The statistical behaviour of raindrops can, therefore, serve as a basis for choosing an appropriate distribution or the normal distribution [*Yesufu,* 1998]. During rainfall, the shape, size and the orientation of raindrops may vary within a given rain storm. Observation has shown that on the average, the drop size distribution and the shape of the raindrops are relatively stable, but changes with the rain rate [*Ajewole*, 1997]. Since 1890's, a number of researchers used different methods to determine the drop size distribution in different climatic regions [*Cruvinel, et al*., 1996]. Among the very earliest methods used to directly measure raindrops size distributions include the stain method [*Weisner*, 1895; *Neuberger*, 1942, *Gillespie*, 1958, *Hall* 1970]; the momentum method [*Joss and Waldvogel*, 1967; *Kinnell*, 1976]; the flour method [*Bentley*, 1904, *Laws and Parsons*, 1943; *Carter et al.*, 1974; *Kohl*, 1974]; the immersion method [*Fuchs and Petrjanoff*, 1937; *May*, 1945]; and the oil

method [*Eigel and Moore*, 1983]. In order to accurately estimate the specific rain attenuation at frequencies above 10 GHz, it is necessary to know the drop size distribution (which is region dependent) for a given rain rate.

The drop size distribution (DSD) represents the probability density of equivolumetric drop diameter *D* being in the unity volume [*Fiser,* 1993]. It is the distribution relating to raindrop sizes. It is often expressed in an exponential form. The discrepancy of different raindrop size distribution models is huge. It varies with the difference quarters, seasons, rainfall types, and other factors [*Xie et al.,* 2011]. The raindrop size is an essential micro-structural property in the modelling and prediction of rain attenuation. They play important roles in meteorology (determination of radar reflectivity and rain rate, classifications of precipitation, flood prediction), in microwave radio communication (determination of rain attenuation and depolarization), and many other applications such as agriculture and insurance business [*Fiser,* 1993]. The attenuation and scattering of electromagnetic waves depend on the raindrop size distribution; therefore, the drop size distribution studies have application in the microwave attenuation modeling [*Marzuki et al.*, 2010]. The general mathematical representation of the drop size distribution model as provided in [*Afullo,* 2011*; Owolawi*, 2011; *Marzuki et al., 2010*] and given as:

$$N(D) = N_c \times f^*(D) \tag{2.38}$$

where N_c is the total concentration per unit volume of rain drops in m^{-3} and $f^*(D)$ is the probability density function (PDF) of the rain drop size (raindrop size distribution function) in mm^{-1}. Various raindrop size distribution models are in use in various regions of the world for estimating radio wave impairment on both terrestrial and earth-space paths. These models have been employed for rain scattering and propagation calculations [*Ajayi et al.,* 1996; *Marshall* and *Palmer,* 1948]. Among the most widely used, especially in the temperate regions, are the Laws and Parsons [*Laws and Parsons*, 1943], Marshal and Palmer [*Marshal* and *Palmer,* 1948], the modified gamma model [*Atla*s and *Ulbrich,* 1974], the Joss et al., [*Joss et al.,* 1968], the lognormal [*Ajayi and Olsen,* 1985] and the Weibull [*Sekine and Lind,* 1982] distribution models. However, in recent times, appreciable numbers of researchers have done similar studies in the tropical, sub-tropical and equatorial regions characterized with heavy rainfall, though with inadequate data. Such studies include the measurement of rain drop size distributions by [*Ajayi and Olsen,* 1985; *Adimula and Ajayi,*1996 in Nigeria; *Lee et al*.2007, T*imothy et al,* 2002, *Kumar et al,* 2010 in Singapore; *Afullo,* 2011, *Adetan and Afullo,* 2012a; 2012b; *Alonge and Afullo,* 2012, *Akuon and Afullo,* 2011 in South Africa and *Kesavan et al,* 2013 in Malaysia]. The next section considers the most commonly used models for raindrop size modelling.

Table 2-1: The L-P Drop size distribution model for different types of rainfall [*Sadiku*, 2000]

Drop Diameter (mm)	Terminal velocity (m/s)	Rainfall Rate (mm/h)								
		0.25	1.25	2.5	5	12.5	25	50	100	150
		Percentage of water volume								
0.5	2.1	28.0	10.9	7.3	4.7	2.6	1.7	1.2	1	1.0
1	3.9	50.1	37.1	27.8	20.3	11.5	7.6	5.4	4.6	4.1
1.5	5.3	18.2	31.3	32.8	31.0	24.5	18.4	12.5	8.8	7.6
2	6.4	3.0	13.5	19.0	22.2	25.4	23.9	19.9	13.9	11.7
2.5	7.3	0.7	4.9	7.3	11.8	17.3	19.9	20.9	17.1	13.9
3	7.9		1.5	3.3	5.7	10.1	12.8	15.6	18.4	17.7
3.5	8.35		0.6	1.1	2.5	4.3	8.2	10.9	15	16.1
4	8.7		0.2	0.6	1	2.3	3.5	6.7	9	11.9
4.5	9.0			0.2	0.5	1.2	2.1	3.3	5.8	7.7
5	9.2				0.3	0.6	1.1	1.8	3	3.6
5.5	9.35					0.23	0.5	1.1	1.7	2.2
6	9.5						0.3	0.5	1	1.2
6.5	9.6							0.2	0.7	1
7										0.3

2.9.1 Laws and Parsons Drop Size Distribution Model

While measuring the proportion of the total volume of water reaching the ground surface, Laws and Parsons proposed empirically the median diameter D_m [*Laws and Parsons*, 1943]:

$$D_m = 1.238R^{0.182} \quad [\text{mm}] \tag{2.39}$$

where R is the precipitation rate (mm/h). The Laws and Parsons model is probably the best known DSD model and has been recommended by the ITU-R for the prediction and calculation of specific rain attenuation in temperate regions. It has been found to be adequate for applications involving statistical results for rain induced attenuation below 30 GHz and for long time bases. This distribution was obtained experimentally from a rudimentary technique [*Battan*, 1964]. It was concluded that the actual drop size distribution on ground could be obtained from the volume distribution with a fall velocity, *v (a)* as:

$$n(a) = \frac{10^3 R\beta_m da}{4.8\pi a^3\, v(a)} \quad [m^{-3}] \tag{2.40}$$

where $\beta_m da$ is the volume fraction percentages, *a* is the radius of raindrop in *m*, *da* is the size interval from $a - \frac{da}{2}$to $a + \frac{da}{2}$ and *R* is the precipitation or rain-rate in mm/h. The Laws-Parsons distribution, which predates the Marshall-Palmer model and is also much used, is an empirically measured *N(D)* which is tabulated numerically rather than expressed mathematically. It is similar to the Marshall-Palmer form except that it has slightly fewer small drops [*Barclay*, 2003]. The Laws and Parsons Model for different types of rain and raindrop sizes have been summarised in Table 2-1.

2.9.2 Marshall and Palmer Drop Size Distribution Model

In 1948, Marshall and Palmer [*Marshall and Palmer*, 1948] proposed the famous negative exponential raindrop size distribution model analytically. This was the first analytical description of the average raindrop size distribution. The model is of the form:

$$N(D) = N_0 \exp(-\Lambda D) \qquad (\text{for } 0 \le D \le D_{max}) \tag{2.41}$$

where *D* is the diameter in millimeters and N_o is a constant often defined as the maximum raindrop size distribution derived from equation (2.41) as:

$$N_0 = \frac{4}{3\pi}\int N(D) D^3 v(D) dD \tag{2.42}$$

where Λ is a constant that tends to increase with rain rates [*Marshall* and *Palmer*, 1948]:

$$\Lambda = 4.1 R^{-0.21} \ [mm^{-1}] \tag{2.43}$$

N_o is usually very close to that of Law and Parsons given as $N_o = 8000 mm^{-1} m^{-3}$. The terminal fall velocity *v (D*) is expressed by Battan [*Battan*, 1964] for diameter between 1 to 4 mm as:

$$v(D) = \sqrt{200.8a} \tag{2.44}$$

A noticeable disadvantage of the Marshall-Palmer (M-P) model is that it overestimates small raindrops below the diameter of about 1.5 mm because of its exponential increase when *D* tends towards zero. Hence, the use of the distribution will lead to higher attenuation value than the actual attenuation at frequencies above 30 GHz, especially outside the temperate region [*Ajewole et al.*,

1999]. According to Hardy [*Hardy*, 1963], equation (2.41) is not satisfactory for small diameters. Even though equations (2.42) and (2.43) are based on measurements for R < 23mm/h, researchers have confirmed that the Marshall-Palmer negative exponential model is well suited for the average DSD at higher rain rates [*Ajayi et al.,* 1996]. The M-P model was developed mainly for temperate climates.

2.9.3 The Modified Gamma Drop Size Distribution Model

Distributions which describe drop size distribution, *N (D)* directly via an analytical expression were first proposed by Marshall and Palmer and later by Joss et al., for different types of rainfall [*Joss et al.,* 1968].The gamma distribution was initially proposed by *Atlas* and *Ulbrich* [1974]. It is expressed in the form:

$$N(D_i) = N_0 D^{\mu} \exp(-\Lambda D) \quad [\ m^{-3}mm^{-1}] \tag{2.45}$$

where *N(D)* is the number of raindrops per cubic meter per millimeter diameter ($mm^{-3}\ m^{-1}$), *D* is the raindrop diameter in mm, *No*, Λ and μ are parameters to be determined through the measured DSD. These input parameters are expressed as a function of rainfall rate as given in equations (2.45a) and (2.45b) where *a, b,* a_g and b_g are the regression coefficients of input parameters with respect to the gamma model

$$N_0 = aR^b \tag{2.45a}$$

$$\Lambda = a_g R^{b_g} \tag{2.45b}$$

In most cases, the parameter μ takes the value of a constant which can be from 0 to 4. In this study, the value of 2 is assumed. The gamma distribution is particularly useful in tropical climate regions where the exponential distribution has been found on numerous occasions to be inadequate [*Adimula* and *Ajayi,* 1996]. The modified gamma distribution model tends to correct the exponential increase of the raindrop per unit volume when the drop diameter *D* tends to zero. This is in contrast to the negative exponential model of Marshall and Palmer. The modified gamma model, suggested by *Ulbrich* [1983] is usually expressed in the form:

$$N(D) = N_0 D^{p} \exp(-\Lambda D^{q}) \quad [m^{-3}mm^{-1}] \tag{2.46}$$

where N_o, p, Λ and q are positive and real constants. One major difficulty in using this distribution is in obtaining these four parameters experimentally. Again, there is the possibility of cutting off both the large and small ends of the raindrop size spectrum for values of *D* in the range 3-5 mm. *Ulbrich*

[1983] observed that not all the gamma distribution parameters are independent. He found theoretically and empirically that the parameters N_0 and p are related through the approximate expression in equation (2.47) where C_N is a constant having the value of 6×10^4 ($m^{-3}cm^{-1-p}$).

$$C_N = e^{3.2p} \tag{2.47}$$

This is advantageous since dual-measurements techniques can be employed to estimate these parameters with N_0 and p expressed in terms of each other. Subsequent work which followed the development of the disdrometer, an instruments capable of automatically recording the size distribution of raindrops, showed that N_o could vary quite considerably, both from one event to another and even within a rain event. The gamma distribution has been found to provide a better fit of drop size distributions at both low and high rainfall rates [*Ulbrich,* 1983].The model has been found adequate in tropical regions of Singapore and Taiwan [*Kumar et al.*, 2010].

2.9.4 Weibull Drop Size Distribution Model

The Weibull distribution, named after Waloddi Weibull (1939) was first proposed by Sekine and Lind [*Sekine* and *Lind,* 1982] for the estimation of rain attenuation at centimeter, millimeter and sub-millimeter ranges, as:

$$N(D) = N_0 \left(\frac{\eta}{\sigma}\right)\left(\frac{D}{\sigma}\right)^{\eta-1} \exp\left\{-\left(\frac{D}{\sigma}\right)^{\eta}\right\} \qquad [m^{-3}mm^{-1}] \tag{2.48}$$

where D is the drop diameter in millimeters, η is the shape parameter, σ is the scale parameter. The parameters η and σ are functions of the precipitation rate R in mm/h. According *to Murthy et al,* [2004], the shape parameter, η is the determinant factor of the Weibull distribution. *Jiang* et al., [1997] considered the Weibull distribution and arrived at the constant input parameters of equation (2.42) as N_o = 1000 mm^{-3}, η = 0.95 $R^{0.14}$ and σ = 0.26$R^{0.42}$ *mm* [*Oguchi,* 1983]. The Weibull distribution is retained for microwave applications for drizzle, widespread, and shower rain cases [*Sekine* and *Chen,* 1985]. The power law regression coefficients of equation (2.48) with respect to the precipitation rate R are given as:

$$N_0 = aR^b \tag{2.49a}$$

$$\eta_\eta = a_\eta R^{b\eta} \tag{2.49b}$$

$$\sigma_\sigma = \mathrm{a}_\sigma R^{b\sigma} \tag{2.49c}$$

Table 2-2: Joss et al. DSD constants [*Joss et al.,* 1968]

Types of Rainfall	N_o $m^{-3}mm^{-1}$	Λ mm^{-1}
Drizzle (J-D)	30000	$5.7\ R^{-0.21}$
Widespread (J-W)	7000	$4.1\ R^{-0.21}$
Shower (J-S)	8000	$4.1\ R^{-0.21}$
Thunderstorm (J-T)	1400	$3.0\ R^{-0.21}$

where a, b, a_η, b_η, a_σ and b_σ are regression coefficients of input parameters corresponding to the Weibull distribution model and R is the rainfall rate in mm/h.

2.9.5 The Joss et al., Drop Size Distribution Model

Joss, Thams and Waldvogel [*Joss et al.*,1968] proposed this model, often referred to as the Joss model by measuring the raindrop size distribution using a disdrometer at Locarno in Switzerland and obtained a similar exponential form of equation (2.41).The distribution models are counted using the disdrometer. Table 2-2 shows the rain drop size distribution parameters of the different types of rain (drizzle, widespread, showers and thunderstorm). Using the disdrometer, *Joss et al.,* [1968] confirmed that there is a large spatial and temporal variability in the raindrop parameters. They also found that for moderate and heavy rainfall, the attenuation calculated from the measured DSD and the measured attenuation are in good agreement. This was however, not the case for light rain. This describes the first model of DSD in relation to the variation of raindrop sizes within each storm [*Ajewole,* 1997].

2.9.6 Lognormal Drop Size Distribution Model

Due to the deficiencies of the negative exponential (Marshall-Palmer) and the modified gamma distribution models in describing the small diameter drops (less than 1.5 mm), researchers have studied the lognormal distribution. According to *Ajayi et al.,* (1985), the lognormal rainfall DSD model is given as:

Table 2-3: Coefficients of lognormal distribution model for tropical region [*Adimula* and *Ajayi*, 1996]

Rainfall type	N_T		μ		σ^2	
	a_o	b_o	A_μ	B_μ	A_σ	B_σ
Drizzle (R < 5 mm/h)	718	0.399	-0.505	0.128	0.038	0.013
Widespread (5 mm/h ≤ R ≤10mm/h)	264	0.232	-0.473	0.174	0.161	0.018
Shower (10mm/h ≤ R ≤ 40 mm/h)	137	0.370	-0.414	0.234	0.223	-0.034
Thunderstorm (R > 40 mm/h)	63	0.491	-0.178	0.195	0.209	-0.030

$$N(D) = \frac{N_T}{\sigma D\sqrt{2\pi}} exp\left\{-\frac{1}{2}\left[\frac{\ln D - \mu}{\sigma}\right]^2\right\} \quad [m^{-3}mm^{-1}] \tag{2.50}$$

where μ is the mean shape parameter, σ is the standard deviation scale parameter , N_T is the concentration of rainfall drops or the sum of rain drops often required for the purpose of fitting the measurements and D is the mean diameter of the raindrop which can be obtained directly from measurement. The lognormal distribution model is more advantageous in the sense that each of its parameters has a clear physical significance which does not appear to be true for the modified gamma distribution model [*Bradley and Stow*, 1974]. Moreover, the parameters; N_T, μ and σ^2 are linearly related to the moments of the drop size distribution [*Ajayi and Olsen*, 1985]. The input parameters N_T, μ and σ are derived from regression techniques and they are dependent on the precipitation rate R in *mm/h* as:

$$N_T = a_o R^{b_o} \tag{2.50a}$$

$$\mu = A_\mu + B_\mu \ln(R) \tag{2.50b}$$

$$\sigma^2 = A_\sigma + B_\sigma \ln(R) \tag{2.50c}$$

where a_o, b_o, A_μ, B_μ, A_σ, B_σ are coefficients of moment regression [*Ajayi et al.*, 1985]. In 1996, *Adimula* and *Ajayi* [1996] further extended the results by making measurements over a period of three years at three different locations in Nigeria. The distributions obtained were confined within four different classes of rain and the optimized values of the coefficients of regression obtained are given in Table 2-3. Sometimes, modeling these parameters as functions of rain rate R may be inadequate as

they assume different values even at the same rain rate. In practice, the DSD parameters are not primarily functions of rain rate *R* only, but also of some other controlling factors such as the type of rainfall [*Paraboni et al.*, 2006].

2.10 Drop Size Distribution, Terminal Velocity and Rain Rate

The fall terminal velocity and shape of raindrops are essential parameters for estimating the rainfall rate and resulting radio wave attenuation. The well-known *Gunn and Kinzer* method [1949] has been used to determine the fall velocity of raindrops. A simple view of the terminal fall velocity of raindrops assumes that when a raindrop falls on the surface of the Earth, it is acted upon by two main forces; gravity and drag. Therefore, a stationary raindrop initially experiences acceleration due to gravity of 9.8 m/s^2, as would any falling body. As gravity increases the speed of the raindrop in its descent, drag retards the downward acceleration of the raindrop. Usually, the air resistance that comes in contact with the water molecules as they fall causes the drag. According to Ajewole [*Ajewole,* 1997], the combination of these two forces (drag and gravity) causes the raindrop to reach a terminal velocity when the drag force is approximately equal to the weight of the raindrop. At this point, a raindrop experiences no further acceleration and therefore falls at a constant velocity. How fast a raindrop falls is a function of the size and weight of the raindrop - the heavier the raindrop, the faster it falls. In addition, the shape of the raindrop and air currents also are factors that contribute to the fall. The drop fall terminal velocity reaches a maximum when the drop size is close to 4 mm [*Gunn and Kinzer*, 1949]. The Gun-Kinzer terminal velocity is given as:

$$v(D) = 9.65 - 10.3\exp(-0.6D) \tag{2.51}$$

where $v(D)$ is the raindrop velocity in m/s, and D is the raindrop diameter in mm. A well-known integral relationship thus exists between drop size distribution or number density *N (D),* terminal velocity *V (D),* and the rainfall rate *R* which must not be violated by any DSD model [*Timothy* and *Sarkar*, 1997]. This relation is expressed as:

$$R = 6\pi \times 10^{-4} \int_0^{\infty} D^3\, N(D) V(D) dD \qquad \left[\frac{mm}{h}\right] \tag{2.52}$$

Equation (2.51) can also be expressed in a discrete form as given by *Ajayi et al.* [1997]:

$$R \approx 6\pi \times 10^{-4} \sum D^{3} N(D)V(D)\Delta D \tag{2.53}$$

where D is the raindrop diameter in mm and ΔD is the diameter interval of drop size class in mm.

2.11 The Specific Rain Attenuation and the Extinction Cross Section

In order to predict accurately the total rainfall attenuation, it is often important to determine the DSD for a given rain rate, which is region-dependent. The two principal requirements for the estimation of the rainfall attenuation in a given geographical location are the drop size distribution, *N (D)* and the rainfall rate, *R.* The total rain specific attenuation can be evaluated by integrating over all the drop sizes as:

$$\gamma\ (dB/km) = 4.343 \times 10^{-3} \int_{0}^{\infty} Q(\lambda, m, D) \times N(D) dD \tag{2.54}$$

where *N (D)* is the drop size distribution, *Q* is the attenuation cross section which is determined by applying the classical scattering theory of Mie for a plane wave impinging upon a spherical absorbing particle. This will be discussed in details in chapter 3.

Another most widely used rain attenuation prediction methods is an empirical relationship between the specific rainfall attenuation α in dB/km and the rain rate *R* in mm/h [*REC. ITU-R P.838-3*, 2005] given as:

$$\gamma = \kappa R^{\alpha} \tag{2.55}$$

where κ and α depend on the operating frequency and rain temperature; and the value of *R* is for an exceedance of 0.01 percent of the time for point rainfall rates with an integration time of 60 seconds. The coefficients κ and α can be horizontally or vertically polarized as presented in [*REC. ITU-R P.838-3*, 2005]. The ITU-R values of the parameters κ and α for the estimation of the specific attenuation is presented in Appendix B-1 for frequencies of 1 to 1000 GHz. It is important to mention that the empirical methods are based on measurements of databases from stations in different climatic zones within a given region. These methods are frequently used for rain attenuation prediction and have yielded good success [*Tamošiūnaitė et al.*, 2011]. The derivation and computation of the extinction cross sections is discussed in the next chapter of this work. The scattering parameters

required for the estimation of the specific rain attenuation in Durban using a scattering method between 2 to 500 GHz is also discussed in chapter 3.

2.12 Review of Raindrop Critical Diameters

The critical raindrop diameters are the range of diameters over which the contribution to the rainfall attenuation is predominant. Within the tropical region and other parts of the globe, a number of researchers have investigated the particular contribution of certain raindrop diameters to the rain attenuation. For instance, in Singapore, *Lakmish et al.*, [2007] and *Lee et al*., [2007] investigated the DSD for Singapore using the lognormal DSD model and identified the critical range of diameters as 0.771mm to 5.3mm. They established that while removing consecutive rain diameters (channels), lower diameters raindrops (< 0.771mm) contribute insignificantly to the overall specific rain attenuation for the selected rain rates. Similarly, the influence of particular raindrop diameters on rain attenuation was also carried out by *Fiser*, [2002] in the Czech Republic. The critical range of diameters contributing to the specific rain attenuation was found to be approximately 0.7-1.5mm. The prevailing contribution to the specific attenuation was formed by raindrops of diameters not exceeding 2 mm. In Malaysia, *Lam et al*. [2011] while investigating the specific raindrop sizes producing major contribution to the total specific attenuation with R = 120.4 mm/h, established that small and medium-size drops contributed more to the rainfall attenuation as frequency increases. The oblate spheroid raindrop shape was however adopted. *Marzuki et al*., [2009] observed in Equatorial Indonesia that the increasing role of small and medium-sized drops to rain attenuation is proportional to frequency of transmission. In their observation, the drop size that produced the largest contribution to the specific attenuation for rain rate of 10mm/h did not exceed 3 mm.

2.13 South Africa Climate and Weather

South Africa is located on latitude 29^{o}'S and longitude 24^{o}'E in the most southern tip of the African continent having a total area of 1,219,912 km [see *http://www.mapofworld.com/latlong/south-africa-lat-long.html*]. With this positioning on the globe, South Africa can be classified as a subtropical region, because the subtropics include all parts of the world just outside 23.4^{o}N and 23.4^{o}S latitude [see *http://en.wikipedia.org/wiki/Tropics*]. South Africa borders other countries like Botswana and Zimbabwe in the central north, Mozambique in north-east, Namibia in north-west. Swaziland and Lesotho are enclosed in the country. South Africa is climatically moderated by surrounding oceans: the Atlantic Ocean in the western part and the Indian Ocean in the eastern part. The country has a coastline of 2,798 km [*South Africa Climate and Weather, in http://www.sa-venues.com/no/weather.html*]. The cold Benguela current pushes northwards from the Antarctic along the Atlantic coastline up to the west coast, and a much warmer stream, the Agulhas current also

moves southwards from the Indian Ocean. The eastern seas 'steady evaporation provides generous rainfall while the Benguela current retains its moisture to cause desert conditions in the west [*South Africa year book*, 1991; http://www.southafrica.info/plantrip/travel_tips/questions/climate.html].

Rainfall is highly seasonal over most of southern Africa. South Africa can be classified into four seasons: summer which occurs from mid-October to mid-February; autumn which occurs from mid-February to April; winter occurs from May to July; and spring which occurs from August to mid-October. These seasons have varying temperatures ranging from -2^{o}C in the winter to 36^{o}C in the summer. Rainfall over the interior northern regions of South Africa follows annual cycle and is almost entirely a summer phenomenon [*Tyson*, 1986]. South Africa has an average annual precipitation of 502 mm, against a world mean of 857 mm. The distribution of rainfall in South Africa is as follows: 21% of the country receives less than 200 mm annually, 48% receives between 200 and 600 mm, while 31% records a total above 600 mm [*South Africa year book*, 1991]. The 400 mm rainfall line divides the country into a wet and a dry western half.

The moist Indian Ocean air masses, which are the chief source of rain over most of the country, gradually lose their moisture as they move towards the western interior. The rainfall distribution pattern in South Africa is also influenced by the orographic effect. This is due to the forced lift of air over high grounds [*Ajayi*, 1989]. The coastal plain has abundant low stratus cloud and fog, particularly during the summer. At night fog tends to advance on to the coastal plain to a depth of 30-50 km, withdrawing again as the land heats up during the day [*South Africa year book*, 1991]. The winter rainfall region is a relatively small area along the western Cape and south west Coast and has a rainfall regime of the Mediterranean type with a conspicuous winter maxima. The rain is often long lasting and not very intense, except along the mountains, where the orographic effect may include heavy showers. Snow occurs on the mountains four to six times during winter, but it usually melts within a few days. Hail and thunderstorm are rare.

The summer rainfall region covers most of the rest of the country, with common light orographic rains along the windward slopes of the eastern escarpment. Over most of the summer months, violent convection storms accompanied by thunder, lighting, sudden squalls and often hail are associated with the rainfall [*http://ww.southafrica.info/plantrip/traveltips/questions/climate.html*]. Between the winter and summer rainfall regions lies a transitional area, where rain comes in all seasons, that is, neither in winter nor in summer, but in autumn and spring. This transitional area can be divided into two sub-regions: a southern coastal strip with annual total of 375 to 875 mm, and a drier inland corridor behind the coastal range with an annual total of 50 to 250 mm [*Brasseur et al*., 1999]. In general, the climatic conditions in South Africa range from Mediterranean in the south-western corner of the country to temperate in the interior plateau, subtropical in the northeast, and a small area in the northwest with a desert climate. Most rainfall in South Africa normally comes in the summer and autumn months. The spring and winter months are drier months; with the exception of Western Cape (Cape Town),

because of its location and Mediterranean nature of climate, it gets most of its rain in winter

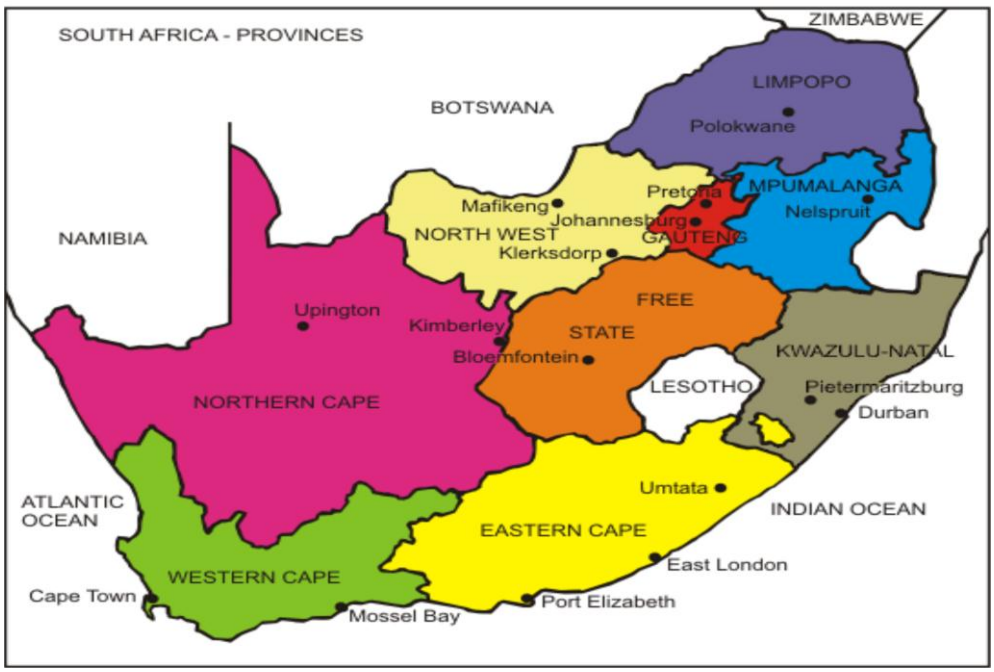

Figure 2-4: Map of South Africa and neighbouring countries [http:\\www.proseo.co.za]

Table 2-4: The ITU-R Model values for World different rain climatic zones

[*ITU-R P. 837-1*, 2008]

Percentage of Time (%)	A	B	C	D	E	F	G	H	J	K	L	M	N	P	Q
1.0	<0.1	0.5	0.7	2.1	0.6	1.7	3	2	8	1.5	2	4	5	12	24
0.3	0.8	2	28	4.5	2.4	4.5	7	4	13	4.2	7	11	15	34	49
0.1	2	3	5	8	6	8	12	10	20	12	15	22	35	65	72
0.03	5	6	9	13	12	15	20	18	28	23	33	40	65	105	96
0.01	8	12	15	19	22	28	30	32	35	42	60	63	95	145	115
0.003	14	21	26	29	41	54	45	55	74	70	105	95	140	200	142
0.001	22	32	42	42	70	78	65	83	55	100	150	120	180	250	170

[*http://www.southafrica.info/travel/advice/climate.html ; Odedina and Afullo*, 2008]. It can be seen that rainfall in South Africa is highly variable and unpredictable throughout the country. Large

fluctuations around the mean annual figure are the rule rather than exception. Like other countries in similar latitudes, South Africa is periodically afflicted by severe and prolonged droughts. However, the droughts often end with severe floods especially during summer [*South Africa year book*, 1991]. *Tyson et al*., [1976] observed that over the period of 1910-1972, much of the summer rainfall area of South Africa experienced a quasi-20-year oscillation [*Tyson et al*., 1976]. This rainfall spectrum shows a clear peak at about twenty year as well as peaks in 2-3 and 3-4 year bands [*Fashuyi et al*., 2006]. The ITU-R has classified regions of the world into 15 rain climatic zones. These are: A, B, C, D, E, F, G, H, J, K, L, M, N, P and Q. This is shown in Table 2-4 (*ITU-R P.837-1, 2, 3, 4, 5*, 2008). Based on the ITU-R classification, South Africa is classified into C, D, E K and N rain climatic zones. However, a study conducted by [*Fashuyi et al,* 2006] using a 5-year rainfall rate data recorded in twelve different geographical locations in South Africa further determined three additional rain climatic zones (M, P and Q) for South Africa.

2.14 Chapter Summary

A theoretical background to this work has been given in this chapter. The rain rate and drop size distribution which are the essential parameters required for the estimation and accurate prediction of the attenuation due to rain in any given locality have been discussed. Different DSD and rain attenuation models are also presented. Scattering and absorption phenomena, which are the two major sources of microwave transmission losses in the lower atmosphere, have been explained. These two phenomena are of major concern to system designers and network planners. The South Africa climate and weather have been discussed. The preceding chapter describes the experimental set up in this research work which includes the data processing and analysis. A comparative analysis of the different methods used for the estimation of the DSD parameters is also discussed.

CHAPTER THREE

RAINDROP SIZE DISTRIBUTION AND ATTENUATION MODELING FOR MICROWAVE PROPAGATION IN SOUTH AFRICA

3.1 Introduction

The attenuation of microwave linear line-of-sight signals due to precipitation limits the propagation path length of line-of-sight communication systems. To understand how this attenuation is influenced by rain, a detailed understanding of the inherent microstructural parameters such as the drop size distributions (DSD) and the corresponding scattering mechanisms at a given operating frequency is important. The raindrop size is an essential micro-structural property in the modelling and prediction of rain attenuation as earlier mentioned in chapter two. In this chapter, the description of instrumentation, data collection, sorting and analysis are discussed. The block diagram of the Joss Waldvogel RD-80 impact disdrometer is described. Based on the DSD measurements from the disdrometer, statistical analysis of different models as discussed under chapter 2 is carried out for Durban, South Africa. A comparative analysis of the two known methods for the parameter estimation is also discussed. The specific attenuation due to rain is computed and compared to the ITU-Recommendation 838-3 standard explained in chapter 2.

3.2 The Joss-Waldvogel (J-W) RD-80 Disdrometer

The Joss-Waldvogel RD-80 disdrometer [*Joss and Waldvogel*, 1967] is an instrument manufactured by Distromet of Basel, Switzerland. It is used to obtain the drop size distribution at a point along the radio path. The measured drop size distribution, which is time dependent, can easily be transformed into rainfall intensities. The disdrometer is typically constructed of a conical Styrofoam body used to transmit the mechanical impulse, caused by vibrations, to two moving coils. When raindrops impact this surface, the downward displacement of the body induces a voltage in a sensing coil. The induced voltage is amplified in the sensor head and applied to a second coil producing an electromagnetic force that restores the body to its rest position. This voltage is processed to convert the vertical momentum of a raindrop into an electronic pulse that is proportional to the raindrop diameter. [*Baltas and Mimikou*, 2002]. The J-W disdrometer device gives a good measure of raindrop size, cheaper to acquire, readily available and has a more sufficient data when compared to other types of disdrometer (e.g. video disdrometer) [*Townsend*, 2011]. The RD-80 disdrometer is capable of measuring not only the rainfall drop size but also the rainfall rate, rainfall accumulation and rain reflectivity [*http://www.distromet.com/83/Product_Description/Data_Aquisition.html*

Sheppard and Joe, 1994]. The equipment set up and the block diagram configurations of the Joss-Waldvogel RD-80 disdrometer are shown in Figures 3-1 and 3-2 respectively. The disdrometer is an enhanced version of the RD-69 that adopts the *Gunn and Kinzer* [1949] concept of rainfall diameter and fall velocity. The system consists of two basic independent units interfaced with a microcomputer. The sampling time T of the disdrometer is 60 seconds with the sampling cross-sectional area, A of 50 cm^2. The disdrometer has an inbuilt unit responsible for the sorting of the raindrops into 20 size intervals (classes or channels) ranging from 0.359 to 5.373 mm at ±5% measurement accuracy. The diameter range for each distinct class is equivalent to $\left(D \pm \frac{\Delta D}{2}\right)$ mm. Appendix C-1 shows the details of the diameter classes, thresholds, intervals and the corresponding fall velocities of the RD-80 disdrometer. *Brawn* and *Upton* [2008] have identified a number of shortcomings (disadvantages) of the disdrometer irrespective of the type, ranging from dead time error, inability to determine the size of large drops under heavy rainstorm, noise caused by strong winds or high acoustics (impact disdrometer), splashing drops or debris landing on the surface of the device, among others. However, one major problem of the disdrometer is its insensitivity to small raindrops in heavy rain. In the presence of large number of large raindrops in intense tropical rain ($R \geq 20$ mm/h), raindrops smaller than 1.0 mm are unrepresented or underestimated. This is due to an automatic threshold in circuitry hat monitors the ambient noise level to reject spurious pulses, but in intense rain high noise level of the drops themselves is interpreted as ambient noise and small drop signals are rejected.

An algorithm supplied by Waldvogel can be used to correct each channel according to the number of impacts in the other channels for the "*dead time"* of the instrument [*Tokay and Short*, 1996; *Tokay et al.*, 2001; *Caracciolo et al.*, 2006; *Kumar et al.*, 2010]. The larger drops produce longer dead times and therefore greater corrections. The Waldvogel algorithm is a multiplication matrix such that it does not increase the counts when the channel has no drops. In this study, rainfall samples with overall sum of drops less than 10 were removed (ignored) from the data samples to compensate for the dead-time errors. In Figure 3-2, the system consists of two basic units: the sensor and the processor. The sensor is exposed to the rain and the processor is used for analog processing and digitizing of the sensor signals. The two units are connected by a pair of wires.

3.3 Data Collection, Processing and Analysis

The Joss-Waldvogel (J-W) RD-80 disdrometer located at the roof top of the Electrical, Electronic and Computer Engineering building, University of Kwa-Zulu Natal, Durban (29°52'S, 30° 58'E), South Africa was used to obtain data samples used in this study. The measurement was taken over a

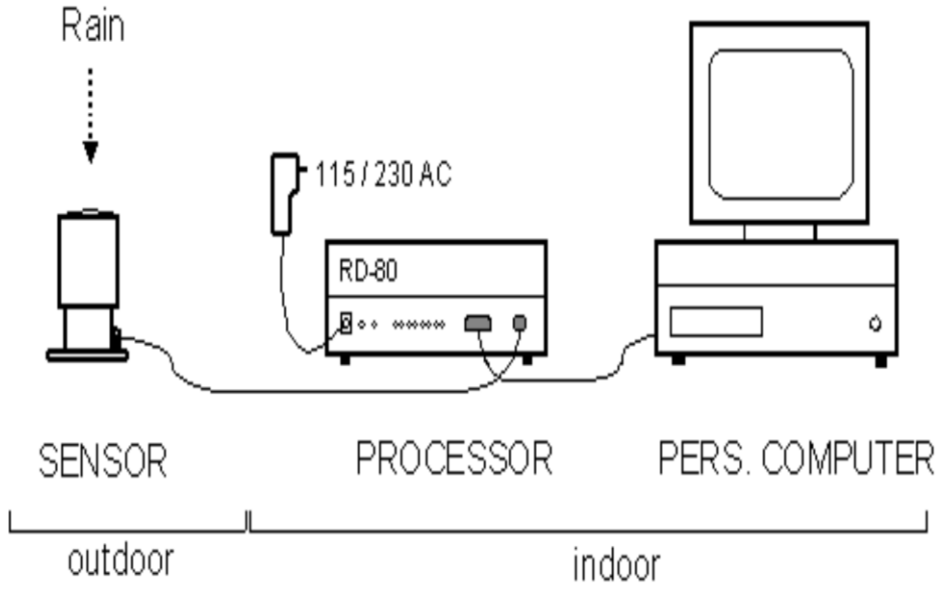

Figure 3-1: Joss-Waldvogel RD-80 impact disdrometer system connected to a personal computer
[RD-80 product information: http://www.disdromet.com/1_index_e.htm].

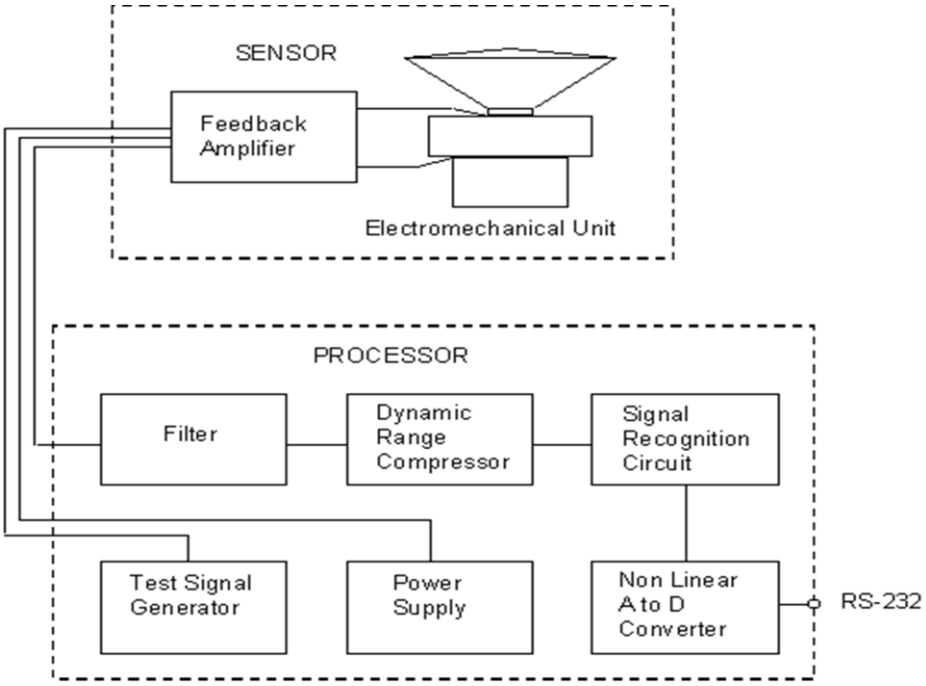

Figure 3-2: Block diagram of RD-80 impact disdrometer

[Source: http://images.worldsoft-cms.info//wcms/ftp/d/distromet.com/siteimages/2274.gif]

period of three (3) years; (2008 to 2010) in Durban at a sampling time of 60 seconds. As earlier stated, the disdrometer used in this work is capable of measuring the rainfall rate, reflectivity, rainfall

accumulation and the raindrop size distribution with accuracy of ±5 %. Rain events (or minutes) with overall sum of drops less than 10 were discarded from the data samples to compensate for the dead-time errors as they are considered to be within the noise level [*Tokay et al.,* 2001]. The location is shielded from noise and abnormal winds. Very minimal equipment outage was observed during the period of data collection at this location.

The integral rain parameters of interest in this work are computed directly from the disdrometer spectra and represented by [*Tokay et al.,* 2001]:

$$P = a\sum_{n=1}^{20} C_n X_n \tag{3.1}$$

where *a* is the product of parameters that are invariant with drop size, C_n is the number of drops in the *n*th channel, and X_n are the moments. Generally, the measured rain drop size distribution $N(D_j)$ from the disdrometer data is the number of raindrops per cubic meter per millimeter diameter ($mm^{-3}\ m^{-1}$) as adopted by [*Bartholomew*, 2009; *Gun and Kinzer*, 1949] and computed as:

$$N(D_j) = \frac{n_j}{v(D_j) \times T \times A \times dD_j}\ (m^{-3}mm^{-1}) \tag{3.2}$$

where n_j is the number of drops measured in the drop size bin, $v(D_j)$ is the terminal velocity of *Gun Kinzer's* [1949] water drops in m/s, *T* is the one-minute sampling time in 60 *s*, *A* is the cross sectional sampling area of the disdrometer given as 50 cm^2 and dD_j is the representative change in diameters interval of the bin in mm. The data was sorted and classified into different types of rain based on rainfall rates *R* in millimeter per hour according to *Timothy et al,* [2002] and *Adimula and Ajayi* [1996] as: drizzle, (0 mm/h ≤ *R*< 5 mm/h), widespread, (5 mm/h ≥ *R* < 10 mm/h), shower, (10 mm/h ≤ *R* < 40 mm/h) and thunderstorm (*R* > 40 mm/h). Over 80,000 data samples were obtained from the disdrometer over a period of 3 years. The minimum and maximum rain rates obtained were 0.003 mm/h and 117.15 mm/h. A summary of this is provided in Table 3-1. The sorted data from the disdrometer was used for the modeling of the various parameters of the DSD models discussed in chapter two.

Table 3-1: Summary of the disdrometer sampled data

Types of Rainfall	Number of Samples	Total Sum of Drops	Observed Maximum Number of Drops Per Sample
Drizzle	57,006	12,798,104	2,532
Widespread	1,114	900,906	2,458
Shower	581	471,112	2,351
Thunderstorm	53	59,833	1,819

3.4 Methods of Parameter Estimation

Estimation of parameters is a fundamental problem in data analysis. Estimation is the process of determining approximate values for parameters of different events. How well the parameters are approximated is a function of the method, the type of data and other factors. A brief discussion of the widely used methods is given by [*Ajayi and Olsen*, 1985] and [*Cohen et al.*, 1980] for estimating the parameters required for DSD modeling is explained in this section. These are the method of moments (MoM) and the maximum likelihood estimation (MLE). These methods of parameter estimation are further used in the preceding section to compare the lognormal DSD model in Durban, South Africa.

3.4.1 Method of Moments Estimation Technique

The method of moments (MoM) was developed by Pearson [*Pearson*, 1895]. The understanding of the moments of the DSD is necessary for the determination of the DSD evolution, and consequently of the rainfall rate [*Caracciolo et al.*, 2006]. The DSD moments represent most of the integral parameters of the drop size distribution. For example, the first moment is defined as the mean, and the second moment the variance. The third moment is the skewness and the 4^{th} moment is the kurtosis. Since the method of moments uses a different function to individually estimate a given parameter, it is often easier and faster to calculate a method of moments estimate when more than one parameter is involved [*Evans*, 2008]. For radar-meteorology, the liquid water content (LWC) is proportional to the third order moment, the rainfall rate, *R*, is proportional to the 3.67 order moment (assuming that the terminal fall velocity is proportional to $D^{0.67}$), and the reflectivity (Z) is proportional to the sixth order moment. [*Caracciolo et al*, 2006]. The method of moments uses the

definition of the DSD moments. Generally, the *n*th order moment, M_n as given by [*Caracciolo et al.*, 2006; *Ajayi and Olsen,* 1985] is expressed as:

$$M_n = \int_0^\infty D^n . N(D) dD \tag{3.3}$$

where *D* is the drop diameter in mm *N(D)* is the appropriate drop size distribution.
Equation (3.3) can be expressed in its discrete form as:

$$M_n = \sum_{i=1}^{N} {D_i}^n N(D_i) \Delta D_i \tag{3.4}$$

Equations (3.2) and (3.3) represent the *n*th moment function obtained from the disdrometer data. The appropriate drop size distribution is denoted by $N(D)$ for N rainfall samples and D_i is the raindrop diameters for N discrete samples in mm and ΔD_i is the change in the diameter interval in mm. This method has been found useful for the estimation of parameters required for the modeling of drop size distribution especially in the tropical regions. Although it was first used by Waldvogel [*Waldvogel,* 1974], a good number of researchers have found it useful. Notable among them include *Ajayi and Olsen* (1985), in some selected locations in Nigeria; *Timothy et al.,* (2002), in Singapore, *Caracciolo et al.,* (2006), at the University of Ferrara in Italy; *Das et al.,* (2010) in tropical India, and *Afullo* (2011) in South Africa. It has been established that the third, fourth and sixth moments are relevant to radio and microwave engineering studies [*Das et al.,* 2010; *Timothy et al.,* 2002]. The moment's estimations for the DSD models as discussed in Chapter 2, section 2.9 above, are derived in the next section.

3.4.1.1 Lognormal Drop Size Distribution Moments Estimation

For the three-parameter lognormal drop size distribution model (see equation (2.50), the moments estimation is expressed as:

$$M_n = N_T . exp\left[n\mu + \frac{1}{2}(n\sigma)^2\right] \tag{3.5}$$

Equation (3.5) gives an estimates of the input parameters, N_T , μ and σ represented by equations (3.5a, b and c). These parameters are sufficient for the representative of the 3rd, 4th and 6th moments as given by [*Timothy et al,* 2002 ; *Yesufu,* 1998].

$$N_T = exp[(24L_3 - 27L_4 + 6L_6)/3] \quad (3.5a)$$

$$\mu = (-10L_3 + 13.5L_4 - 3.5L_6)/3 \quad (3.5b)$$

$$\sigma^2 = (2L_3 - 3L_4 + L_6)/3 \quad (3.5c)$$

L_3, L_4 and L_6 are considered the natural logarithms of the measured moments M_3, M_4 and M_6. These moments are related to the rain rate, the kinetic energy and radar reflectivity which are essential in rainfall retrieval and hydrological studies [*Caracciolo et al.*, 2006]. They are computed from the observed spectrum for each event.

3.4.1.2 Modified Gamma Drop Size Distribution Moments Estimation

For the gamma DSD model given in equation (2.45), the *n*th moment function of the DSD, M_n, is expressed as:

$$M_n = N_0 \frac{\Gamma(\mu + n + 1)}{\Lambda^{\mu+n+1}} \quad (3.6)$$

By using $n_1 = 3$, $n_2 = 4$, $n_6 = 6$, the gamma DSD parameters as given by *Tokay and Short* [1996], *Kozu and Nakamura*, [1991], and *Caracciolo et al.*, [2006] are obtained as follows:

$$\mu = \frac{11G - 8 + [G(G+8)]^{\frac{1}{2}}}{2(1-G)} \quad (3.7)$$

$$G = \frac{{M_4}^3}{{M_3}^2 M_6} \quad (3.8)$$

$$N_o = \frac{\Lambda^{\mu+4} M_3}{\Gamma(\mu+4)} \quad (3.9)$$

$$\Lambda = \frac{(\mu+4)M_3}{M_4} = \frac{(\mu+4)}{D_m} \quad (3.10)$$

where $D_m \left(= {M_4}/{M_3}\right)$ is the mass –weighted average diameter, and G is the third moment of the mass spectrum normalized by ${D_m}^3$. In this study, the method of moments was applied for a fixed value of μ assumed to be 2. Research has shown that the two moments M_3 and M_4 are adequate to represent the input parameters from the disdrometer measurements. These moments are also related to

the rain rate, the kinetic energy and radar reflectivity which are essential in rainfall retrieval and hydrological studies [*Caracciolo et al.*, 2006].

3.4.1.3 Negative Exponential Drop Size Distribution Moments Estimation

For the negative exponential DSD model represented by equation (2.41), the moment function is derived from the gamma DSD moments functions [*Kozu and Nakamura*, 1991] and expressed as:

$$M_n = N_0 \frac{\Gamma(n+1)}{\Lambda^{n+1}} \tag{3.11}$$

with $\mu = 0$ in equations (2.41) and (3.9), the moment function is estimated as:

$$\Lambda = \frac{(4M_3)}{M_4} \tag{3.11a}$$

$$N_0 = \frac{\Lambda^4 M_3}{\Gamma(4)} \tag{3.11b}$$

3.4.2 The Maximum Likelihood Estimation Technique

Another useful method of parameter estimation is the maximum likelihood estimation (MLE). The maximum likelihood estimation method is a statistical method of estimation. The method originally due to Gauss was developed by Fisher [*Fisher*, 1922]. He based his work on that of *Pearson* (1895) who promoted several estimation methods, in particular the method of moments. The MLE is extremely useful with simple, normal data. However with more complicated models, maximum likelihood alone may not result in a closed form solution. The method maximizes the likelihood or the product of the density functions of a sample. The measured raindrop size distribution can be approximated as the product of the total number of raindrops sizes, *N (D)* and the probability density function (PDF) of the distribution.

$$N(D) = PDF \times N_T(D) \tag{3.12}$$

For example, the PDF for the lognormal distribution as given by Cohen et al., [*Cohen et al.*, 1980] is;

$$f(D_i|\mu,\sigma^2) = (2\pi\sigma^2)^{-\frac{1}{2}}(D_i)^{-1}exp\{[-\ln D_i - \mu]^2/2\sigma^2\}\ \sigma^2 > 0 \tag{3.13}$$

(i = 1, 2 …n), where n is the sample size. Taking the product of the probability densities of the individual D_i, equation (3.13) solves to give:

$$\mathrm{L}(D_1 \ldots\ldots D_n|\mu,\sigma^2) = \prod_{i=1}^{n}[f(D_i|\mu,\sigma^2)] \tag{3.14}$$

$$= \prod_{i=1}^{n}\left((2\pi\sigma^2)^{-1/2}{D_i}^{-1}exp\left[\frac{[-(\ln(D_i)-\mu)^2]}{2\sigma^2}\right]\right) \tag{3.15}$$

$$= (2\pi\sigma^2)^{-n/2}\prod_{i=1}^{n}{D_i}^{-1}\,exp\left[-\sum_{i=1}^{n}-\ln D_i-\mu\right]^2\Big/_{2\sigma^2} \tag{3.16}$$

Taking the natural logarithms of the likelihood function in equation (3.16), the parameters $\hat{\mu}$ and $\hat{\sigma}$, which maximize $\mathrm{L}(D_i|\mu,\sigma^2)$ can be determined. This is done by taking the gradient of the log-likelihood function, L with respect to μ and σ^2 and setting it to zero.

$$\frac{\partial \ln L}{\partial \mu} = \frac{\sum_{i=1}^{n}\ln(D_i)}{\hat{\sigma}^2} - \frac{2n\hat{\mu}}{2\hat{\sigma}^2} = 0; \qquad \frac{n\hat{\mu}}{\hat{\sigma}^2} = \frac{\sum_{i=1}^{n}\ln(D_i)}{\hat{\sigma}^2} \tag{3.17}$$

Similarly,

$$\frac{\partial \ln L}{\partial \sigma} = \frac{n}{\sigma} + \frac{1}{\hat{\sigma}^3}\sum_{i=1}^{n}[\ln D_i - \mu]^2 = 0 \tag{3.18}$$

$$= -\frac{n}{2\hat{\sigma}^2} + \frac{\sum_{i=1}^{n}(\ln(D_i)-\hat{\mu})}{2(\hat{\sigma}^2)^2} = 0 \tag{3.19}$$

From equations (3.17) and (3.18), the maximum likelihood estimators are given in (3.19) and expressed as:

$$\hat{\mu} = \frac{\sum_{i=1}^{n}\ln(D_i)}{n} \tag{3.19a}$$

$$\hat{\sigma}^2 = \frac{\sum_{i=1}^{n}\left(\ln(D_i) - \frac{\sum_{i=1}^{n}\ln(D_i)}{n}\right)^2}{n} \tag{3.19b}$$

3.5 Drop Size Distribution Parameterization for Durban, South Africa

In this section, by using the method of moments estimation technique described in section 3.41, different input parameters for the described models in section 2.9, namely, Weibull, modified gamma, lognormal and the negative exponential are proposed for Durban. The parameters of these models are

based on different rainfall regimes as given by [*Ajayi and Olsen*, 1985] and the annual rainfall. The

Table 3-2: Estimated input drop size distribution fit-parameters for different DSD models based on rainfall regimes in Durban, South Africa

Input parameters	WEILBULL RDSD MODEL		
	N_{ow}	σ_w	η
Drizzle	$455.41R^{0.4526}$	$2.3979R^{-0.138}$	$0.6509R^{0.108}$
Widespread	$563.25R^{0.0938}$	$2.4185R^{-0.016}$	$0.5925R^{0.2591}$
Shower	$714.83R^{-0.077}$	$2.4688R^{-0.049}$	$0.5647R^{0.285}$
Thunderstorm	$60.928R^{0.6577}$	$2.5563R^{-0.066}$	$1.2017R^{0.059}$
Input parameters	**MODIFIED GAMMA RDSD MODEL**		
	N_{om}	μ_m	Λ
Drizzle	$85998R^{-0.12}$	2	$6.4146R^{-0.162}$
Widespread	$120535R^{-0.608}$	2	$6.7906R^{-0.24}$
Shower	$223906R^{-1.061}$	2	$7.5184R^{-0.312}$
Thunderstorm	$3005.6R^{0.2158}$	2	$3.881R^{-0.117}$

Input parameters	LOGNORMAL RDSD MODEL					
	N_T		μ_l		$\sigma^2{}_l$	
	a_o	b_o	A_μ	B_μ	A_σ	B_σ
Drizzle	284.81	0.4301	-0.3312	0.1252	0.0755	0.0106
Widespread	342.25	0.1085	-0.3981	0.243	0.0784	-0.0008
Shower	452.27	-0.095	-0.4794	0.2952	0.0725	0.0049
Thunderstorm	41.46	0.6178	0.2183	0.0875	0.0621	0.0085

Input parameters	NEGATIVE EXPONENTIAL RDSD MODEL	
	Λ	N_o
Drizzle	$4.2764R^{-0.162}$	$8257R^{0.2045}$
Widespread	$4.5271R^{-0.24}$	$10327R^{-0.127}$
Shower	$5.0123R^{-0.312}$	$15649R^{-0.436}$
Thunderstorm	$2.5873R^{-0.117}$	$788.34R^{0.45}$

Table 3-3: Estimated input drop size distribution fit-parameters for different RDSD models based on annual (overall) rainfall in Durban, South Africa

WEILBULL RDSD MODEL					
N_{ow}		σ_w		η	
$427.25R^{0.4281}$		$2.4553R^{-0.129}$		$0.6665R^{0.1171}$	
MODIFIED GAMMA RDSD MODEL					
N_{om}		μ_m		Λ	
$78259R^{-0.156}$		2		$6.3209R^{-0.168}$	
LOGNORMAL RDSD MODEL					
N_T		μ_l		$\sigma^2{}_l$	
a_o	b_o	A_μ	B_μ	A_σ	B_σ
268.07	0.4068	-0.3104	0.1331	0.0738	0.0099
NEGATIVE EXPONENTIAL RDSD MODEL					
Λ			N_o		
$4.2139R^{-0.168}$			$7738.3R^{0.1794}$		

results are presented in Tables 3-2 and 3-3 for different rainfall regimes and the annual (overall) respectively.

3.6 Variability of DSD Modeling in Durban, South Africa

This section considers the variability of the developed drop size distribution models with rain rates using the estimated input parameters in Table 3-3. The different DSD models are fitted to the raindrop size distribution as spectra observed from the J-W disdrometer at Durban. The plots are shown in Figures 3-3 to 3-7, where the measured and modelled DSD data and the raindrop diameters are compared for different models. Firstly, an intrinsic change in the shapes of the DSD is observed as rain rate increases. In other words, the coverage area (diameter region) of the drop size distribution gets wider as the rain rate increases. In figure 3-3 (R = 3.41 mm/h), the lognormal model underestimates the measured data in the diameter range of 0.35 to about 1 mm. The Weibull and

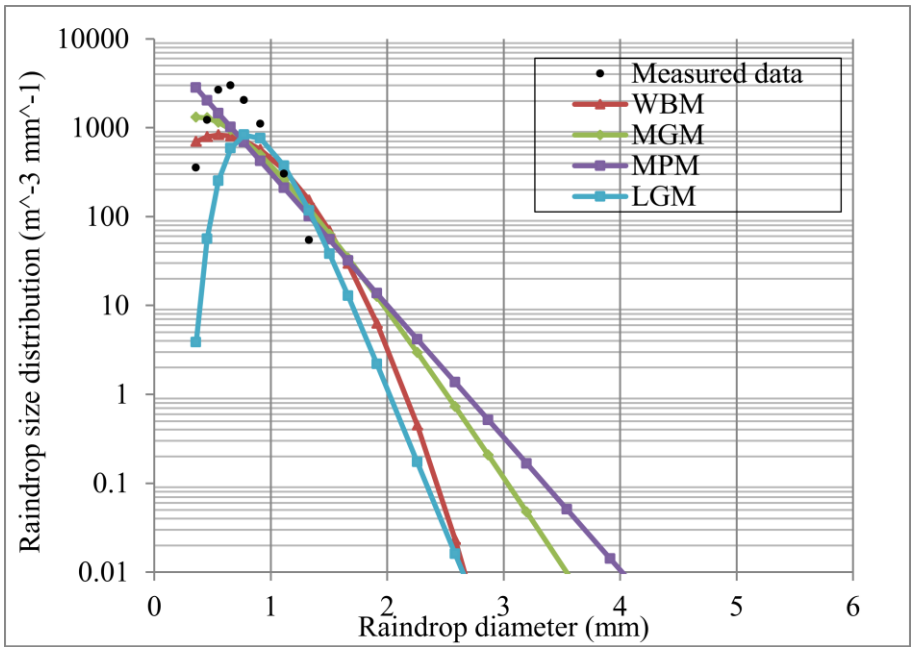

Figure 3-3: Different DSD models for Durban (R = 3.41 mm/h)

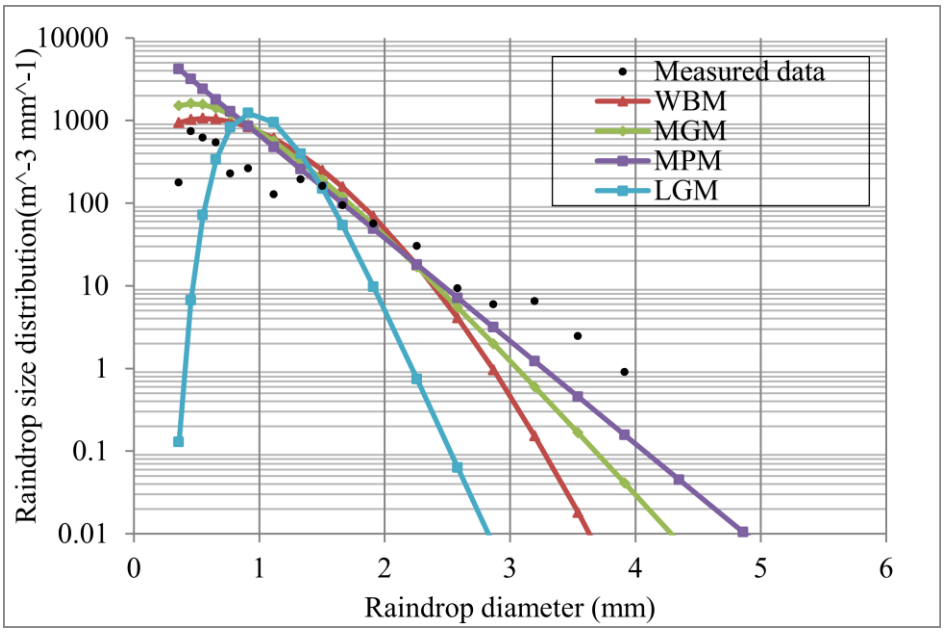

Figure 3-4: Different DSD models for Durban (R = 9.91 mm/h)

modified gamma models seem to perform better when compared with the measured data at this low rain rate. At the rain rate of 9.91 mm/h, the Weibull model also shows a good agreement with the measured data when compared with other models. At rain rate of about 25 mm/h, the shape of the

DSD gets wider in the abscissa region. At this rain rate, the lognormal model gives a better fit. As

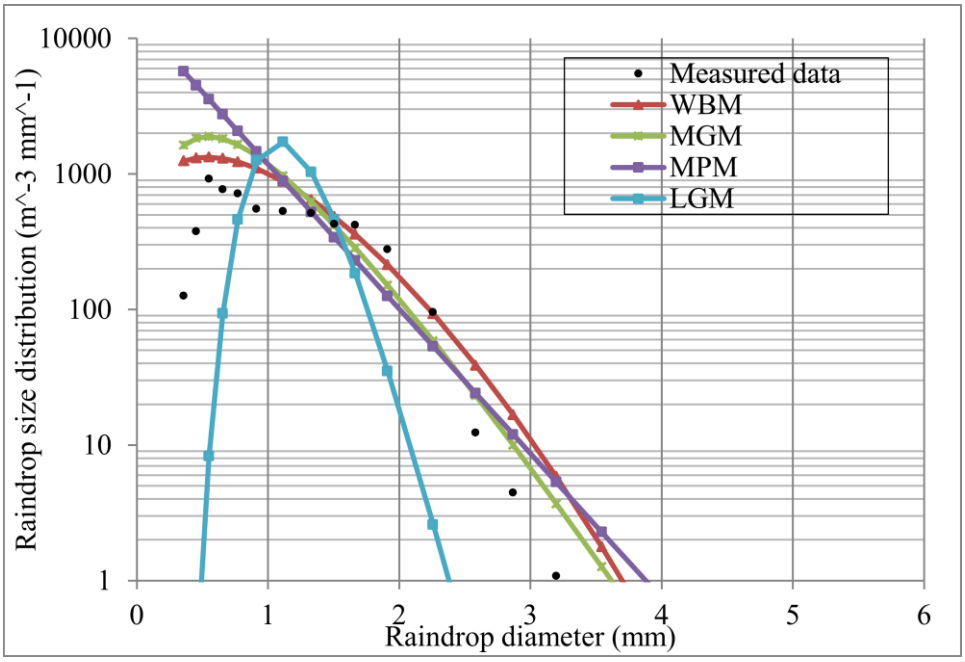

Figure 3-5: Different DSD models for Durban (R = 24.78 mm/h)

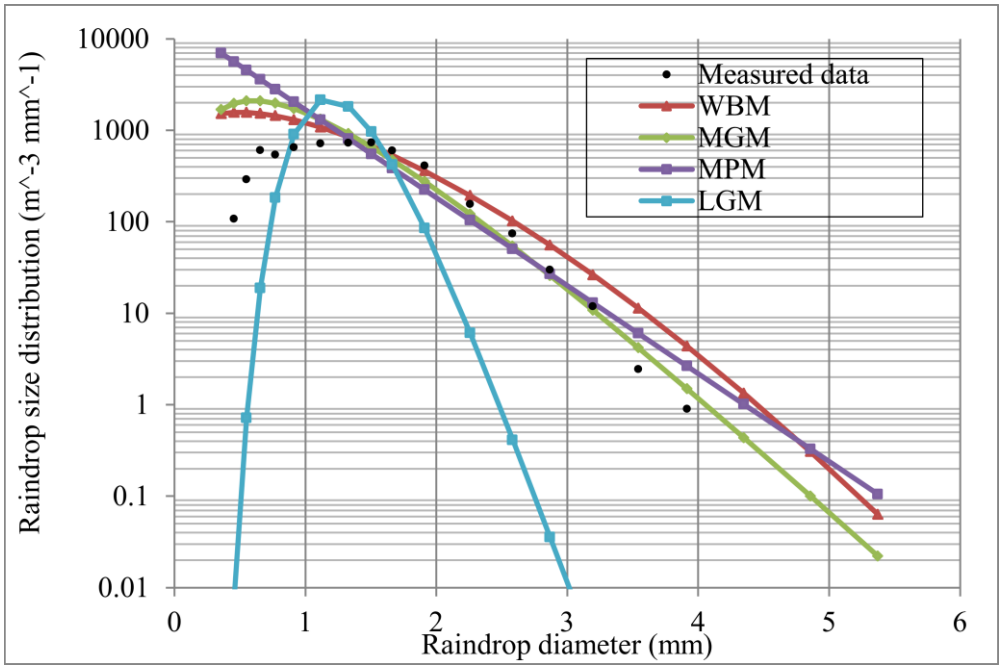

Figure 3-6: Different DSD models for Durban (R = 46.14 mm/h)

the rain rate increases, the distribution of the droplets gets wider. The lognormal DSD shows a good agreement with the observed DSD spectra from the disdrometer but underestimates at the smaller diameter ranges (Figures 3-5 to 3-7). In other words, the modelled DSD and measured DSD show a

proper fitting along a range of diameters. In general, the Marshal-Palmer DSD obviously overestimates the measured data for all the rain rates considered at the lower and higher drop diameter bounds, showing the inadequacy of the standard model in the region. It is obvious that the drop diameter increases for all the models as the rain rate increases. Although the gamma DSD also gives a

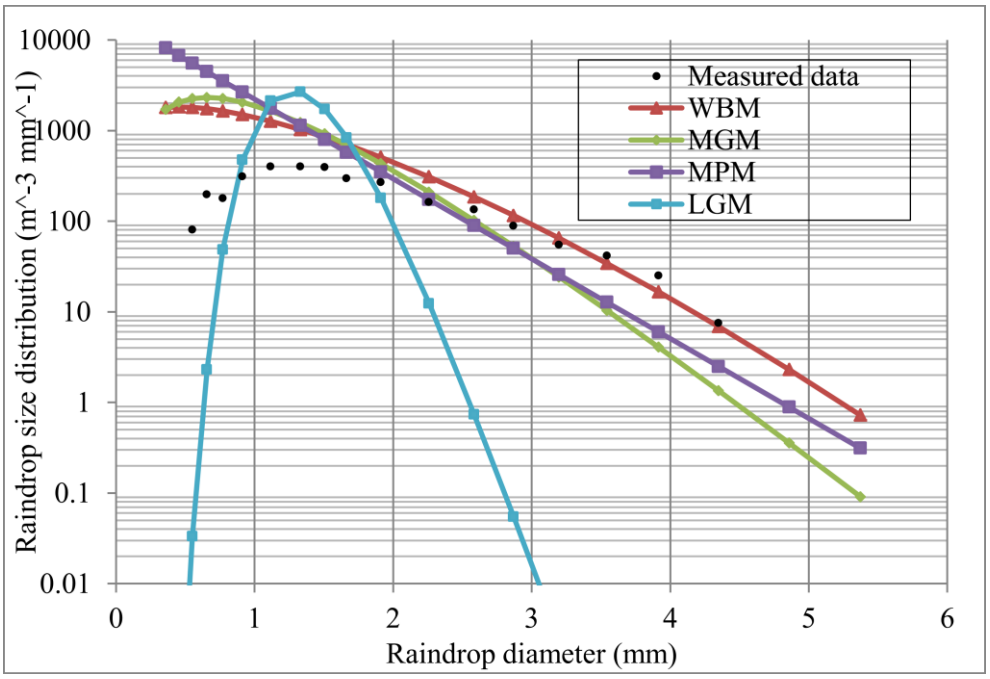

Figure 3-7: Different DSD models for Durban (R = 77.70 mm/h)

better fit with the measured data, the lognormal model shows overall good agreement with the measured DSD especially at higher rain rate is more relevant for network planning.

3.7 Comparison of the Two Methods to Evaluate DSD Parameters

In this section, two methods of parameter estimation discussed in section 3.4 above are compared for the lognormal raindrop size distribution model in Durban, South Africa. Parameter estimates with the method of moments is found to give best fit compared to the maximum likelihood estimation technique. Large deviation errors were observed between the measured and modeled raindrop size distributions with the MLE estimates over the rainfall rates considered. Tables 3.4 and 3.5 show the parameters estimates for the different types of rainfall using the MoM and the MLE techniques respectively. The measured data was compared with different rainfall types. The selected rainfall rates in mm/h are 3.47 (drizzle), 8.20 (widespread), 16.78 (shower) and 84.76 (thunderstorm). These are shown in Figures 3-8 to 3-11 with their probability density functions. In Figures 3-8 and 3-10, the lognormal model underestimates the measured data at the lower diameter bands for all rain rates while the drizzle has the highest peak with the thunderstorm, drizzle, widespread and shower having the

Table 3-4: Estimated parameter of lognormal model for Durban using the MoM technique

Coefficient	Drizzle	Widespread	Shower	Thunderstorm
a_0	284.81	342.25	452.27	41.461
b_0	0.4301	0.1085	-0.095	0.6178
A_μ	-0.3312	-0.3981	-0.4794	0.2183
B_μ	0.1252	0.2431	0.2952	0.0875
A_σ	0.0755	0.0784	0.0725	0.0621
B_σ	0.0106	-0.0008	0.0049	0.0085

Table 3-5: Estimated parameter of lognormal model for Durban using the MLE technique

Coefficient	Drizzle	Widespread	Shower	Thunderstorm
a_0	266.78	263.3	458.11	225.9
b_0	0.5662	0.4225	0.1222	0.3871
A_μ	-0.224	-0.2214	-0.3605	-0.6496
B_μ	0.1239	0.1339	0.209	0.2755
A_σ	0.213	0.1691	0.1647	0.8082
B_σ	0.0423	0.0897	0.1024	-0.083

least peaks in the order for both the MoM and MLE techniques as shown in Figures 3-9 and 3-11. Thunderstorm has the least occurrence as drizzle dominates Durban for most part of the annual rainfall experienced. The same observation is made in Table 3-1.

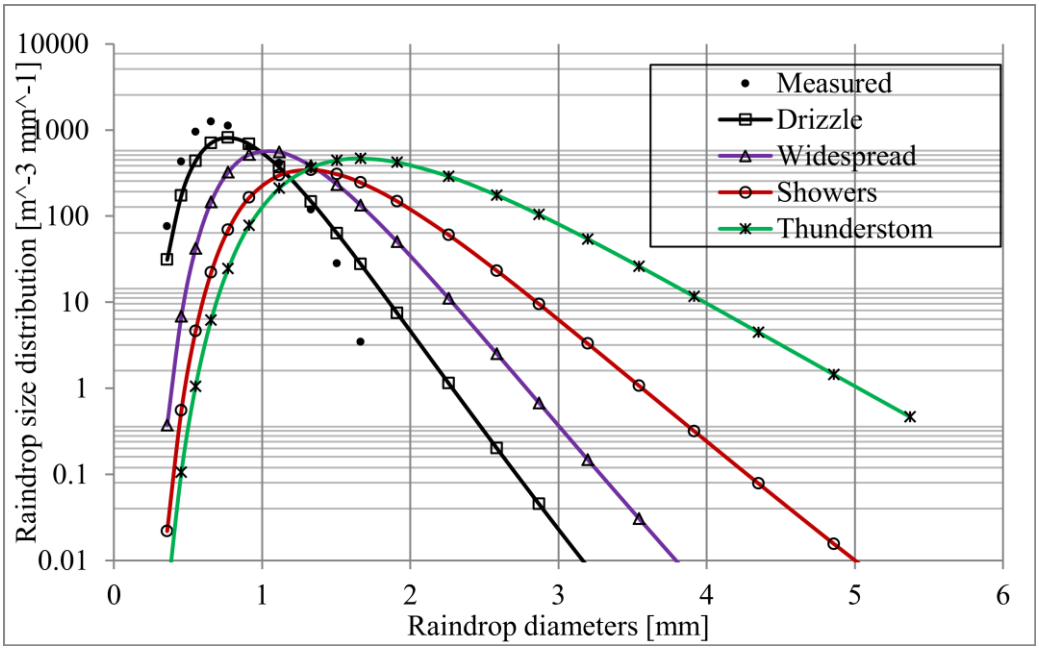

Figure 3-8: Lognormal DSD for different rainfall regimes using MoM technique

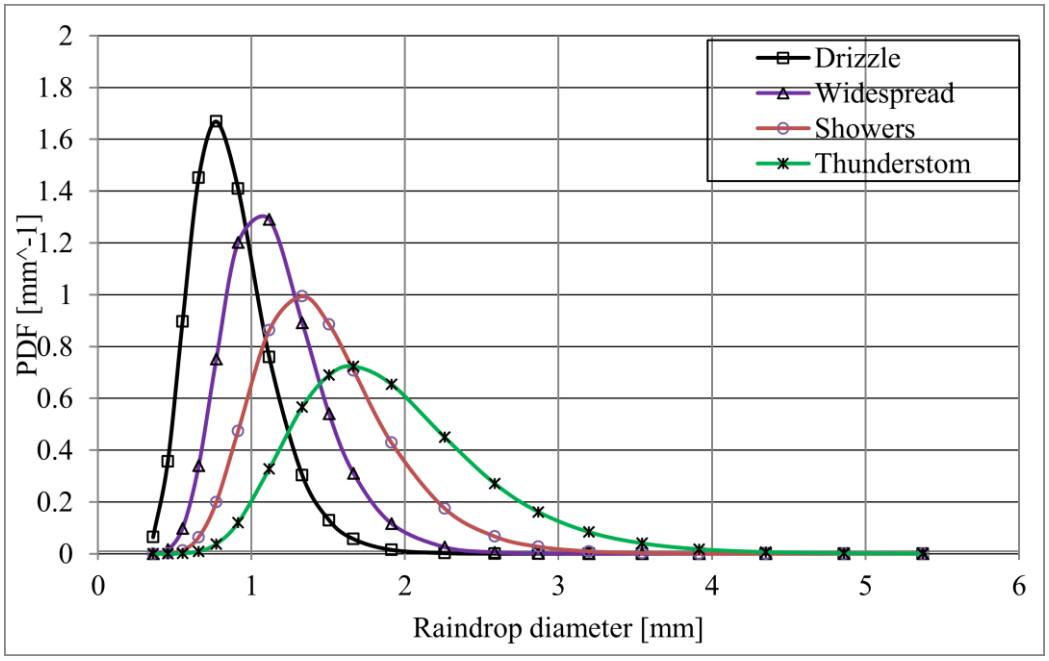

Figure 3-9: PDFs at different rainfall regimes using MoM technique.

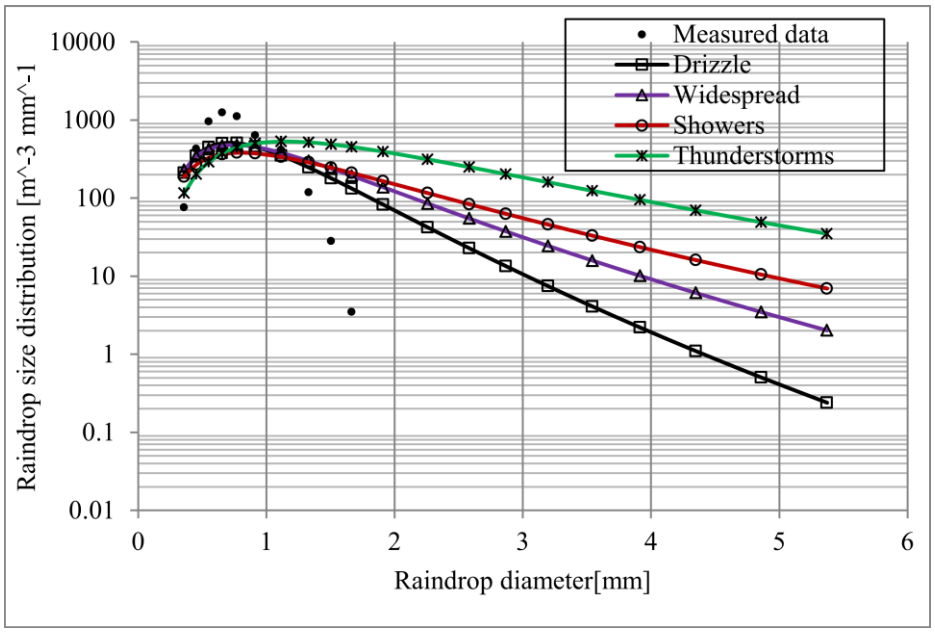

Figure 3-10: Lognormal DSD for different rainfall regimes using MLE technique

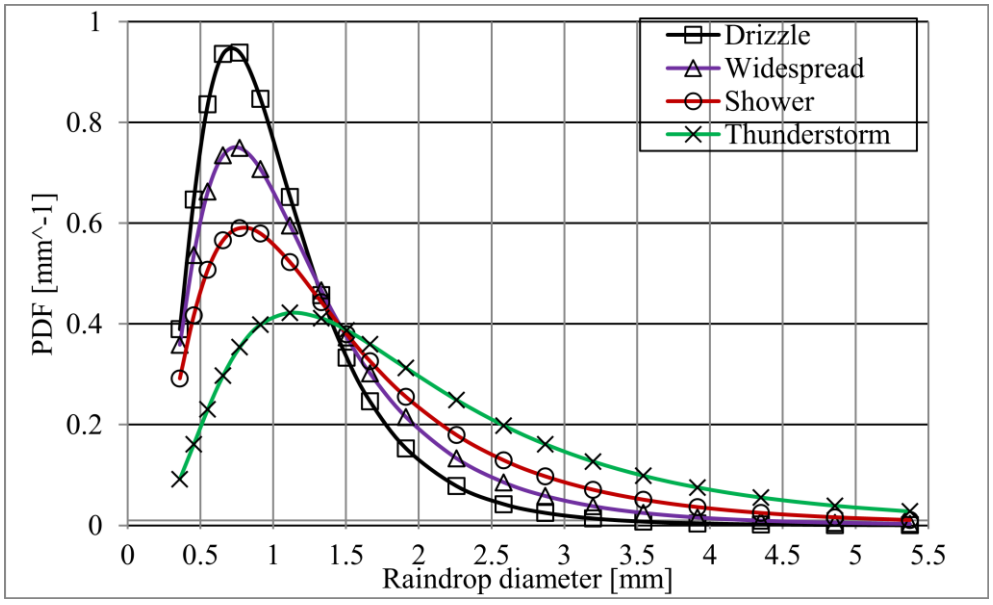

Figure 3-11: PDFs at different rainfall regimes using MLE technique

Statistical error between these methods is computed using the root mean square error represented by equation (3.20). The measured and modeled DSDs are compared. The root mean square (RMS) error shows the deviation of the method from the observed or measured data for different rain rate values. The method witht the least error is considered the best method. The MLE

Table 3-6: Root mean square error for MoM and MLE techniques for different rain rates

Rain rate (mm/h)	RMSE	
	MoM	MLE
5	0.1104	3.8408
10	0.0609	7.6318
20	0.2099	12.5480
40	0.0572	22.0287
60	0.6068	37.2215

technique shows a larger deviation error from the measured data while the MoM reveals a fairly better agreement with the measured data (see Table 3-6). This deviation can also be observed in Figures. 3-12 and 3-13 for rain rate values of 5 mm/h and 120 mm/h respectively. The Root Mean Square Error (RMSE) is expressed as:

$$RMSE = \sqrt{\frac{1}{n}\sum_{j=1}^{n}\left[\hat{F}(X_i) - F(X_i)\right]^2} \tag{3.20}$$

where $\widehat{F}(X_i)$ is the measured data obtained from the disdrometer using (3), $F(X_i)$ is the modeled data and *n* is the number of classes or channels considered.

3.8 The Dielectric Spectra Properties of Water

The relative dielectric constant of water often referred to as the complex permittivity is given as:

$$\epsilon = \epsilon' + i\epsilon'' \tag{3.21}$$

where ϵ' and ϵ'' are real and loss parts, $i = \sqrt{-1}$. The functional dependence of $\in (f, T)$ on frequency and temperature shows that there is an interaction mechanism between EM radiation and the water molecules forming a liquid [*Liebe et al*, 1991]. The frequency dependence of the permittivity of water is given by the well-known Deybe equation and it is sufficient to describe $\in (f)$ up to 100 GHz. Above 100 GHz, additional resonance and relaxation terms have to be considered.

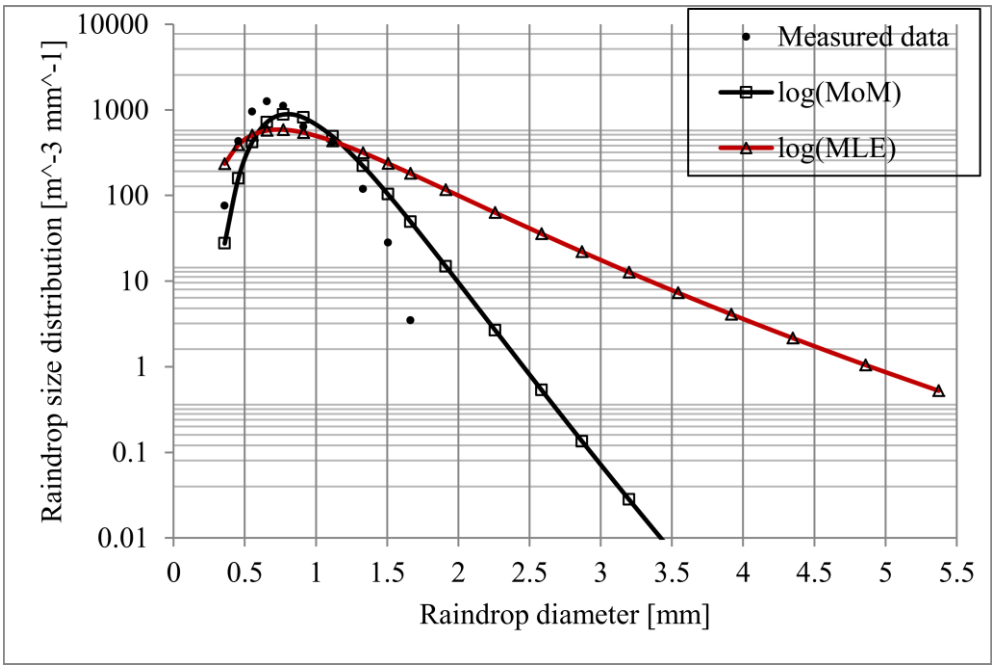

Figure 3-12: Comparison of lognormal models using MoM and MLE techniques (R=5 mm/h)

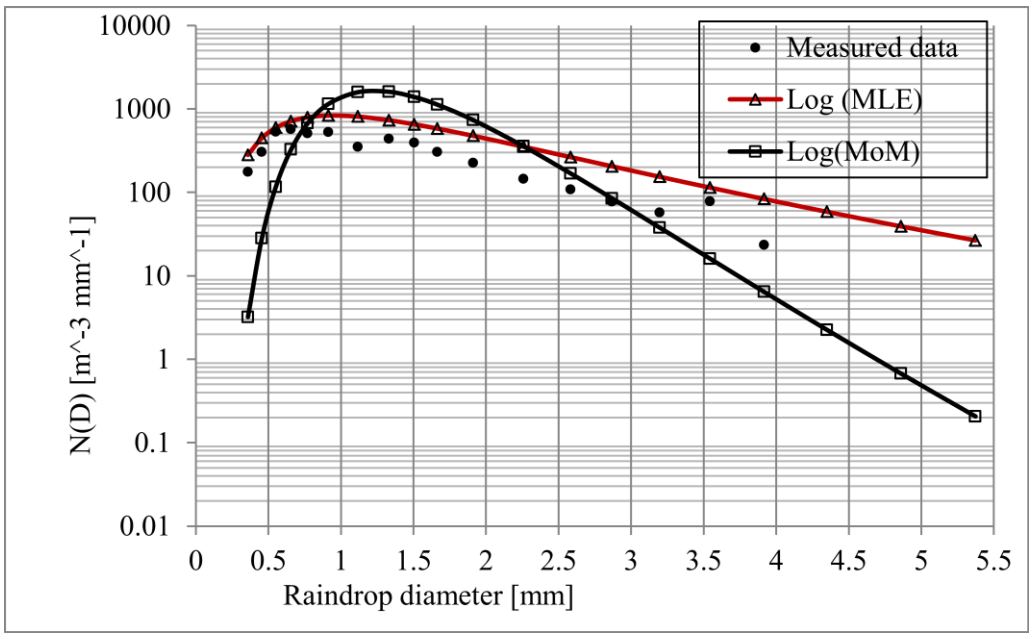

Figure 3-13: Comparison of lognormal models using MoM and MLE (R=120 mm/h)

The single Debye model (shape) is represented by [*Liebe et al*, 1991]:

$$\epsilon_D\,(f,T) = \frac{(\epsilon_o - \epsilon_\infty)}{1 - i(f/\gamma_D} + \epsilon_\infty \qquad (3.22)$$

According to *Liebe et al.*[1991], the static dielectric constant $\in_o (T)$ at $(-20^o \leq T \leq 60^o C)$ with least square fit results in the simple expression (3.23) as:

$$\in_o (T) = 77.66 - 103.3\theta \tag{3.23}$$

where

$$\theta = 1 - \frac{300}{[273.15 + T]} \tag{3.24}$$

$$\in_\infty = 0.066 \in_o \tag{3.25}$$

$$\gamma_D = 20.27 + 146.5\theta + 314\theta^2 \tag{3.26}$$

Above 100 GHz, the double Debye model is used to model the complex dielectric constant of water which is frequency dependent. The double Debye model is a slight modification of the single model given as:

$$\in_{DD} (f,T) = \in_o - f\left[\frac{(\in_o - \in_1)}{(f + i\gamma_1)} + \frac{(\in_1 - \in_2)}{(f + i\gamma_2)}\right] \tag{3.27}$$

where

$$\in_1 = 0.0671 \in_o \tag{3.28}$$

$$\gamma_1 = 20.20 + 146.4\theta + 316\theta^2 \tag{3.29}$$

$$\in_2 = 3.52 + 7.52\theta \tag{3.30}$$

$$\gamma_2 = 39.8\gamma_1 \tag{3.31}$$

Liebe et al, [1991] further formulated a model for the spectra dependence of $\in (f)$ that is valid for frequencies up to 1 THz. However, above 1 THz, experimental data were found deficient both in quality and quantity. In this study, a Mie scattering MATLAB code was developed to calculate the complex dielectric constant of water for frequencies in the range 1GHz to 500 GHz. The ambient temperature of 20^o C was assumed in this work.

3.9 Computation of the Extinction Cross Sections

According to *Cullen and Kumar* [1970], the extinction cross section is the region of interaction in which the influence of the rain droplets absorption and scattering mechanisms on the EM wave energy is highest. A hydrometeor that has a physical cross section has absorption, scattering and total attenuation cross sections [*Oguchi*, 1983]. The absorption cross section, Q_A corresponds to the power absorbed by the hydrometeor (raindrop in this case), the scattering cross section, Q_S is equivalent to

the power scattered in all directions and the total attenuation cross section Q_T corresponds to the total power removed from the hydrometeor [*Townsend*, 2011]. *Mulangu and Afullo* [2009] employed the Mie scattering approach and the dielectric model of Liebe to determine the scattering coefficients and rain attenuation distribution for four locations in Botswana, using rain rate values of $R_{0.01}$=68.9 mm/h, $R_{0.01}$=137.06 mm/h, $R_{0.01}$=86.87 mm/h, and $R_{0.01}$=64.4 mm/h, for Gaborone, Selebi-Phikwe, Francistown and Kasane, respectively, over the frequency range of 1-1000 GHz. Their results reveal that the extinction coefficients depended more strongly on temperature at the lower frequency range than at the higher ranges for the lognormal distribution of *N (D)*.

Similarly, *Odedina and Afullo* [2010] determined the forward scattering amplitudes for the spherical raindrops for all raindrop sizes at different frequencies by using the Mie scattering theory. The real parts of the extinction cross-sections were used to generate appropriate models at different frequencies. The total cross section Q_t is directly related to the attenuation of the transmitted signal, and is given by:

$$Q_t = -\left(4\pi/_k\right)\mathbf{I}\mathrm{m}\left[\hat{e} \times f\left(\check{\mathrm{K}}_1\check{\mathrm{K}}_2\right)\right] \tag{3.32}$$

where $k = 2\pi/_\lambda$ is the wave number, $\hat{e}$ is the unit vector of the polarization state of the wave and $f\left(\check{\mathrm{K}}_1\check{\mathrm{K}}_2\right)$ is the scattering amplitude and polarization state of the scattered wave, obtained from the solution of the boundary value. The scattered amplitude depends on K_1, K_2 the frequency, size, shape and the polarisation of the incident wave. For forward scattering (used in this study), $\check{\mathrm{K}}_1 = \check{\mathrm{K}}_2$. Depending on the frequency of the incident signal and the shape of the raindrop, the absorption and scattering can be modeled using different methods. These methods include the Rayleigh theory, Mie theory or the T-Matrix method. The Mie theory which assumes spherical raindrop is used in this work. In the Mie scattering theory, the real part and forward scattering functions are used to estimate the scattering parameters. According to *Mie* [1908], the forward scattering amplitude is computed as:

$$S(0) = \frac{1}{2}\sum_{n=0}(2n+1)[a_n(m,\alpha) + b_n(m,\alpha)] \tag{3.33}$$

where $a_n(m,\alpha)$ and $b_n(m,\alpha)$ are the Mie scattering coefficient which are functions of the complex refractive index of pure water, *m* and α is dependent on the ambient temperature and the frequency of the rain droplets [*Deirmendjian, et al.*, 1961]. The *n*th truncation of the infinite series was computed by *Mulangu et al*. [2009] as:

$$n_{max} = \alpha + 4\alpha^{\frac{1}{3}} + 2, \qquad \text{for} \quad (\alpha = k\overline{a}) \tag{3.34}$$

where α is the particle size for all wavelengths of the raindrops and $\overline{a}$ is the radius for assumed spherical droplets. The solutions of the Mie scattering parameters describe the scattered field

contributions from the multi poles induced in the sphere (see equation (3.29), such as raindrop, can be evaluated as given by [*Odedina*, 2010; *Mätzler*, 2002; *Sadiku*, 2000]:

$$a_n(\mathrm{m},\alpha) = \frac{m^2\Psi_n(m\alpha)[\alpha\Psi_n(\alpha)]' - \Psi_n(\alpha)[m\alpha\Psi_n(m\alpha)]'}{m^2\Psi_n(m\alpha)\left[\alpha\Phi_n{}^{(1)}(\alpha)\right]' - \Phi_n{}^{(1)}(\alpha)[m\alpha\Psi_n(m\alpha)]'} \tag{3.35}$$

$$b_n(\mathrm{m},\alpha) = \frac{\Psi_n(\alpha)[m\alpha\Psi_n(m\alpha)]' - \Psi_n(m\alpha)[\alpha\Psi(\alpha)]'}{\Phi_n{}^{(1)}(\alpha)[m\alpha\Psi_n(m\alpha)]' - \Psi_n(m\alpha)\left[\alpha\Phi_n{}^{(1)}(\alpha)\right]'} \tag{3.36}$$

where $\Psi_{\mathrm{n}}(\alpha)$ and $\Phi_{\mathrm{n}}{}^{(1)}(\alpha)$ are given by [*Arfken and Weber*,2003]:

$$\Psi_{\mathrm{n}}(\alpha) = \sqrt{\frac{\pi}{2\alpha}}.\mathrm{J}_{\mathrm{n}+\frac{1}{2}}(\alpha) \tag{3.37}$$

$$\Phi_{\mathrm{n}}{}^{(1)}(\alpha) = \sqrt{\frac{\pi}{2\alpha}}.\mathrm{H}_{\mathrm{n}+\frac{1}{2}}(\alpha) \tag{3.38}$$

Note that

$J_{n+\frac{1}{2}}(\alpha)$= half-integral order of Bessel function,

$H_{n+\frac{1}{2}}(\alpha)$= half-integral order of Hankel function,

$\alpha = \frac{\pi D}{\lambda}$.

Based on the above equations, the MATLAB programs developed by Mätzler's [2002; 2003] were used to compute *S (0)* from the Mie computations. According to *Van der Hulst* [1957], the extinction cross section Q_t can be estimated by the product of a factor and the real part of the scattering function. This is expressed by equation (3.35) as:

$$Q_{ext}(D) = \frac{4\pi}{k^2}Re[s(0)] \tag{3.39}$$

A reduced power law relation was proposed for Durban by *Odedina and Afullo* [2010] at $20^o\mathrm{C}$ for frequencies up to 35 GHz to compute the power law coefficients k_{ext} and ζ_{ext} of Q_{ext} in equation (3.40) as:

$$Q_{ext}(D) = k_{ext}\overline{a}^{\zeta_{ext}} \tag{3.40}$$

Table 3-7: Numerical values of the extinction cross sections power law coefficients at frequency of 1 to 500 GHz

Frequency (GHz)	Complex refractive index	k_{ext}	ς_{ext}
1	8.9339 + j0.2437	0.0006	3.0806
2	8.9014 + j0.4843	0.0027	3.2737
4	8.7763 + j0.9442	0.0191	3.7875
6	8.5830 + j1.3599	0.0851	4.3988
8	8.3396 + j1.7196	0.217	4.5805
10	8.0649 + j2.0188	0.3857	4.5272
12	7.7755 + j2.2594	0.5866	4.4443
15	7.3405 + j2.5234	0.955	4.3453
16	7.1994 + j2.5892	1.0939	4.3164
18	6.9272 + j2.6934	1.3883	4.2576
19.5	6.7332 + j2.7509	1.6169	4.2104
20	6.6705 + j2.7667	1.6936	4.194
23	6.3171 + j2.8321	2.1474	4.0885
25	6.1026 + j2.8532	2.4567	4.0186
28	5.8107 + j2.8603	2.8544	3.9035
30	5.6345 + j2.8530	3.1204	3.8323
35	5.2500 + j2.8072	3.7452	3.6639
40	4.9322 + j2.7383	4.3106	3.5077
45	4.6668 + j2.6586	4.8223	3.3646
50	4.4428 + j2.5752	5.2855	3.2353
60	4.0869 + j2.4099	6.0493	3.0094
70	3.8182 + j2.2560	6.625	2.8209
90	3.4421 +j1.9907	7.4097	2.5284
100	3.3061 + j1.8778	7.6874	2.4156
150	2.9154 + j1.5083	8.3061	2.0691
200	2.7103 + j1.2655	8.3464	1.9293
250	2.5871 + j1.1051	8.2291	1.8785
300	2.5029 + j0.9932	8.0777	1.8672
350	2.4395 + j0.9115	7.935	1.87
400	2.3882 + j0.8493	7.8144	1.875
500	2.3067 + j0.7597	7.6315	1.8812

where $\overline{a} = D/2$ is the radius of the raindrops in centimeters. The result is only valid for raindrops in the centimeters unit and up to frequency of 35 GHz. In this study, the raindrops are assumed spherical and the coefficients are computed to frequency up to 500 GHz using the regression fitting technique. The results for the power law coefficients for frequencies between 1 to 500 GHz for Durban are given in Table 3-7 below and used in this work. At frequency above 150 GHz in Table 3-7, the double

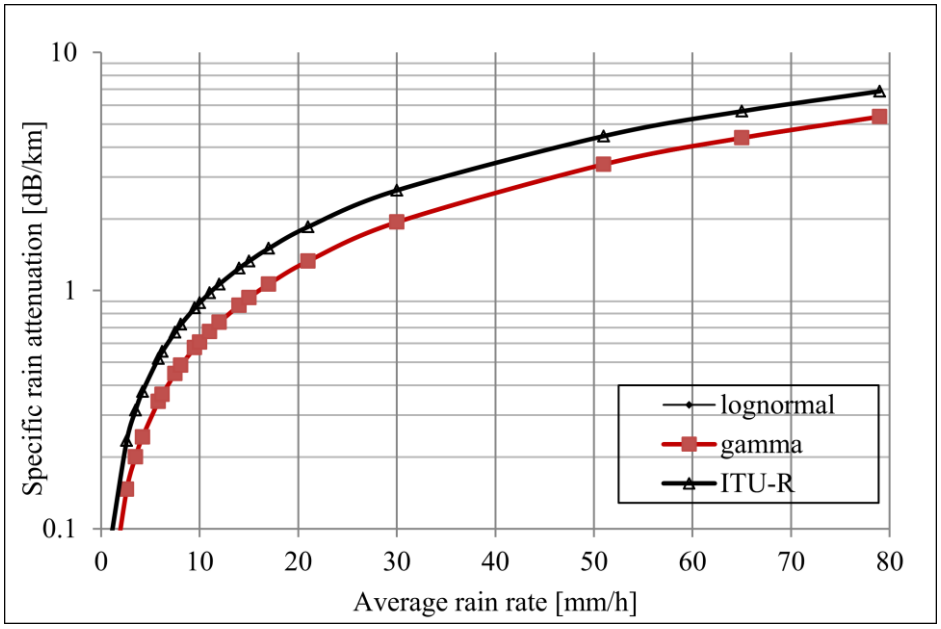

Figure 3-14: Specific rain attenuation for Durban at 15 GHz

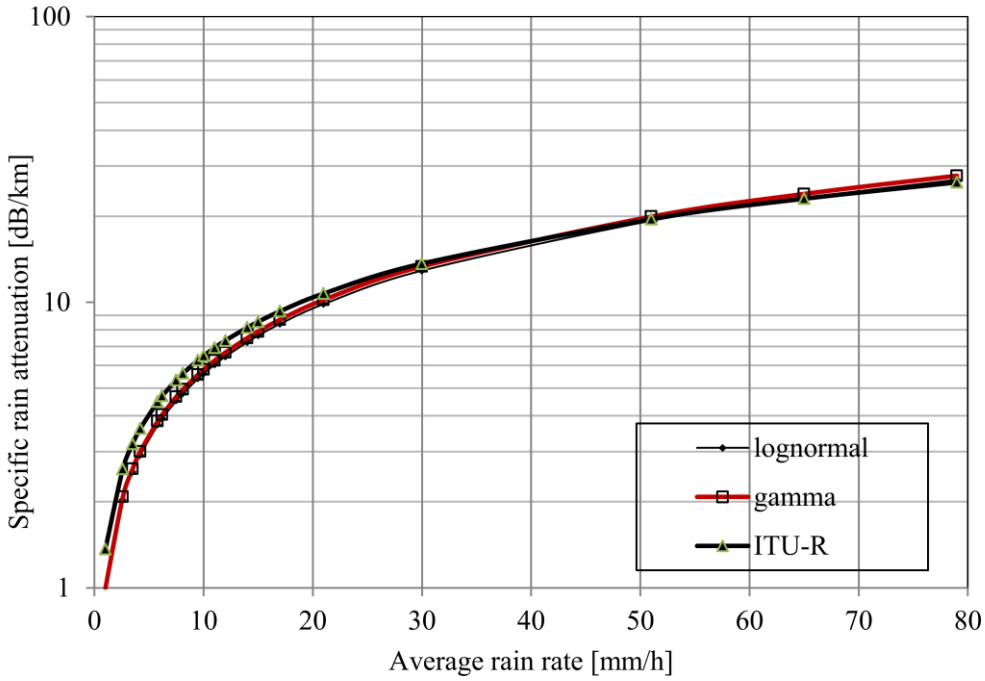

Figure 3-15: Specific rain attenuation for Durban at 100 GHz

Debye method was used. The other results showing the scattering amplitudes and Q_{ext} at some selected frequencies are presented in the Appendices D-1 to D-5.

Table 3-8: Specific rain attenuation for Durban at different frequencies (R = 65 mm/h)

Frequency (GHz)	Attenuation			
	Lognormal dB/km	Modified gamma dB/km	ITU-R dB/km	Measured Data dB/km
2	0.0073	0.0073	0.0052	0.0075
10	1.0486	1.0744	1.8049	1.3192
15	2.5678	2.6124	3.9115	3.1496
19.5	4.2323	4.3772	5.6621	5.1986
20	4.5248	4.5799	5.8606	5.4289
25	6.5365	6.5835	8.0571	7.6366
50	14.4085	14.4233	17.2975	14.7686
60	16.8243	16.9125	19.3790	16.5559
70	18.8203	19.0322	20.8386	17.8858
90	21.9302	22.4947	22.5735	19.7199
100	23.1755	23.9445	23.0421	20.3931
150	26.7442	28.4428	23.6329	21.9990

Table 3-9: Root mean square error for specific rain attenuation at different rain rates

Rain Rate (mm/h)	RMSE		
	Lognormal	Modified gamma	ITU-R
3.41	0.1933	0.2402	0.5526
5.00	1.1167	1.1786	1.4407
9.98	0.7561	0.8687	1.2569
20.35	0.6847	0.8774	1.3545
35.77	0.4285	0.6826	1.2769
51.06	0.9821	1.3074	1.4584
71.07	2.8885	3.2905	2.5965
84.76	3.0408	3.4641	2.3466
117.15	4.0162	4.4387	2.1316

3.10 Computation of the Specific Attenuation Due to Rain in Durban

The drop size distribution reflects the distribution of raindrop sizes as a function of the rain rate [*Nader*, 1998]. The choice of DSD is essential as it greatly affects the resultant specific attenuation. In this section, the lognormal and modified gamma DSD models have been chosen for the purpose of analysis as they have been found suitable for DSD modeling in the South Africa region. The specific attenuation is computed and compared with the ITU-R (vertical) model. The specific attenuation is a function of frequency and temperature. The specific attenuation will therefore vary with frequency. The variation of the specific attenuation at different frequencies between 2-150 GHz with critical rain rate *R* of 65 mm/h is shown in Table 3-8. The lognormal and gamma models compare favourably well with the measured data up to frequency of about 60 *GHz*. At frequency of above 70 GHz, the two models over-estimate the measured data. A larger deviation is observed at frequency of 150 *GHz* at the same rain rate. Using the average rain rates of 3.40 mm/h and 46.14 mm/h, the models are compared with the ITU-R (V) model at frequencies of 15 GHz and 100 GHz as shown in Figures 3-14 and 3-15. The specific rain attenuation of the two models at both selected frequencies is very close. The ITU-R leads to higher attenuation at both frequencies but more noticeable at the 15 GHz frequency when compared with the two models. The error estimation is also shown in Table 3-9.

3.11 Chapter Summary

In this chapter, the experimental set up, data acquisition, processing and analysis using the J-W RD-80 impact disdrometer have been discussed. The dead time error of the disdrometer was minimized by disregarding the total sum of drops less than 10 for a given rain event. Parameters estimates for different DSD models have been proposed for Durban, South Africa. The two models - modified gamma and lognormal distribution models - compare reasonably well with measured data and are both suitable for the modeling of raindrop size distributions in the region. In this chapter, two methods of parameter estimation (MoM and MLE) are compared. The MLE technique gave a larger deviation error from the measured data while the MoM revealed a fairly better agreement with the measured data.

CHAPTER FOUR

ANALYTICAL APPROACH TO CRITICAL DIAMETERS IN RAINDROP SIZE DISTRIBUTION

4.1 Introduction

The critical diameters are the range of diameters where the rain attenuation is predominant. In this chapter, the critical raindrop diameters influencing the specific rain attenuation in Durban, South Africa is investigated using the spherical raindrop shape at temperature T = 20°C. Similarly, the critical diameter at which the rain attenuation is optimum at a typical equatorial region of Butare, Rwanda, in Central Africa, is also investigated. The total rainfall attenuation over a differential change in diameter is computed by integrating over all the raindrop sizes and determining the differential change in the attenuation obtained over a fixed diameter interval, dD_j. The diameter ranges contributing 90%, 99%, 99.5%, 99.9%, 99.99% and 100% to the total specific attenuation are also discussed. This range of diameters constitutes the surface area under the curve and along the abscissa regions. An analytical approach is adopted to determine the peak diameter D_p where the specific rain attenuation is maxima. The specific attenuation γ is expressed as:

$$\gamma = \int_{d_0}^{d_{max}} Q_{ext}(D)N(D)dD \qquad (\frac{dB}{km}) \tag{4.1}$$

where $Q_{ext}(D)$ is the extinction cross sections given as:

$$Q_{ext}(D) = \kappa D^{\alpha} \tag{4.2}$$

N (D) is the drop size distribution model in m^{-3} mm^{-1} which in this case can be lognormal or gamma, *D* is the raindrop diameters in mm, κ and α are frequency dependent parameters. By substituting the expressions for the extinction cross section and drop size distribution (DSD) model (lognormal DSD model in this case) of equations (4.2) and (2.50), the differential specific rain attenuation can be maximized as derived below:

$$\Delta\gamma = \kappa D^{\alpha} * \frac{N_T}{\sigma D\sqrt{2\pi}} exp\left\{-\frac{1}{2}\left[\frac{\ln(D)-\mu}{\sigma}\right]^2\right\} \Delta D \tag{4.3}$$

$$\Delta\gamma = \kappa D^{\alpha-1} * \frac{N_T}{\sigma\sqrt{2\pi}} exp\left\{-\frac{1}{2}\left[\frac{\ln(D)-\mu}{\sigma}\right]^2\right\} \Delta D \quad (4.4)$$

At the peak diameter *D*, $\frac{\Delta\gamma}{\Delta D} = 0$ and ΔD is fixed and constant,

$$(\alpha-1)D^{\alpha-2} - D^{\alpha-1}\left[\frac{1}{\sigma D}\frac{(\ln D-\mu)}{\sigma}\right]^2 = 0 \quad (4.5)$$

$$(\alpha-1) = \frac{1}{\sigma^2}(\ln D-\mu) \quad (4.6)$$

It follows from equation (4.6) therefore,

$$D_p = exp[\sigma^2(\alpha-1)+\mu] \quad (4.7)$$

The maximum specific rain attenuation peaks at the diameter, D_p (in mm) given by the expression 4.7.

Table 4-1 (a) to (d) shows the different rainfall regimes with their respective critical diameters. The estimated values of μ and σ in Table 3-4 have been used for the purpose of analysis while α is a frequency dependent parameter as provided in Table 3-8. It can be observed that the peak diameters D_p at which the differential attenuation is maximum increases as the rain rate increases with varying input parameters. As the operating frequency increases, the peak diameter, D_p at which the specific rain attenuation is maximum reduces. The peak attenuation for the drizzle and widespread occurs between $0.7 \leq D \leq 1.5$ mm whereas for the shower and thunderstorm rainfall, the specific rain attenuation peaks between $1.3 \leq D \leq 2.7$ mm at all frequencies. The input parameters μ and σ in equation (4.7) used in Table 4-1 are regime-dependent. The peak diameter D_p is frequency-dependent since α is frequency dependent.

4.2 The Critical Diameters for Rainfall Attenuation in Southern Africa

Attenuation on radio propagation paths is generally caused by various atmospheric components such as gases, water vapor, clouds and rain. Rain attenuation, caused by scattering and absorption by the water droplet is one of the most important signal impairments influencing the attenuation of microwave (3-30 *GHz*) and millimeter wave (30 -300 GHz) *Mathews* [1965]. The nearly linear relationship existing between the rainfall rate *R* (mm/h) and the specific attenuation at 35 GHz has been known since 1940s and has been successfully tested experimentally for estimating path-averaged rainfall rate in the early 1960s. This linearity was also found to be independent of the (rain) drop size distribution DSD, by *Kültegin and Daisley* [2011].

Table 4-1: Rainfall regimes and the peak diameters for maximum attenuation at 10-100 GHz in Durban

(a)

Drizzle						
Rain rate (mm/h)	**10 GHz**	**19.5 GHz**	**25 GHz**	**40 GHz**	**60 GHz**	**100 GHz**
0.5	0.837282	0.819398	0.808757	0.781082	0.755001	0.725056896
1	0.937165	0.915015	0.90186	0.867735	0.835696	0.799057637
1.5	1.001028	0.976039	0.961214	0.922815	0.886841	0.845798761
2	1.048962	1.021789	1.005681	0.964002	0.925016	0.880611039
2.5	1.087718	1.058747	1.041584	0.997211	0.955755	0.908597272
3	1.120444	1.089934	1.071868	1.025193	0.981627	0.932122655
3.5	1.148881	1.117018	1.098159	1.049462	1.004047	0.95248767
4	1.174096	1.141023	1.121454	1.070949	1.023882	0.970487943
4.5	1.196797	1.162624	1.142411	1.090267	1.041703	0.98664746

(b)

Widespread						
Rain rate (mm/h)	**10 GHz**	**19.5 GHz**	**25 GHz**	**40 GHz**	**60 GHz**	**100 GHz**
5.5	1.333592	1.301439	1.282351	1.232861	1.186432	1.13338217
6	1.361755	1.328953	1.309478	1.258986	1.211615	1.157487212
6.5	1.388187	1.354776	1.33494	1.283507	1.235253	1.180114173
7	1.413117	1.379131	1.358954	1.306636	1.25755	1.201457619
7.5	1.436728	1.402199	1.381699	1.328543	1.278669	1.221674717
8	1.459172	1.424127	1.40332	1.349368	1.298745	1.240894398
8.5	1.480574	1.445037	1.423938	1.369227	1.317891	1.259223846
9	1.50104	1.465033	1.443655	1.388218	1.336201	1.276753208
9.5	1.520659	1.484202	1.462556	1.406425	1.353755	1.29355909

Table 4-1: Rainfall regimes and the peak diameters for maximum attenuation at 10-100 GHz in Durban

(c)

Shower						
Rain rate (mm/h)	**10** GHz	**19.5** GHz	**25** GHz	**40** GHz	**60** GHz	**100** GHz
10	1.641879	1.598873	1.573385	1.507458	1.445819	1.375649
12	1.738137	1.692131	1.664871	1.594383	1.528509	1.453554
15	1.86366	1.813703	1.784111	1.70762	1.636176	1.554932
17.5	1.955629	1.902751	1.871435	1.790509	1.714951	1.629065
20	2.038957	1.983415	1.950526	1.865556	1.786249	1.696133
22.5	2.115399	2.057398	2.023059	1.934359	1.851594	1.757579
25	2.186204	2.125915	2.090225	1.998053	1.912071	1.814429
30	2.314374	2.249913	2.211762	2.113266	2.021426	1.917183
35	2.428585	2.360378	2.320018	2.215846	2.11875	2.008586

(d)

Thunderstorm						
Rain rate (mm/h)	**10** GHz	**19.5** GHz	**25** GHz	**40** GHz	**60** GHz	**100** GHz
40	2.388614	2.318931	2.277735	2.171537	2.07273	1.960839
60	2.505148	2.429412	2.384676	2.269492	2.162511	2.041591
65	2.528816	2.451836	2.406373	2.289346	2.180689	2.057921
75	2.571689	2.492443	2.445657	2.325273	2.213569	2.087442
80	2.591262	2.510976	2.463583	2.341661	2.22856	2.100895
85	2.609783	2.528511	2.480542	2.357159	2.242734	2.11361
90	2.627367	2.545156	2.496638	2.371866	2.256181	2.125669
100	2.66009	2.576124	2.526582	2.399216	2.281178	2.148078
120	2.717682	2.630606	2.57925	2.44729	2.325091	2.187415

The study of drop size distribution (DSD) is, however, vital for several application areas such as satellite meteorology, microwave communications, cloud physics and soil erosion *Harikumar* [2009]. The drop size distribution is an important parameter for the estimation of attenuation due to rain at microwave and millimeter- wave frequency applications because it governs all the microwave and rainfall integral relation.

It has been established that modeling of DSD in tropical and temperate regions is not the same. This is due to the presence of heavy rainfall in tropical regions compared to temperate regions. When compared to temperate regions where a large database exists, measurements of drop size distributions in tropical regions are few. The negative exponential function, as proposed by *Marshall and Palmer*

[1948] or the *Laws and Parsons*, [1943] and the gamma distribution model often characterize modeling of raindrop size distributions in the temperate region. However, there is so much uncertainty in the preponderance and estimation of small diameter raindrops due to limitation in the sensitivity of the measuring equipment. These models grossly overestimate the concentration of the small diameter raindrops in the tropical regions hence the *Ajayi and Olsen* [1985] model was proposed and found suitable for the modeling of tropical rain drop size distributions and equally adequate for the determination of the specific attenuation. In this section, the influence of critical raindrop diameters on the specific rain attenuation in Durban (29°52'S, 30° 58'E), South Africa is investigated. The total rainfall attenuation is evaluated by integrating over all the raindrop sizes and the differential change in the attenuation is observed over a given range of drop size diameters. The major contribution to the specific attenuation for the DSD models considered is created by the raindrop diameters not exceeding 2 mm especially at higher frequencies. The three parameter lognormal and gamma distribution models are employed for the purpose of analysis. The overall and seasonal values of $R_{0.01}$ as determined by *Alonge* and *Afullo* [2012] for Durban are used.

4.3 Rainfall Rate and DSD models in Durban

Several works have been done by researchers on rainfall attenuation and raindrop size distribution in the tropical and equatorial regions, as well as in Durban (29°52'S, 30°58'E), South Africa. *Owolawi* [2006] estimated the Marshal-Palmer (M-P) parameters for Durban and defined the intercept parameter (drop density per unit volume), *No*. In his findings, he established a power law relation for the intercept given by $N_0 = a_1 R^{a_2}$ with a_1 and a_2 estimated as, 1500 and 0.26 respectively. In 2010, *Odedina and Afullo* [2010] proposed the lognormal and the modified gamma distribution models as best fit for the measurements of rainfall in Durban. *Afullo* [2011], while studying the rain drop size distribution model for the eastern coast of South Africa, established that the optimized lognormal and gamma DSD models compete favourably well with the DSD obtained for same tropical regions using the Biweight kernel estimation technique for Durban. *Alonge and Afullo* [2012] considered the rainfall drop size distributions for different seasons- summer, autumn, winter and spring; they established that the lognormal model is suitable for summer and autumn; the modified gamma for winter and Weibull distribution is best for the spring season in Durban. The values of $R_{0.01}$ for the different seasons were also estimated.

Recently, *Adetan and Afullo* [2012a; 2012b] in separate studies compared the two methods to evaluate the lognormal raindrop size distribution model in Durban and the three-parameter raindrop size distribution modeling for microwave propagation in South Africa. They established that the method of moment (MoM) provides a better technique to estimate the DSD parameters in Southern Africa with the lognormal model giving the best fit. In their findings, they showed that the three-parameter lognormal DSD gives a better fitting and performance when compared with the gamma

distribution model. However, the gamma distribution model is also adequate as the error deviation is minimal. *Akuon and Afullo* [2011] derived the rain cell sizes for the southern Africa and estimated the overall $R_{0.01}$ for Durban as 60 mm/h. The seasonal and overall values of $R_{0.01}$ determined by *Alonge* and *Afullo,* [2012] and *Akuon* and *Afullo*, [2011] are used in this work for the evaluation of the drop size distribution, *N (D)* parameters required for the estimation of the rainfall specific attenuation.

It is worth mentioning at this juncture that no work has been done to determine the influence of particular raindrop channels (or diameters) at which the rain attenuation is affected significantly in Durban and the Southern Africa region. Therefore this study, seeks to investigate these critical diameters that produce a major contribution to the total specific attenuation in Durban. The Mie scattering approximation at temperature of 20^{o}C for spherical raindrop shape is adopted for the estimation of the scattering functions *k* and α. In this section, the lognormal and gamma distribution models are used to characterize the measured rain drop size distribution *N (D),* in Durban as determined in *Adetan* and *Afullo* [2012b] (see Table 3-3).

4.4 Raindrop Size Distribution Models

This section considers the measurements of the raindrop size distribution models employed in the computation of the specific attenuation. There are several DSD models used for raindrop distribution modeling across the temperate and tropical regions. In this section, the three-parameters lognormal and gamma DSD models are employed for the estimation of the rainfall attenuation.

Generally, the measured rain drop size distribution $N(D_j)$ from the disdrometer data is the number of raindrops per cubic meter per millimeter diameter (mm^{-3} m^{-1}) as adopted by [*Bartholomew*, 2009; *Gunn and Kinzer*, 1949] and given earlier in equation (3.2); where n_j is the number of drops measured in the drop size bin, $v(D_j)$ is the terminal velocity of Gun Kinzer's [*Gunn and Kinzer*, 1949] water drops in m/s, *T* is the one-minute sampling time in 60 s, *A* is the measurement area of the disdrometer given as 0.005 m^2 and dD_j is the representative change in diameter interval of the bin in mm. As earlier stated, this work considers the analysis of the data in 0.1 mm diameter interval from consecutive channels (bins). The precipitation rate, *R* (mm/h) can be determined from the measured DSD data as stated in equations (2.33) and (2.35) and given again as equations 4.8 and 4.9, respectively [*Bartholomew*, 2009; *Gunn and Kinzer*, 1949]:

$$\left.\begin{aligned} R &= \frac{1}{6.A.T}\pi\sum_{j=1}^{20} n_j {D_j}^3 \\ &= 6.28318536\times 10^{-3}\sum_{j=1}^{20} {D_j}^3 n_j \end{aligned}\right\}\left[\frac{mm}{h}\right] \qquad (4.8)$$

$$\left.\begin{aligned} R &= 6\pi \times 10^{-4} \int_0^{\infty} {D_j}^3 . V(D_j) . N(D_j) dD_j \ \ [mm/h] \\ &= \ 1.88496 \times 10^{-3} \sum_{j=1}^{20} {D_j}^3 . V(D_j) . N(D_j) dD_j \end{aligned}\right\} \tag{4.9}$$

Equation (4.9) must not be violated by any DSD. The lognormal and gamma DSD parameters as determined in *Adetan and Afullo* [2012a] are used in this section. The shape parameter μ is assumed 2 for the gamma model. The scatter plots for the input parameters N_T, μ and σ of the lognormal model are shown in Figure 4-1.

4.5 Evaluation of the Specific Rainfall Attenuation and the Extinction Cross Sections

The specific attenuation of microwave signals due to rain in equation (4.1) can be re-written as:

$$\gamma = 4.343 \times 10^{-3} \int_0^{D_{max}} Q_{ext}(D, \lambda, m) . N(D) dD \ \ [\frac{dB}{km}] \tag{4.10}$$

where Q_{ext} is the extinction cross sections which are dependent on the drop diameter D, the wavelength λ, and the complex refractive index of water drop m, which in turn is a function of the frequency and temperature. The extinction cross section Q_{ext} is found by applying the classical scattering theory of Mie for a plane wave impinging upon a spherical absorbing particle discussed in Chapter 3. The Mie scattering theory is applied under the assumption that each spherical raindrop illuminated by a plane wave is uniformly distributed in a rain filled medium. Similarly, it is assumed that the distance between adjacent drops is large enough to avoid any interaction between them. For more accurate modeling, the raindrops should be modeled as oblate spheroids. The cross sections Q_{ext} are expressed by *Hulst* [1957], and *Bohren and Huffman* [2004] and stated in equation (4.11) as:

$$Q(D, \lambda, m) = \frac{\lambda^2}{2\pi} \sum_{n=1}^{\infty} (2n+1) \mathrm{Re}[a_n + b_n] \tag{4.11}$$

where a_n and b_n are the Mie scattering coefficients. The expression of the extinction cross sections, Q_{ext} provided by *Odedina and Afullo* [2010] as a frequency-dependent, power law function with coefficients, k and α is given in equation (4.12) and adopted in this section; where k and α are the coefficients that depend on rain rate, temperature, polarization and canting angle.

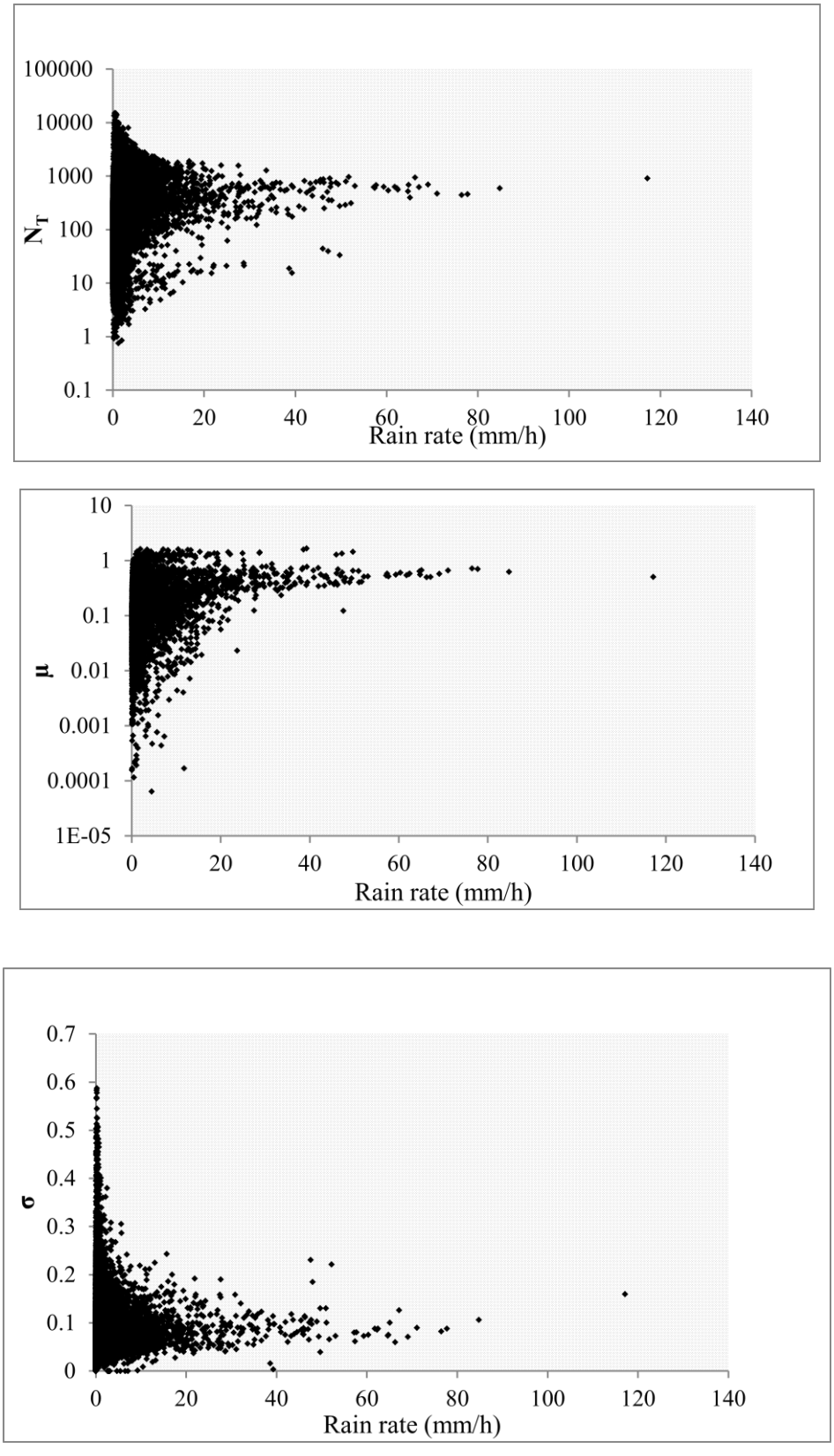

Figure 4-1: Scatterplot of the lognormal DSD parameters; N_T, μ and σ against rainfall rate R for the disdrometer data in Durban, South Africa.

$$Q_{ext}(D) = k\left(\frac{D}{2}\right)^{\alpha} \tag{4.12}$$

Mätzler's MATLAB [*Mätzler*, 2002] functions are used for the estimation of k and α. Table 4-2 shows the computed values of k and α of the power law relation in equation (4.12) at frequencies of 2.5 to 100 GHz (see Table 3-8). The total rainfall attenuation therefore is evaluated by integrating over all the raindrop sizes. The total specific rain attenuation is computed numerically over the raindrop diameters as:

$$\gamma = 4.343 \times 10^{-3} \int_{d_1}^{d_{max}} k\left(\frac{D_j}{2}\right)^{\alpha} \times \frac{N_T}{\sqrt{2\pi} \times \sigma \times D_j} exp\left[-0.5\left(\frac{\ln(D_j) - \mu}{\sigma}\right)^2\right] dD_j \tag{4.13}$$

Equation (4.13) is solved from the incremental values of the specific rain attenuation of (4.14):

$$\mathrm{d}\gamma = 4.343 \times 10^{-3} \frac{kN_T}{2^{\alpha}\sigma\sqrt{2\pi}} \left[{D_j}^{\alpha-1}.e^{-t}\right].dD_j \tag{4.14}$$

where

$$t = \frac{1}{2}\frac{\left(\left(\ln D_j\right) - \mu\right)^2}{\sigma} \tag{4.15}$$

Similarly, the total rain attenuation using the extinction cross sections in equation (4.12) and integrating over the drop diameters gives the specific attenuation for the gamma DSD model in equation (2.45) as:

$$\gamma = 4.343 \times 10^{-3} \int_{d_1}^{d_{max}} k\left(\frac{D_j}{2}\right)^{\alpha} \times N_0 {D_j}^{\mu} \exp(-\Lambda j)\, dD_j \tag{4.16}$$

$$d\gamma = 4.343 \times 10^{-3} \frac{kN_0}{2^{\alpha}} \left[{D_j}^{\alpha+2}.e^{-\Lambda D_j}\right] dD_j \quad ; \quad (\mu = 2) \tag{4.17}$$

4.6 Overall Determination of Critical Diameters in Durban

The critical diameters are the range of diameters over which the contribution to the rainfall attenuation is predominant. Figures 4-2 and 4-3 show the overall critical diameters versus the specific rainfall attenuation for the lognormal and gamma DSD models using the overall $R_{0.01}$ of 60 mm/h as determined by [*Akuon and Afullo*, 2011]. In Figure 4-2, it can be observed that the greatest shift of the attenuation towards raindrops of lower diameter occurs at the diameter D~1.4 mm at 10 GHz; while at 100 GHz, it was observed to occur at D~1.1 mm. For the gamma model in Figure 4-2, the maximum

Table 4-2: k and α values at f = 2.5-100 GHz (T = 20°C)

Frequency (GHz)	k	α
2.5	0.0048	3.3911
10	0.3857	4.5272
19.5	1.6169	4.2104
25	2.4567	4.0186
40	4.3106	3.5077
60	6.0493	3.0094
80	7.0623	2.6621
100	7.6874	2.4156

shift occurs around D~1.3 mm at 10 GHz and diameter D~0.9 mm at 100 GHz. This compares well with the results obtained by *Fiser* [2002]. The specific attenuation therefore is directly proportional to the surface area under the curve and above the diameters (x-axis).

Tables 4-3 and 4-4 show the total attenuation created by drop sizes in the diameter interval of 0.1 to 7 mm for the two models. The total specific rainfall attenuation increases with increasing frequency. At frequency above 40 GHz, it is observed as illustrated in Table 4-5 for the annual (overall) determination of the critical diameters that the drop size diameters creating the prevailing contribution to the total attenuation for all the rain rates considered did not exceed 3 mm (about 90%). Similar results are obtained at the selected frequencies for different seasons. This is illustrated in Tables 4-6 and 4-7. Similarly, the role of small drop diameters increases with the increasing frequency for the DSD models as the prevailing contribution of raindrops diameters to the specific attenuation does not exceed 2 mm, especially at higher frequencies. This is observed in Tables 4-8 and 4-9 for the DSD models. Detailed results are shown in Appendix E for the annual and rainfall regimes.

4.7 Seasonal Determination of Critical Diameters in Durban

The values of $R_{0.01}$ for summer (50.48 mm/h), winter (53.37 mm/h), autumn (72.15 mm/h) and spring (18.51 mm/h) seasons as determined by [*Alonge and Afullo*, 2012] for Durban are used to estimate the seasonal critical range of diameters in this chapter. Figures 4-4 and 4-5 show the specific attenuation and the range of raindrop diameters at f =10 GHz, 40 GHz and 100 GHz for the gamma and lognormal DSD models, respectively. It is observed that higher rainfall rates cause higher rainfall specific attenuation and the specific attenuation increases with increasing frequency for all seasons.

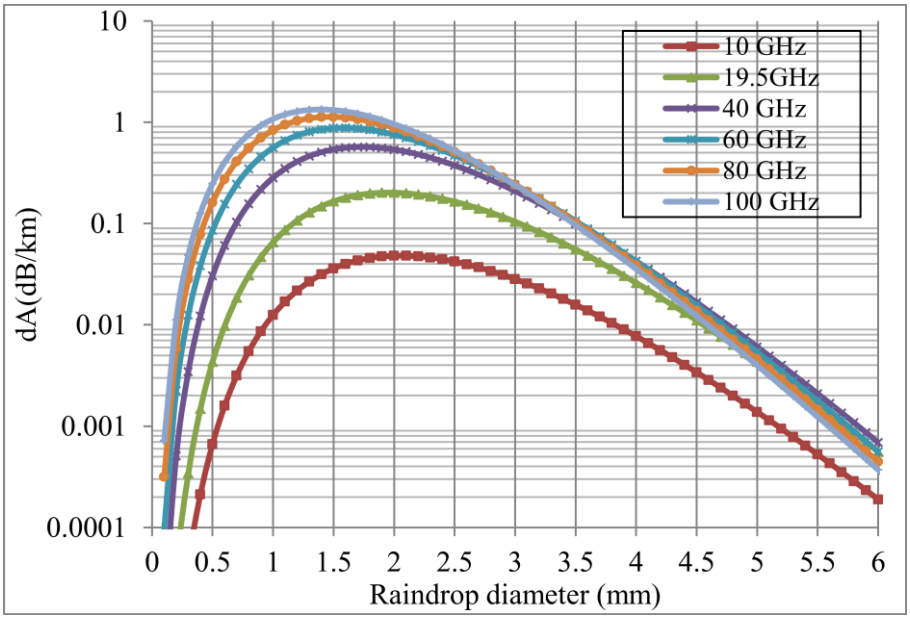

Figure 4-2: Overall specific attenuation against the drop size diameters at various frequencies using the lognormal DSD model ($R_{0.01}$ = 60 mm/h) [*Akuon and Afullo*, 2011]

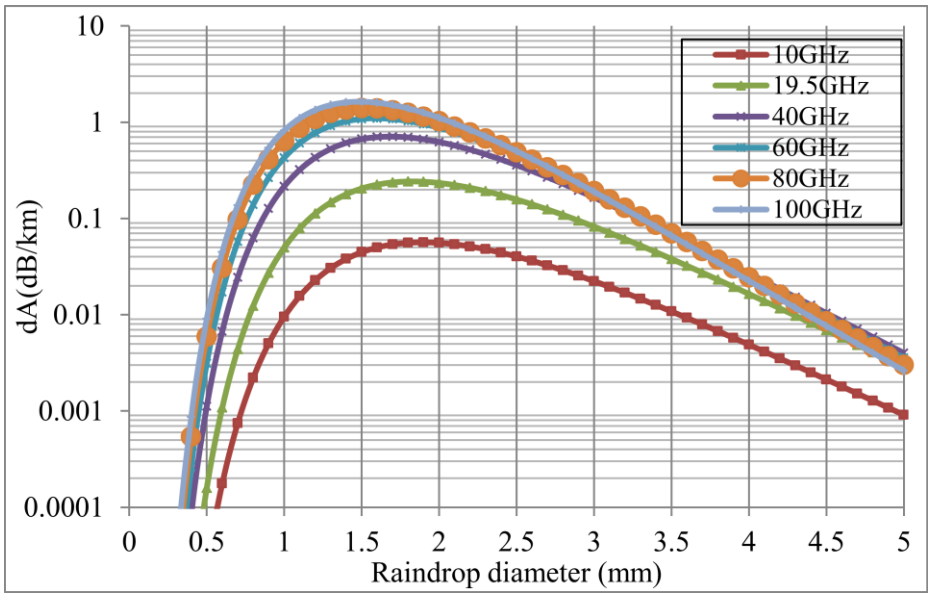

Figure 4-3: Overall specific attenuation against the drop size diameters at various frequencies using the gamma DSD model ($R_{0.01}$ = 60 mm/h) [*Akuon and Afullo*, 2011].

Table 4- 3: Overall specific rainfall attenuation created by drops in the diameter range $0.1 \geq D \geq 7$ mm at various frequencies using the lognormal gamma DSD models with $R_{0.01}$ from [*Akuon and Afullo*, 2011].

Frequency (GHz)	L-M	G-M
	γ (dB/km)	γ (dB/km)
10	0.961007	0.985026
19.5	3.977033	4.027874
40	10.73367	10.72919
60	15.72329	15.80689
80	19.23337	19.6010
100	21.82271	22.58165

The wide gap between the spring and the other seasons may be due to the low $R_{0.01}$ values recorded for spring season in the region.

Similarly as observed in section 4.6, the largest contributions to the specific attenuation for DSD models considered are due to raindrop diameters not greater than 2 mm, for all the seasons. Tables 4-10 and 4-11 show the contributions of the drop sizes in the range 0.1 mm $\leq D \leq$ 2.0 mm, 0.5 mm $\leq D \leq$ 2.5 mm, 1.0 mm $\leq D \leq$ 3.0 mm, 1.5 mm $\leq D \leq$ 3.5 mm and 4.0 mm $\leq D \leq$ 7.0 mm for the seasonal and overall determination of critical diameters, respectively. Over 80% of the attenuation at all frequencies for the models is contributed by drop diameters in the range 1.0 mm $\leq D \leq$ 3.0 mm for the overall and seasonal values of $R_{0.01}$. The summer and winter seasons tend to have similar critical diameters at the same frequency range as shown in Table 4-10. At frequency $f \geq 80$ GHz, the critical range of diameters for the gamma DSD model occurs in the range 0.5 mm $\leq D \leq$ 2.5 mm. The highest contribution to the attenuation in the diameter range 4.0 mm $\leq D \leq$ 7.0 mm is observed during the autumn season to be 6.05% (Table 4-10). This is very low and insignificant. Therefore, larger diameters contribute little to the specific attenuation.

Table 4-4: Seasonal specific rainfall attenuation created by drops in the diameter range $0.1 \geq D \geq 7$ mm at various frequencies using the lognormal and gamma DSD models with $R_{0.01}$ from [*Alonge and Afullo*, 2012].

Season	Frequency (GHz)	L-M	G-M
		γ (dB/km)	γ (dB/km)
Winter ($R_{0.01}$=50.48mm/h)	10	0.843837	0.865123
	19.5	3.514999	3.559706
	40	9.621152	9.614014
	60	14.23015	14.30342
	80	17.52132	17.85711
	100	19.97118	20.67386
Summer ($R_{0.01}$=53.37mm/h)	10	0.793249	0.813361
	19.5	3.314549	3.356609
	40	9.133414	9.125235
	60	13.57084	13.63964
	80	16.76166	17.08379
	100	19.14682	19.82421
Autumn ($R_{0.01}$=72.15mm/h)	10	1.179336	1.208381
	19.5	4.830721	4.893022
	40	12.75207	12.75333
	60	18.39855	14.30342
	80	22.27487	22.69526
	100	25.09265	25.94920
Spring ($R_{0.01}$=18.51mm/h)	10	0.260292	0.267478
	19.5	1.150270	1.164359
	40	3.356328	3.563353
	60	5.771739	5.792821
	80	7.540564	7.692947
	100	8.957303	9.305668

Table 4-5: Percentage fraction (%) of the overall specific attenuation created by particular diameter intervals to the total specific attenuation at different frequencies for the lognormal and gamma DSD models. $R_{0.01}$ from [*Akuon and Afullo*, 2011]

Frequency (GHz)	G-M		L-M		
	Diameter range (mm)	$\sum\gamma$ (dB/km)	Diameter range (mm)	$\sum\gamma$ (dB/km)	% Contribution
10	0.7-3.5	0.8885	1.0-3.3	0.8681	90
	0.8-5.3	0.9759	0.6-4.6	0.9514	99
	0.7-5.4	0.9797	0.9-5.6	0.9562	99.5
	0.6-6.3	0.9837	0.5-5.9	0.9600	99.9
	0.3-6.8	0.9849	0.4-6.7	0.9609	99.99
	0.2-6.9	0.9850	0.3-6.9	0.9601	100
40	0.6-3.1	9.6613	0.8-2.9	9.6996	90
	0.7-5.7	10.616	0.4-4.0	10.605	99
	0.6-5.8	10.678	0.6-4.5	10.683	99.5
	0.4-5.6	10.718	0.5-5.3	10.723	99.9
	0.3-6.7	10.728	0.5-6.4	10.732	99.99
	0.2-6.7	10.729	0.3-6.8	10.733	100
80	0.5-2.8	17.744	0.6-2.6	17.329	90
	0.5-4.2	19.380	0.6-3.7	19.029	99
	0.5-5.9	19.485	0.7-4.3	19.140	99.5
	0.3-5.3	19.585	0.4-4.7	19.208	99.9
	0.2-6.5	19.599	0.5-6.6	19.232	99.99
	0.2-6.9	19.600	0.3-6.7	19.233	100
100	0.5-2.7	20.387	0.5-2.5	19.551	90
	0.4-4.0	22.374	0.6-3.6	21.590	99
	0.3-4.2	22.475	0.4-3.9	21.706	99.5
	0.3-5.4	22.564	0.4-4.7	21.801	99.9
	0.2-5.9	22.579	0.5-6.1	21.820	99.99
	0.1-6.9	22.581	0.4-6.7	21.822	100

Table 4-6: Percentage fraction (%) of the seasonal specific attenuation created by particular diameter intervals to the total specific attenuation at f = 10 GHz with $R_{0.01}$ from [*Alonge and Afullo*, 2012]

Season	G-M		L-M		
	Diameter range (mm)	$\sum\gamma$ (dB/km)	Diameter range (mm)	$\sum\gamma$ (dB/km)	% Contribution
Winter ($R_{0.01}$=50.48 mm/h)	0.8-3.5	0.7858	0.6-3.2	0.7665	90
	0.4-4.8	0.8533	0.3-4.5	0.8356	99
	0.6-5.1	0.8606	0.9-5.5	0.8392	99.5
	0.5-6.1	0.8645	0.7-6.1	0.8432	99.9
	0.4-6.7	0.8650	0.3-6.6	0.8437	99.99
	0.3-6.8	0.8651	0.2-6.9	0.8438	100
Summer ($R_{0.01}$=53.37 mm/h)	0.4-3.4	0.7359	0.6-3.2	0.7245	90
	0.8-5.7	0.8070	0.7-4.5	0.7861	99
	0.7-5.6	0.8099	0.9-5.6	0.7890	99.5
	0.7-5.9	0.8126	0.5-5.5	0.7921	99.9
	0.4-6.7	0.8132	0.3-6.6	0.7931	99.99
	0.3-6.9	0.8133	0.3-6.9	0.7932	100
Autumn ($R_{0.01}$=72.15 mm/h)	0.5-3.6	1.0908	1.0-3.4	1.0634	90
	0.4-4.8	1.1932	1.0-5.2	1.1703	99
	0.6-5.4	1.2027	0.8-5.3	1.1735	99.5
	0.5-6.1	1.2071	0.6-6.3	1.1786	99.9
	0.3-6.7	1.2082	0.6-6.8	1.1791	99.99
	0.2-6.8	1.2084	0.2-6.9	1.1793	100
Spring ($R_{0.01}$=18.51 mm/h)	0.7-2.9	0.2416	0.8-2.6	0.2359	90
	0.4-3.8	0.2639	0.3-3.7	0.2582	99
	0.6-4.8	0.2663	0.7-4.0	0.2590	99.5
	0.5-5.7	0.2672	0.7-5.3	0.2599	99.9
	0.3-6.1	0.2674	0.5-5.6	0.2602	99.99
	0.2-6.8	0.2675	0.2-6.9	0.2603	100

Table 4-7: Percentage fraction (%) of the seasonal specific attenuation created by particular diameter intervals to the total specific attenuation at f = 100 GHz with $R_{0.01}$ from [*Alonge and Afullo*, 2012]

Season	G-M		L-M		
	Diameter Range (mm)	$\sum\gamma$ (dB/km)	Diameter Range (mm)	$\sum\gamma$ (dB/km)	% Contribution
Winter ($R_{0.01}$=50.48 mm/h)	0.4-2.6	18.613	0.6-2.5	18.095	90
	0.5-4.0	20.374	0.3-3.6	19.801	99
	0.4-4.6	20.584	0.4-3.8	19.861	99.5
	0.3-5.9	20.660	0.6-5.5	19.958	99.9
	0.2-6.1	20.672	0.4-6.1	19.969	99.99
	0.2-6.8	20.673	0.3-6.7	19.971	100
Summer ($R_{0.01}$=53.37 mm/h)	0.6-2.7	17.874	0.6-2.5	17.439	90
	0.5-4.6	19.613	0.4-3.5	18.959	99
	0.4-4.5	19.732	0.6-3.9	19.059	99.5
	0.3-6.4	19.811	0.6-4.9	19.127	99.9
	0.2-6.2	19.823	0.5-6.3	19.145	99.99
	0.2-6.8	19.824	0.3-6.5	19.147	100
Autumn ($R_{0.01}$=72.15 mm/h)	0.5-2.8	23.507	0.3-2.6	22.562	90
	0.4-4.0	25.668	0.2-3.7	24.820	99
	0.4-4.6	25.828	0.5-4.1	24.972	99.5
	0.3-5.7	25.932	0.4-4.7	25.057	99.9
	0.2-6.2	25.947	0.5-6.2	25.090	99.99
	0.2-6.8	25.948	0.2-6.7	25.092	100
Spring ($R_{0.01}$=18.51 mm/h)	0.6-2.4	8.384	0.7-2.1	8.119	90
	0.4-4.0	9.237	0.6-3.1	8.895	99
	0.3-3.5	9.260	0.4-3.1	8.910	99.5
	0.5-5.6	9.293	0.5-3.8	8.943	99.9
	0.2-6.9	9.304	0.4-4.8	8.956	99.99
	1.0-6.9	9.306	0.2-6.6	8.957	100

Table 4-8.Contributions (dB/km) of raindrop diameters to specific attenuation at f = 10-100 *GHz* using gamma DSD model at some selected raindrop diameters $R_{0.01}$ from [*Akuon and Afullo*, 2011]

D (mm)	10 GHz	19.5 GHz	40 GHz	60 GHz	80 GHz	100 GHz
0.5	0.00066458	0.00432229	0.03052364	0.0854693	0.1614904	0.24739323
1	0.01251707	0.06535861	0.28359016	0.5621624	0.83493096	1.07817132
1.5	0.03605435	0.16556628	0.54028250	0.8750749	1.12895735	1.31919274
2	0.04814263	0.20181959	0.53804413	0.7550666	0.88150815	0.95953242
2.5	0.04218448	0.16477267	0.37552693	0.4715396	0.50945100	0.52486476
3	0.02831760	0.10440091	0.20932425	0.2400162	0.24340260	0.23974637
3.5	0.01581624	0.05553190	0.09991122	0.1060903	0.10197876	0.09670172
4	0.00772147	0.02598769	0.04256851	0.0422914	0.03881020	0.03561027
4.5	0.00340138	0.011028519	0.01663003	0.0155800	0.01372448	0.01223253
5	0.00138164	0.004332728	0.00606713	0.0053933	0.0045803	0.00397772
5.5	0.00052558	0.001599184	0.00209427	0.0017753	0.00145862	0.00123731
6	0.00018939	0.00056059	0.00069061	0.0005605	0.00044687	0.00037103
6.5	6.52142E-05	0.0001881	0.0002191	0.0001709	0.00013253	0.00010788
7	2.16018E-05	6.08923E-05	6.73133E-05	5.0601E-05	3.82336E-05	3.05609E-05

Table 4-9: Contributions (dB/km) of raindrop diameters to specific attenuation at f = 10-100 *GHz* using lognormal DSD model at some selected raindrop diameters $R_{0.01}$ from [*Akuon and Afullo*, 2011]

D (mm)	10GHz	19.5GHz	40GHz	60GHz	80GHz	100GHz
0.5	2.44494E-05	0.00015901	0.00112294	0.003144345	0.00594109	0.009101391
1	0.009552573	0.04987928	0.21642554	0.4290216	0.63718848	0.822820544
1.5	0.044693481	0.20523825	0.66974166	1.084755054	1.39947113	1.635289547
2	0.055845165	0.23410953	0.62412799	0.875872843	1.02254422	1.113051905
2.5	0.040321344	0.15749524	0.35894122	0.450713399	0.48695032	0.501683318
3	0.022364563	0.08245333	0.16531926	0.189559075	0.19223352	0.189345918
3.5	0.010830001	0.03802486	0.06841311	0.072644183	0.06982883	0.06621543
4	0.004884991	0.0164411	0.02693095	0.026755673	0.02455326	0.02252883
4.5	0.002126469	0.00689479	0.01039674	0.009740292	0.00858025	0.007647515
5	0.000911798	0.00285933	0.00400393	0.003559268	0.00302271	0.002625054
5.5	0.000389847	0.00118617	0.0015534	0.001316832	0.00108191	0.000917759
6	0.000167452	0.00049565	0.00061059	0.000495645	0.0003951	0.000328043
6.5	7.2591E-05	0.00020948	0.00024395	0.000190284	0.00014752	0.000120094
7	3.18489E-05	8.9777E-05	9.9244E-05	7.46042E-05	5.63702E-05	4.50578E-05

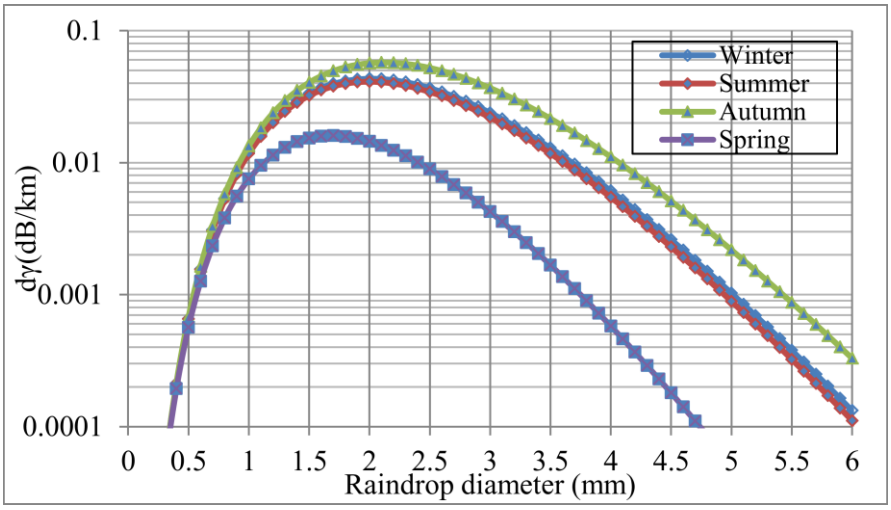

(a)

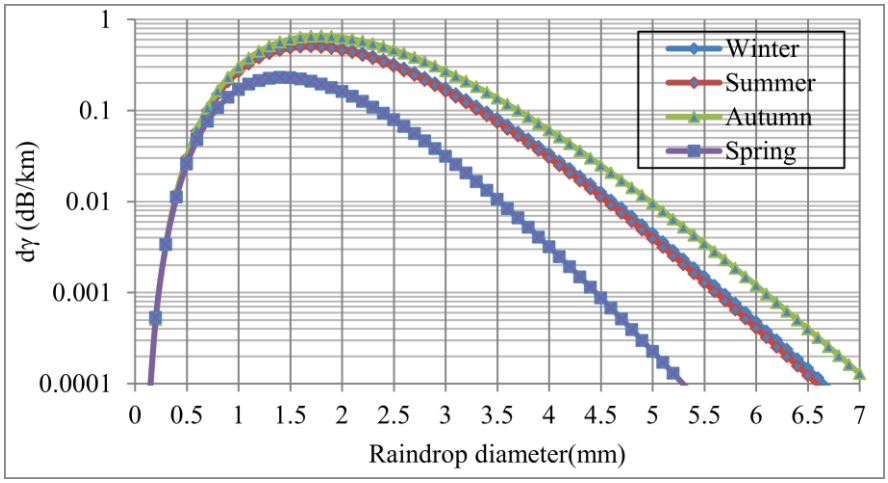

(b)

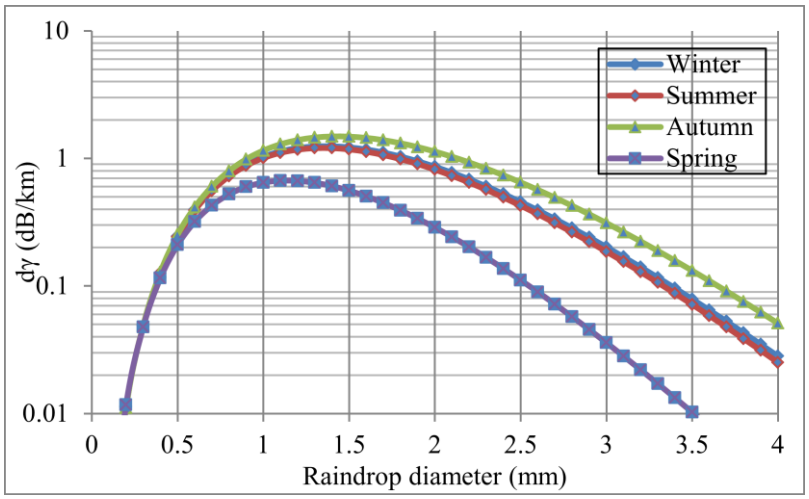

(c)

Figure 4-4: Seasonal specific attenuation against the drop size diameters (mm) at (a) *f* = 10GHz (b) *f* = 40 GHz (c) *f* = 100 GHz for the gamma DSD model

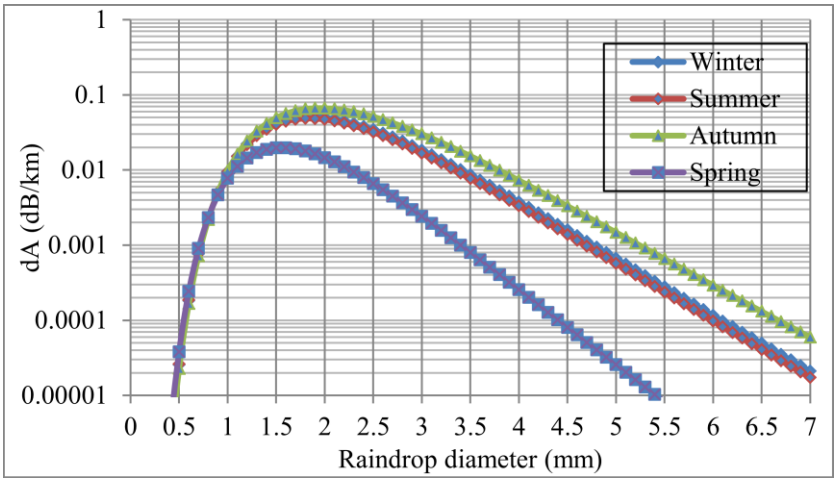

(a)

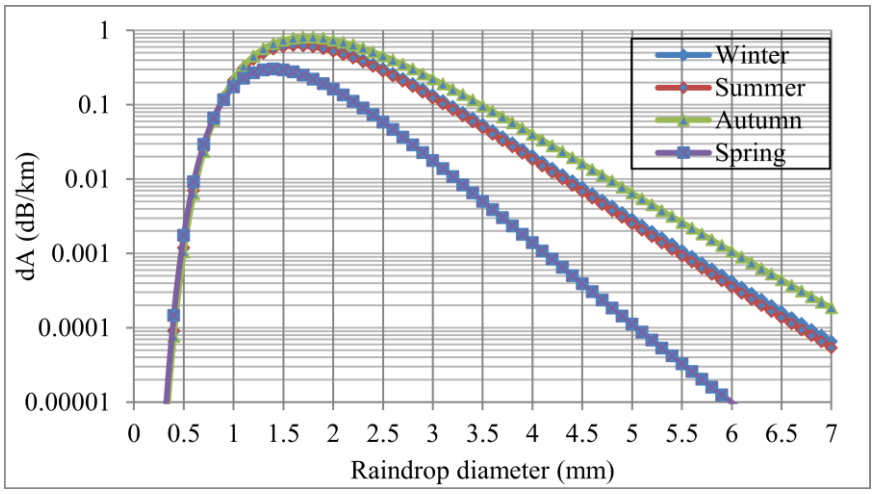

(b)

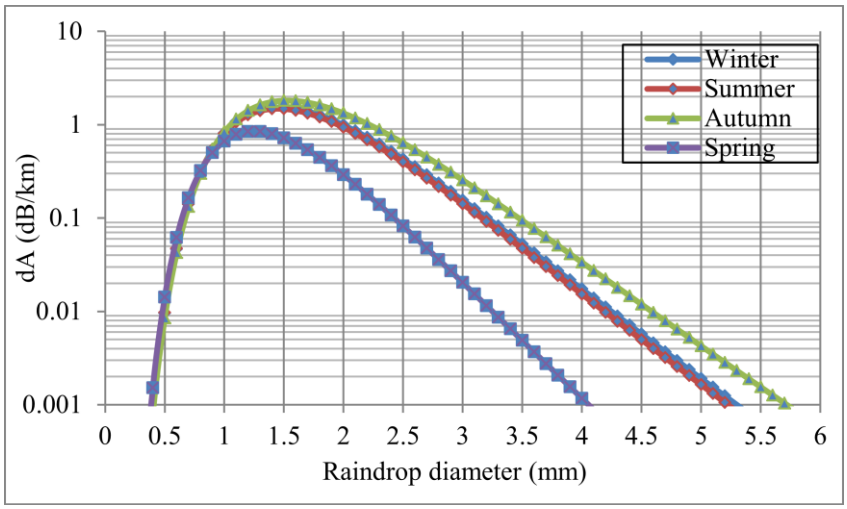

(c)

Figure 4-5: Seasonal specific attenuation against the drop size diameters (mm) at (a) *f* = 10GHz (b) *f* = 40GHz (c) *f* = 100 GHz for the lognormal DSD model

Table 4-10: Percentage (%) fraction of the attenuation created by range of raindrop diameters (*mm*) to the total attenuation within the given diameter range for different seasons with $R_{0.01}$ from [*Alonge and Afullo*, 2012]

Season	*f* (GHz)	L-M	G-M	L-M	G-M	L-M	G-M	L-M	G-M	L-M	G-M
		0.1 ≤ *D* ≤ 2	0.1≤ *D* ≤ 2	0.5 ≤ *D* ≤ 2.5	0.5 ≤ *D* ≤ 2.5	1.0≤ *D* ≤ 3.0	1.0≤ *D* ≤ 3.0	1.5 ≤ *D* ≤ 3.5	1.5 ≤ *D* ≤ 3.5	4.0≤ *D* ≤7.0	4.0≤ *D* ≤7.0
Winter	10	48.42	41.58	72.89	64.82	86.35	79.43	80.23	77.32	2.79	4.32
	19.5	52.67	46.35	76.30	69.02	88.11	81.45	78.79	75.84	2.18	3.42
	40	61.92	57.29	82.96	77.57	90.79	83.94	74.00	70.17	1.21	1.93
	60	68.13	65.01	86.87	82.72	91.65	83.69	69.43	64.24	0.77	1.23
	80	72.18	70.18	89.19	85.73	91.74	82.39	65.76	59.28	0.56	0.88
	100	74.89	73.69	90.65	87.53	91.55	80.86	62.96	55.41	0.44	0.68
Summer	10	49.59	42.54	73.91	65.79	86.94	80.06	79.98	77.27	2.58	4.04
	19.5	53.83	47.32	77.24	69.94	88.61	81.97	78.42	75.66	2.01	3.19
	40	63.01	58.23	83.71	78.32	91.07	84.19	73.39	69.73	1.11	1.79
	60	69.13	65.88	87.49	83.34	91.79	83.75	68.68	63.65	0.71	1.14
	80	73.11	70.99	89.73	86.25	91.78	82.31	64.94	58.61	0.51	0.81
	100	75.77	74.45	91.13	87.97	91.52	80.69	62.10	54.71	0.39	0.63
Autumn	10	42.21	36.52	67.16	59.45	82.71	75.67	80.94	77.05	4.17	6.05
	19.5	46.47	41.20	70.96	63.92	85.02	78.27	80.19	76.31	3.29	4.86
	40	56.01	52.20	78.57	73.27	88.88	82.17	76.79	72.15	1.89	2.83
	60	62.59	60.21	83.18	79.13	90.55	83.00	73.02	67.09	1.23	1.84
	80	66.98	65.69	85.99	82.67	91.17	82.45	69.81	62.61	0.90	1.33
	100	69.97	69.47	87.77	84.87	91.35	81.43	67.28	59.00	0.72	1.04
Spring	10	70.77	60.57	89.02	81.47	93.16	87.54	69.18	71.45	0.47	1.02
	19.5	74.16	65.01	90.81	84.27	93.12	87.38	65.86	67.82	0.35	0.77
	40	80.89	74.32	93.99	89.36	92.01	84.89	57.75	58.23	0.17	0.39
	60	84.93	80.20	95.67	91.89	90.36	81.16	51.61	50.44	0.10	0.23
	80	87.39	83.86	96.59	93.06	88.78	77.52	47.25	44.74	0.07	0.15
	100	88.95	86.21	97.14	93.55	87.44	74.44	44.16	40.63	0.05	0.12

4.8 Regime Analysis of Critical Raindrop Diameters in Durban

The influence of critical raindrop diameters on the specific rainfall attenuation in Durban, South Africa using various rainfall regimes is analyzed in this section. Different rain rate values representing drizzle (below 5mm/h), widespread (5-20 mm/h) shower (20-50 mm/h) and thunderstorm

Table 4-11: Percentage (%) fraction of the attenuation created by range of raindrop diameters (mm) to the total attenuation within the given diameter range with $R_{0.01}$ from [*Akuon and Afullo*, 2011]

Frequency (GHz)	L-M	G-M	L-M	G-M	L-M	G-M	L-M	G-M	L-M	G-M
	0.1 ≤ D ≤ 2	0.1 ≤ D ≤ 2	0.5 ≤ D ≤ 2.5	0.5 ≤ D ≤ 2.5	1≤ D ≤ 3	1≤ D ≤ 3	1.5 ≤ D ≤ 3.5	1.5 ≤ D ≤ 3.5	4 ≤ D ≤ 7	4 ≤ D ≤ 7
10	45.97	39.58	70.71	62.75	85.02	78.04	80.64	77.32	3.28	4.94
19.5	50.24	44.32	74.28	67.06	86.99	80.29	74.46	76.12	2.57	3.93
40	59.63	55.31	81.31	75.94	90.13	83.33	75.19	71.03	1.45	2.25
60	65.99	63.16	85.50	81.37	91.30	83.50	70.92	65.42	0.93	1.44
80	70.19	68.46	88.00	84.59	91.60	82.49	67.42	60.63	0.68	1.04
100	73.02	72.08	89.59	86.54	91.54	81.15	64.71	56.85	0.53	0.81

(above 50 mm/h) as classified according to [*Ajayi and Olsen*, 1985; *Adimula and Ajayi*, 1996] are selected for the purpose of analysis over the measured raindrop size distribution. The three-parameter lognormal and gamma DSD models with shape parameter of 2 are used to estimate the parameters required to investigate the drop sizes which produce a major contribution to the total specific rainfall attenuation for the selected rain rate values. The attenuation created by drops in the diameter intervals $0.1 \geq D \geq 7.0$ mm at various frequencies of transmission is shown in Tables 4-12 and 4-13 for gamma and lognormal models, respectively.

The total specific attenuation increases with increasing frequencies and rain rate. The highest and prevailing contribution to the specific attenuation occurs at $D \sim 2$ mm for the stratiform (drizzle or widespread) and convective (shower or thunderstorm) rain types shown in Figures 4-6 and 4-7 for the gamma and lognormal models, respectively. The total percentage fraction formed by drops in the diameter range 0.5 mm $\leq D \leq$ 2.5 mm and 1.0 mm $\leq D \leq$ 3.0 mm are found to be most critical for the specific rain attenuation for the stratiform (drizzle and widespread) and convective (shower and thunderstorm) rainfall types. As stated earlier, the contribution of larger diameters to the total attenuation is very low and virtually insignificant when compared to the medium and smaller diameters. Hence, the diameter ranges 0.5 mm $\leq D \leq$ 2.5 mm are critical to attenuation in Durban being a coastal region characterized by drizzle.

Table 4-12 Rain attenuation created by drops in the diameter range 0.1 mm ≥ D ≥ 7.0 mm at various frequencies for gamma model

frequency (GHz)	R =1.41 mm/h	R= 14.21mm/h	R= 44.52 mm/h	R= 77.70 mm/h
10	0.015406	0.19953	0.70762	1.31181
20	0.08133	0.92552	3.07908	5.53309
30	0.18647	1.84412	5.72388	9.94386
40	0.31899	2.78129	8.11154	13.6706
100	1.33609	7.62494	18.0329	27.4400

Table 4-13 Rain attenuation created by drops in the diameter range 0.1 mm ≥ D ≥ 7.0 mm at various frequencies for the lognormal model

frequency (GHz)	R =1.41 mm/h	R= 14.21mm/h	R= 44.52 mm/h	R= 77.70 mm/h
5	0.0057	0.0239	0.0754	0.2049
10	0.0433	0.2014	0.6899	2.0193
19.5	0.2093	0.9014	2.9032	8.0519
40	0.7903	2.8815	8.1216	20.0556
60	1.4570	4.7398	12.1929	27.8055
80	2.0836	6.2730	15.1661	32.7638
100	2.6307	7.5191	17.4093	36.2179

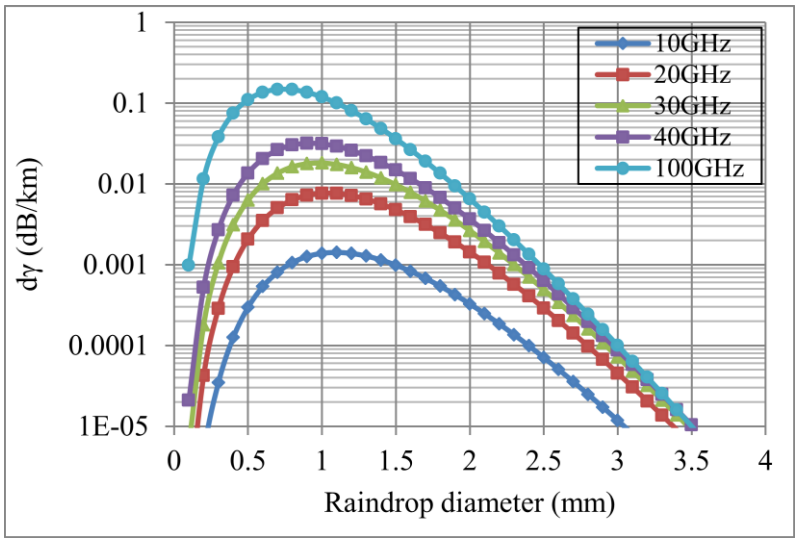

(a)

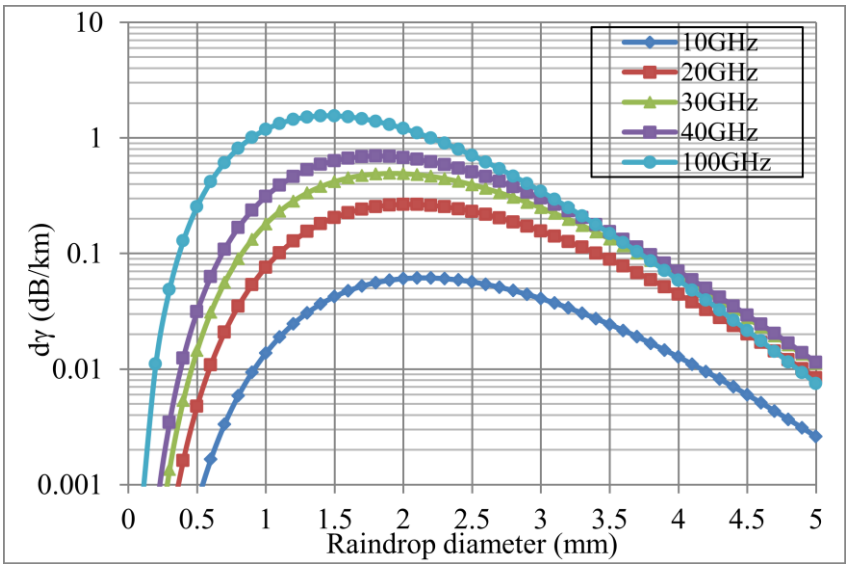

(b)

Figure 4-6: Rainfall attenuation and raindrop diameters for rainfall regimes at various frequencies for (a) R= 1.41 and (b) R= 77.70 mm/hr using gamma DSD model.

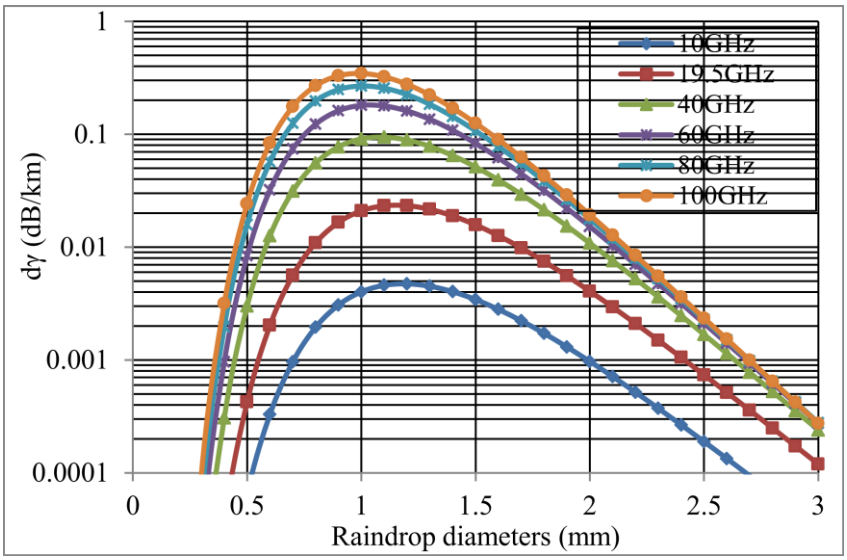

(a)

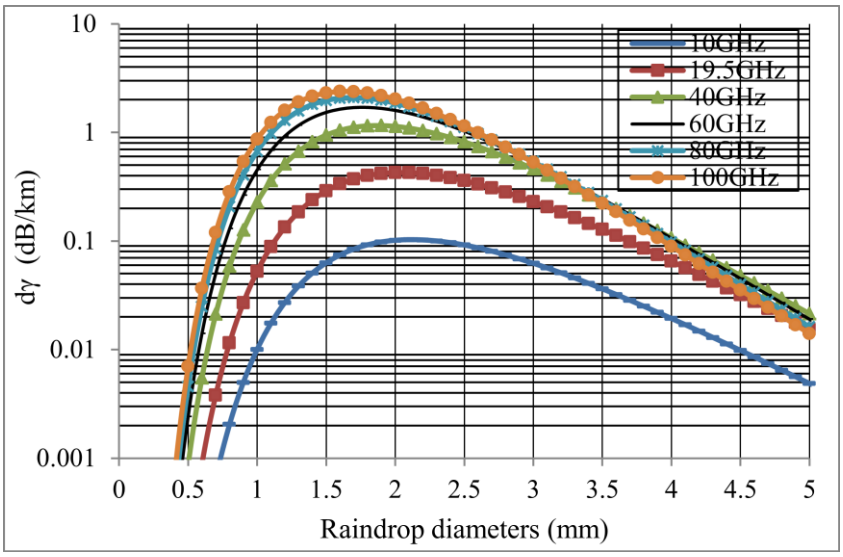

(b)

Figure 4-7: Rainfall attenuation and raindrop diameters for rainfall regimes at various frequencies for (a) R= 3.68 mm/h and (b) R= 120 mm/h using lognormal DSD model.

4.8 Chapter Summary

This chapter considered the critical range of diameters over which the specific rainfall attenuation is highest. For the DSD models considered, the maximum (peak) value of the rain attenuation was found to occur for the drop diameters in the range 0.5 mm ≤ D ≤ 2.5 mm and 1.0 mm ≤ D ≤ 3.0 mm for both the seasonal and overall values of $R_{0.01}$ as well as for the different rainfall regimes in Durban. Over 80% of the attenuation at frequencies of 2-100 GHz for both the DSD models is created by drop diameters in the range 1.0 mm ≤ D ≤ 3.0 mm for both the overall and seasonal values of $R_{0.01}$. The summer and winter seasons tend to have similar critical diameters at the same frequency. For instance, at a frequency of 80 GHz and above, the critical range of diameters for the gamma DSD model occurs in the range 0.5 mm ≤ D ≤ 2.5 mm. However, at larger diameters in the range 4.0 mm ≤ D ≤ 7.0 mm, the highest percentage contribution to rainfall attenuation was observably small (6.05%). The highest contribution of raindrops diameters to the specific rain attenuation was created by drop diameters not exceeding 2 mm, especially at higher frequencies. This confirms the results obtained by [*Lee et al*, 2007 and *Lakshmi et al*, 2007 in Singapore; *Fiser*, 2002 in Czech Republic; *Lam et al*, 2011 in Malaysia; *Marzuki et al*, 2009 in Equatorial Indonesia]. The percentage contribution as created by the given range of diameters at various frequencies and seasons to the total specific attenuation was also investigated. At frequency above 40 *GHz*, the drop size diameter that gives the largest contribution to the total attenuation for all the rain rates considered does not exceed 3 mm (90%). This is similar to the results obtained by [*Marzuki et al*, 2009].

Furthermore, the critical diameters are seen to coalesce around the peak diameter, D_p at which the maximum attenuation occurs. The peak diameter was found to be $D_p = exp[\sigma^2(\alpha - 1) + \mu]$. It should be noted that D_p is frequency dependent, since α is dependent on frequency. The parameters, μ and σ in Table 4-1 are region-dependent. A good understanding of this rainfall attenuation characteristic will be helpful to properly design adequate fade margin levels, achieve the expected quality of service in a radio communication system operating in the South Africa region and for the purpose of link budget design by the engineers and service providers in this particular area.

CHAPTER FIVE

COMPARATIVE ANALYSIS OF DROP SIZE DISTRIBUTION AND CRITICAL DIAMETERS FOR EQUATORIAL AND SUB-TROPICAL AFRICA

5.1 Introduction

Raindrops measurements obtained from Butare (2.6^{o}S, 29.74^{o}E), Rwanda, in Central Africa, and Durban (29^{o}52'S, 30^o 58'E), South Africa using the Joss-Waldvogel (J-W) RD-80 disdrometer are used for the analysis of the drop size distribution (DSD) and specific rainfall attenuation modeling in the central and southern African countries identified as equatorial (Butare) and sub-tropical (Durban) regions. The influence of the raindrop diameters that are critical to the measured rain rate and specific rain attenuation at operating frequencies of 10-150 GHz is investigated using the estimated $R_{0.01}$ values for Butare and Durban. The drop size distribution (DSD) and the rainfall rate distribution have been considered as most essential parameters for the prediction of rain attenuation. Measurements used for the analysis in Butare were taken at the National University of Rwanda for a period of nine months in 2012. The Mie scattering approximations [*Mätzler,* 2002] at temperature of 20^{o}C for spherical raindrop shape is adopted for the estimation of the scattering functions. The three-parameter lognormal and gamma distribution models are used to characterize the measured drop size distribution *N (D)* at these locations. The influence of the disdrometer bins on the DSD and specific rain attenuation using selected values of rain rate representing stratiform and convective rain types [*Timothy et al,* 2002] is also studied. The contribution of the critical raindrop diameters to the specific attenuation due to rain using the estimated $R_{0.01}$ values for these locations is also investigated. The rain rate distribution characteristics and $R_{0.01}$ values at various percentages of exceedence for central and southern Africa is discussed briefly in section 5.2.

5.2 Rain rate distribution characteristics in central and southern Africa

Tropical, subtropical and equatorial regions are characterized by high-intensity rainfall, enhanced frequency of rainfall occurrence and increased presence of large raindrops when compared to temperate regions with moderate/low rain intensity [*Ajayi*, 1990]. Oftentimes rain in the tropics occur in form of cells which are a complex mixture of stratiform and convective types, with the convective rain contributing over 70 percent of the total rainfall in most cases [*Timothy et al,* 2002, *Ajayi*, 1990].

Figure 5-1: Map of Rwanda showing some of the neighboring countries

[Source: https://www.google.co.za/#q=map+of+rwanda]

The rainfall characteristics in South Africa have been discussed in section 2.13. This will no longer be stressed in this chapter (see section 2.13).

Rwanda is a land-locked country located in Central Africa, only two degrees south of the equator, surrounded by the Democratic Republic of the Congo, Uganda, Tanzania and Burundi [Figure 5-1]. The country is characterized with two rainy seasons per annum (February to May and September to December). During these seasons, heavy downpours occur almost daily, alternating with sunny weather. Rainfall is heaviest in the southwest and lightest in the east. At Gisovu, in the West, near Kibuye, annual rainfall averages 1600 mm; at Gabiro, in the northeast, 780 mm*;* and at Butare, in the south, 1150 mm. [http://www.nationsencyclopedia.com/Africa/Rwanda-CLIMATE.html]. The second largest city in Rwanda, Butare, where the measurement was taken using the disdrometer installed at the National University of Rwanda, is situated in the South and borders Burundi to the South. The city is at an elevation of 1772 meters above mean sea level. Rwanda is generally surrounded by mountains. Disdrometer measurements obtained from Durban and Butare are used to estimate the rain rate exceeded for 0.01 % of time in South Africa and Rwanda. The percentage of time the rain rates is exceeded was utilized in this work to compute the specific attenuation over the frequency range of 10 to 150 GHz .Table 5-1 and Figure 5-2 show the complementary cumulative distributions

Table 5-1: Estimated rain rate distribution at various percentages of exceedence in South Africa and Rwanda.

Percentage of time rain rate is exceeded (%)	Durban (South Africa)	Butare (Rwanda)
2	6.62	15.65
1	10.53	26.24
0.5	16.21	35.96
0.3	20.96	44.01
0.2	24.26	50.88
0.1	32.33	65.61
0.05	47.57	70.69
0.03	51.67	71.19
0.02	57.35	71.59
0.01	66.25	73.88

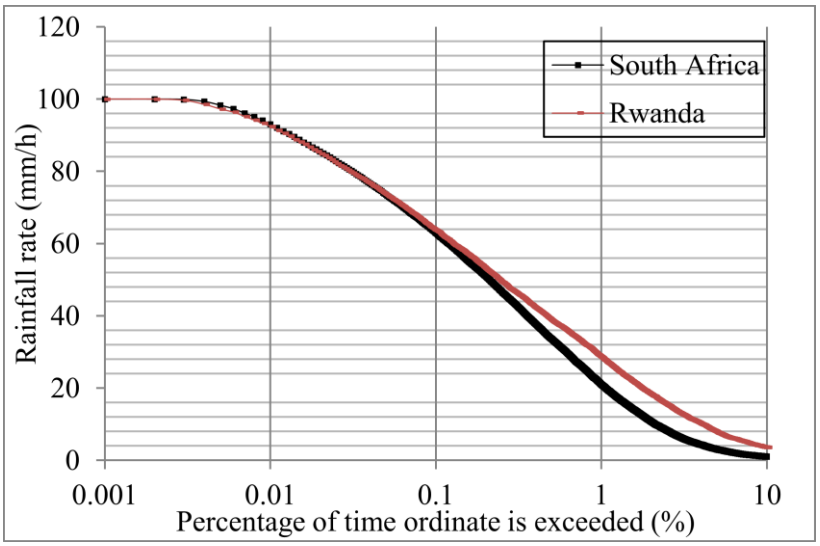

Figure 5-2: Complementary cumulative distributions of rain rate measured in South Africa and Rwanda.

functions (CDDF) of the rainfall rate R (mm/h), exceeded for various percentages of time P (%) obtained at Durban and Butare.

5.3 Data Collection and Analysis

The measurements were taken over a period of 9 months in Butare, Rwanda and one year in Durban, South Africa. The minimum and maximum rain rates obtained were 0.003 mm/h and 117.15 mm/h for Durban, 0 .003 mm/h and 78.15 mm/h for Butare respectively. Rain events with overall sum of drops less than 10 were discarded from the data samples to compensate for the dead- time errors. The location is shielded from unwanted winds, hence, very minimal equipment outage was observed during the period of data collection in these locations. The selected rain rate values were taken from the rain events that occurred on the 15^{th} of April 2012 at Butare and 25^{th} of April 2009 at Durban. Tables 5-2 and 5-3 show the threshold of the drop size bins and the measured drops for the selected rain rates at Butare and Durban respectively. The asterisks (*) represent lack of rain drops in the bin. This lack of raindrops becomes more prominent at lower channels as the rain rate increases. A more detailed discussion of these Tables is provided under section 5-5.

5.4 Estimation of DSD Input Parameters and Modeling

The various input parameters for the DSD models already discussed in Section 2.10.3 and 2.10.6 for Butare and Durban is represented in Table 5-4. The method of moments discussed in section 3.41 is used to estimate these parameters in this section It should be mentioned that these parameters are functions of rain rate and the value of μ for the gamma DSD model is assumed to be 2 at these locations. Figures 5-3 (a) to (d) show the parameter fittings for the proposed DSD models at these locations at the rain rate values of 3.5, 10, 25 and 50 mm/h, respectively. In general, the gamma model overestimates the measured data at all rain rates as the drop diameter and rain rate increases. The lognormal model underestimates the measured DSD between the diameter range of 0.4 and 1.1 mm at Durban especially at low rain rate values. Maximum *N (D)* is observed for the two models at $D \geq 0.7$mm. It is observed that *N (D)* becomes wider as the rain rate increases. This shows that larger raindrops occur at higher rain rates (see Tables 5-2 and 5-3).

Table 5-2: Drop size bins and measured raindrops from disdrometer for the selected rain rates at Butare

Date of rain event: 15-04-2012							
Time of rain event		**05:13**	**05:09**	**11:07**	**10:31**	**10:26**	**10:20**
Rain rate (mm/h)		**1.27**	**3.69**	**9.53**	**25.32**	**62.60**	**78.51**
Bins i	**Mean Diameter** D_i	**Raindrops**					
1	0.359	5	1	*	*	*	*
2	0.455	6	1	*	*	*	*
3	0.551	30	11	1	*	*	*
4	0.656	31	40	4	*	*	*
5	0.771	12	24	8	*	*	*
6	0.913	28	34	34	11	*	*
7	1.112	94	74	100	34	*	*
8	1.331	13	103	85	38	7	3
9	1.506	*	26	43	37	11	20
10	1.656	*	15	56	35	59	52
11	1.912	*	5	64	75	122	130
12	2.259	*	*	22	53	122	131
13	2.584	*	*	1	31	90	101
14	2.869	*	*	1	16	55	80
15	3.198	*	*	*	23	50	71
16	3.544	*	*	*	12	28	31
17	3.916	*	*	*	3	20	21
18	4.35	*	*	*	1	4	10
19	4.859	*	*	*	*	1	3
20	5.373	*	*	*	*	*	*
Total number of drops		**219**	**334**	**419**	**369**	**569**	**653**

Table 5-3: Drop size bins and measured raindrops from disdrometer for the selected rain rates at Durban

Date of rain event: 25-04-2009							
Time of rain event		**17:02**	**16:41**	**16:46**	**16:05**	**16:52**	**16:51**
Rain rate (mm/h)		**1.67**	**3.49**	**8.45**	**19.48**	**47.56**	**117.15**
Bins i	**Mean Diameter** D_i	**Raindrops**					
1	0.359	7	3	*	*	*	*
2	0.455	23	2	2	*	*	*
3	0.551	24	1	16	1	1	*
4	0.656	24	*	20	1	3	*
5	0.771	22	2	15	*	8	*
6	0.913	33	1	22	3	54	7
7	1.112	43	1	21	13	182	74
8	1.331	28	8	18	5	191	115
9	1.506	17	4	9	4	132	145
10	1.656	3	8	11	5	117	172
11	1.912	3	4	9	17	172	327
12	2.259	*	1	4	20	114	274
13	2.584	*	4	3	6	43	155
14	2.869	*	5	4	9	30	127
15	3.198	*	6	10	23	5	27
16	3.544	*	*	4	21	2	4
17	3.916	*	1	2	6	1	8
18	4.350	*	*	2	2	*	5
19	4.859	*	*	1	*	*	7
20	5.373	*	*	*	1	10	20
Total number of drops		**227**	**51**	**173**	**137**	**1065**	**1467**

Table 5-4: Proposed input parameters for Butare and Durban

Lognormal DSD models		
Parameters	**Butare (Rwanda)**	**Durban (South Africa)**
a_o	93.34	215.15
b_o	0.2371	0.3203
A_μ	-0.0337	-0.2519
B_μ	0.1835	0.1562
A_σ	0.0731	0.073
B_σ	0.0076	0.0096
Gamma DSD models		
μ	2	2
N_o	$12020R^{-0.439}$	$5340R^{-0.307}$
Λ	$4.8049R^{-0.21}$	$5.9786R^{-0.19}$

5.5 Comparison with Other DSD Models

A comparative analysis of the proposed models for these locations with observations over other countries in the tropical, sub-tropical and equatorial regions is illustrated in Figures 5-4 (a) and (b) at R = 25 and 100 mm/h respectively using the parameters in Table 5-5. The lognormal *N(D)* coefficients for the countries shown in Table 5-5 are those obtained from [*Ajayi and Olsen*, 1985] for Nigeria, [*Maitra*, 2004] for India, [*Kesavan et al*, 2013] for Malaysia, and [*Timothy et al*, 2002] for Singapore. For the two rain rates considered, the Indian *N(D)* gives the highest peak followed by Singapore. The India and Singapore distributions however show the narrowest distributions compared to other countries in the regions. Although the DSD for Rwanda and Nigeria covers a wider distribution up to 5.5 mm, they have the lowest DSDs compared to other countries. Malaysia and South Africa distributions are similar at diameters below 1 mm at these rain rates.

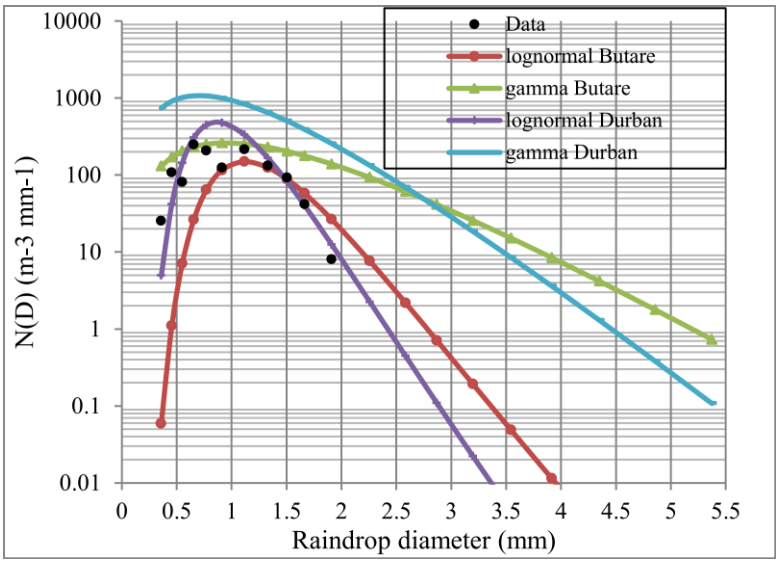

(a)

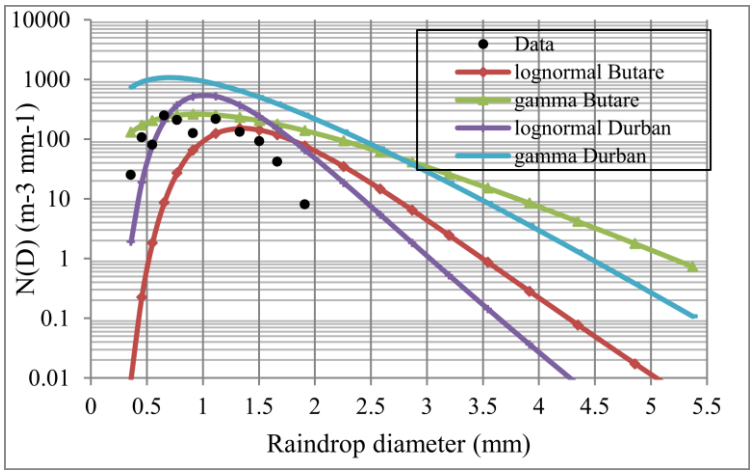

(b)

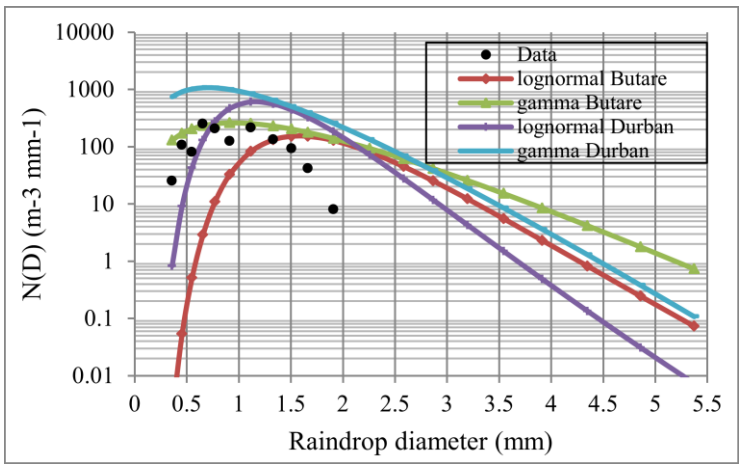

(c)

Figure 5-3: Drop size distribution and raindrop diameters at (a) R = 3.5 mm/h (b) R= 10 mm/h (c) R= 25 mm/h (d) R = 50 mm/h

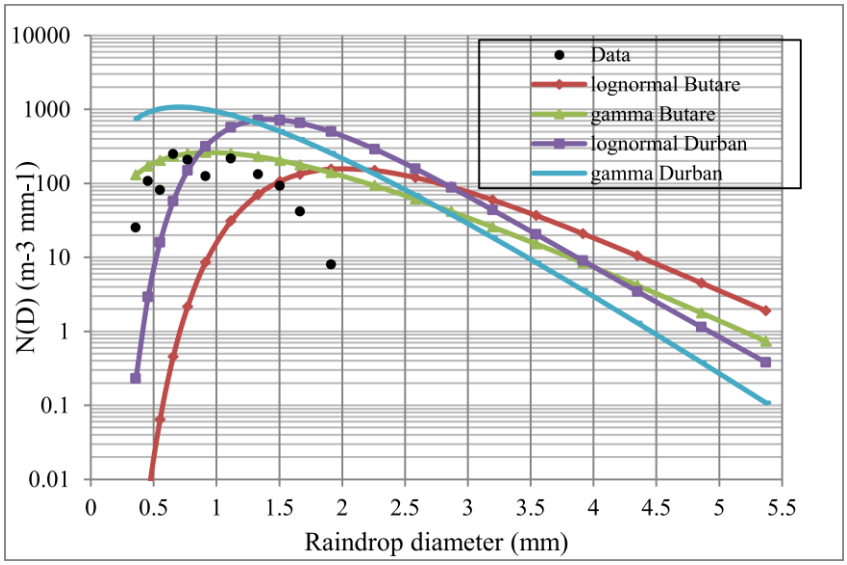

(d)

Figure 5-3: Drop size distribution and raindrop diameters at R = 50 mm/h

- Data is the measured data from the disdrometer

Table 5-5: Coefficients of lognormal for some tropical countries

Coefficients	Rwanda	South Africa	Nigeria	Malaysia	India	Singapore
a_0	93.34	215.15	108	45.325	546	276.18
b_0	0.2371	0.3203	0.363	0.6703	0.469	0.3815
A_μ	-0.0337	-0.2519	-0.195	-0.3914	-0.538	-0.4286
B_μ	0.1835	0.1562	0.199	0.1873	0.017	0.1458
A_σ	0.0731	0.073	0.137	0.4072	0.0689	0.1564
B_σ	0.0076	0.0096	0.013	-0.0586	0.076	0.00913

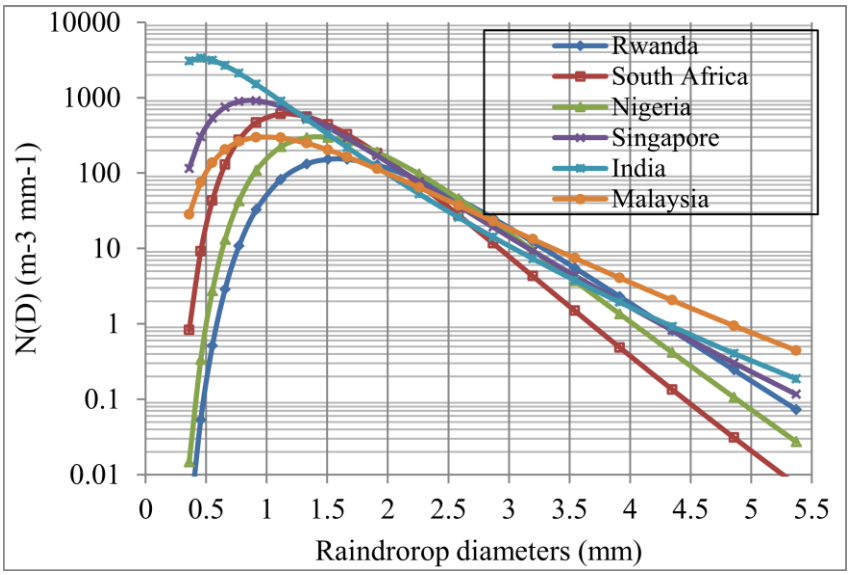

(a)

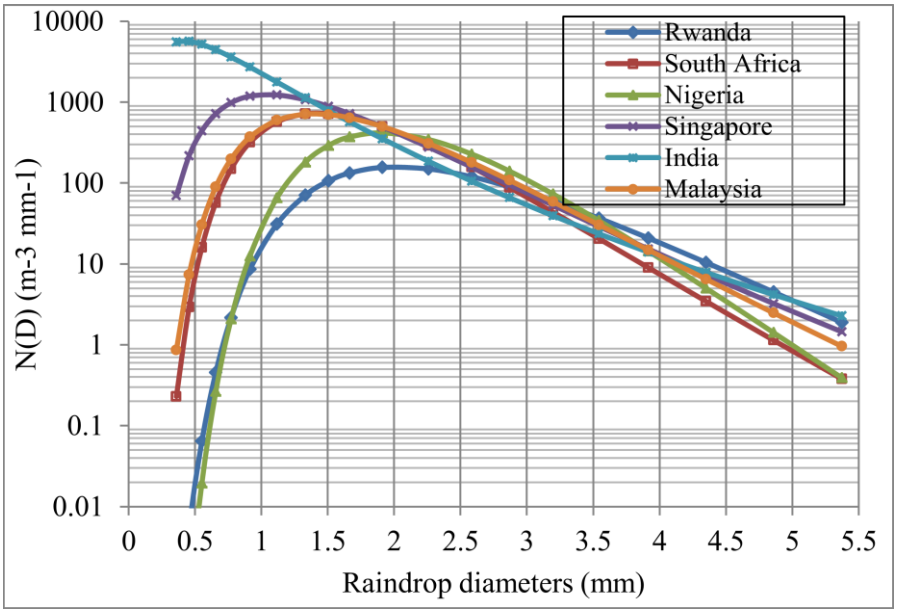

(b)

Figure 5-4: Comparison of the drop size distribution variations in the tropical, sub-tropical and equatorial regions (a) R = 25 mm/h (b) R = 100 mm/h.

5.6 The Role of Raindrop Diameters on Measured Rain Rate and Attenuation

The effect of the bins removal on the measured rainfall rate and attenuation due to rain is discussed in this section. Firstly, the influence of the bins removal on the measured rain rate using equation (2.33) is illustrated in Figures 5-5 and 5-6 for Butare and Durban respectively. The gamma and lognormal DSD models are used. The bins are removed (with or without raindrops) in consecutive and alternate manners. It is observed that the measured rain rate does not alter significantly as lower bins 1 to 4 are removed. Similarly, the removal of the larger diameters does not affect the measured rain rate.

As observed in Tables 5- 2 and 5-3, the largest raindrop for lower rain rates (1.27 and 3.69 mm/h) at Butare and (1.67 and 3.49 mm/h) at Durban occurred mostly in bins 7 and 8. As the rain rate increases, lower bins tend to contain low or no drops while the maximum drops is observed in bins 11 and 12 for Butare and Durban. The critical raindrop channels therefore lies at the center of the disdrometer bin for $D \geq 0.771$mm. Table 5-6 illustrates the effect of bins removal on the specific rain attenuation and rain rate for the two models at a given frequency at Butare and Durban respectively. The specific rain attenuation increases with increased rain rate and frequency. When the lower bins are removed, the computed specific rain attenuation at the two stations is not altered but the larger diameters affect the specific attenuation as observed in Tables 5-6(a) and (b). The measured rain rates and specific rain attenuation are less affected by the removal of lower bins while the removal of larger channels (bins) greatly affects the specific rain attenuation especially as the rain rate increases.

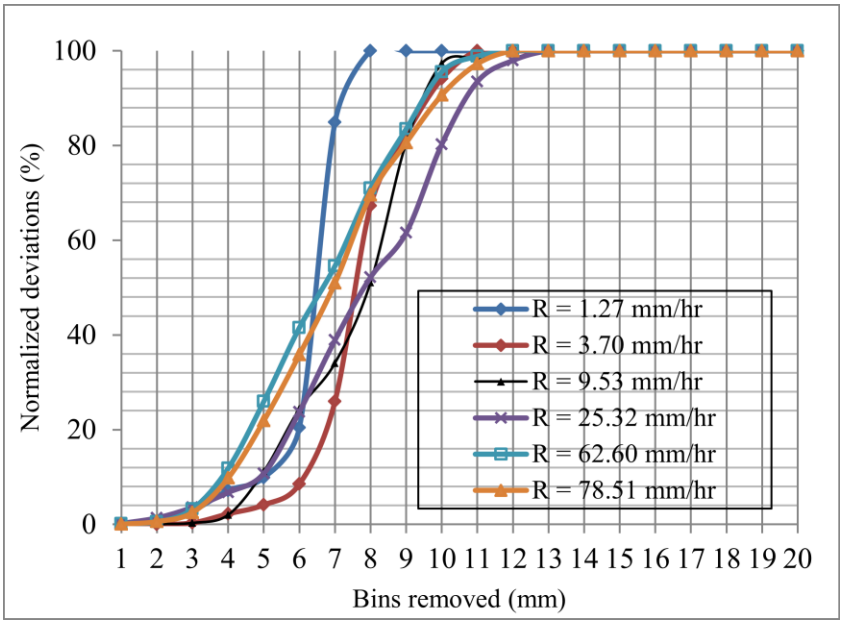

(a)

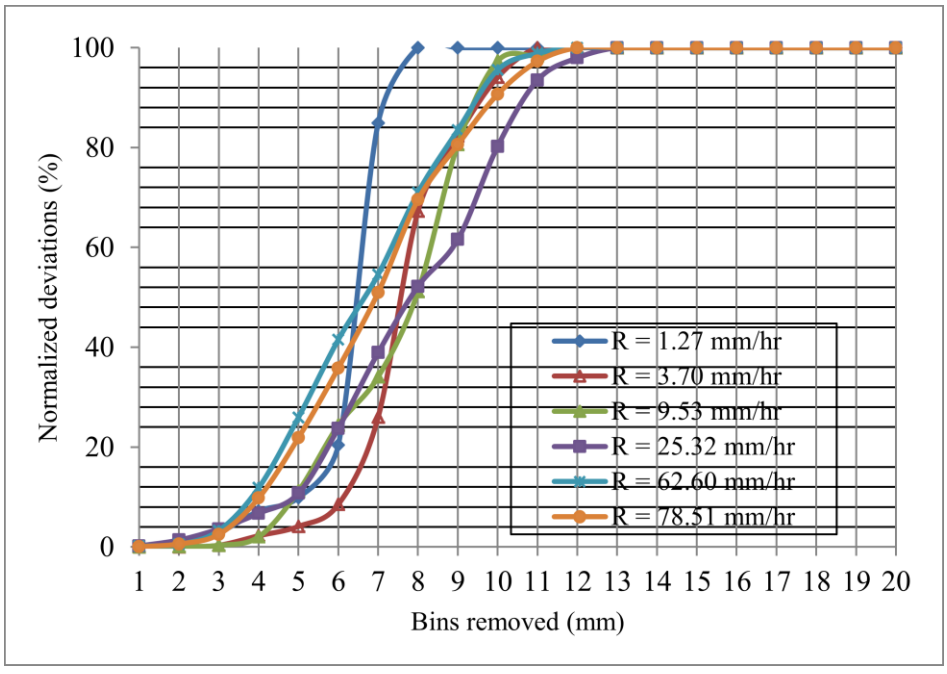

(b)

Figure 5-5: Normalized deviation of bins removal for gamma and lognormal models at Butare

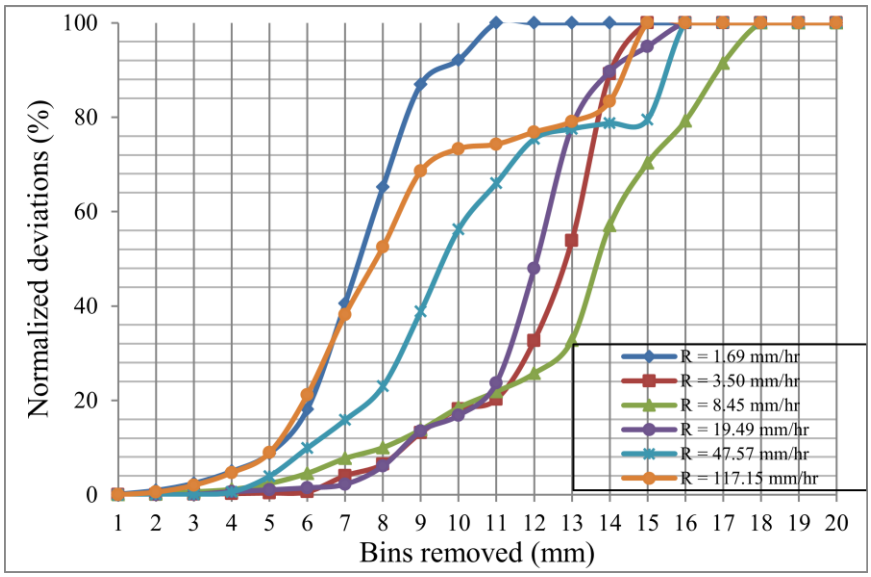

(a)

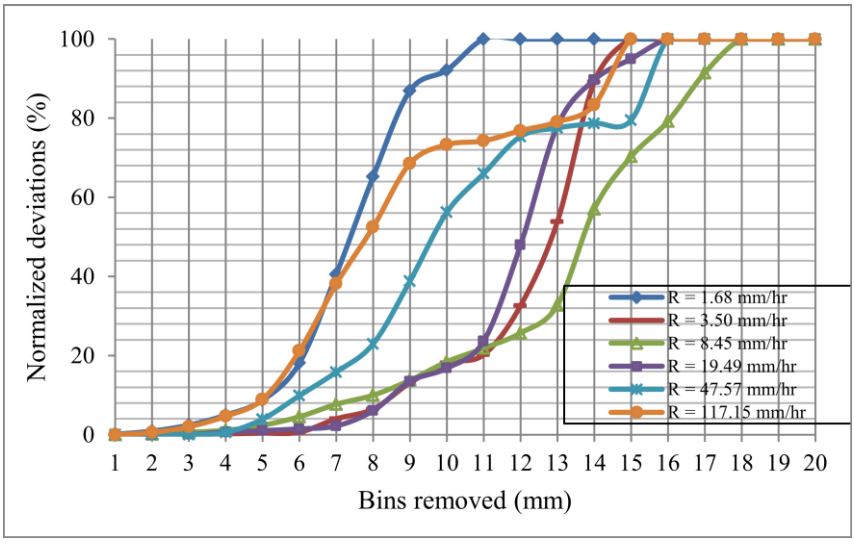

(b)

Figure 5-6: Normalized deviation of bins removal for gamma and lognormal models at Durban

Table 5-6 (a): Rain attenuation with bins removal at *f* = 19.5, 35 and 40 GHz for gamma and lognormal DSD models for Butare, Rwanda.

19.5 GHz						
	Gamma model			**Lognormal model**		
Rain rate (mm/h)	All bins B1-B20	Bins removed B1-B4	Bins removed B17-B20	All bins B1-B20	Bins removed B1-B4	Bins removed B17-B20
1.27	0.076	0.071	0.076	0.076	0.070	0.076
3.69	0.242	0.236	0.242	0.240	0.234	0.240
9.53	0.668	0.668	0.668	0.666	0.665	0.666
25.32	1.877	1.877	1.750	1.893	1.893	1.763
62.60	4.682	4.682	3.922	4.844	4.844	4.033
78.51	5.820	5.820	4.730	6.073	6.073	4.895
35 GHz						
Rain rate (mm/h)	**Gamma model**				**Lognormal model**	
	All bins B1-B20	Bins removed B1-B4	Bins removed B17-B20	All bins B1-B20	Bins removed B1-B4	Bins removed B17-B20
1.27	0.215	0.200	0.215	0.218	0.203	0.218
3.69	0.601	0.588	0.601	0.606	0.593	0.606
9.53	1.490	1.489	1.490	1.508	1.506	1.508
25.32	3.764	3.764	3.533	3.837	3.837	3.599
62.60	8.617	8.617	7.334	8.930	8.930	7.569
78.51	10.511	10.511	8.697	10.958	10.958	9.015
			40 GHz			
	Gamma model				**Lognormal model**	
Rain rate (mm/h)	All bins B1-B20	Bins removed B1-B4	Bins removed B17-B20	All bins B1-B20	Bins removed B1-B4	Bins removed B17-B20
1.27	0.264	0.246	0.264	0.267	0.250	0.267
3.69	0.711	0.696	0.711	0.719	0.704	0.719
9.53	1.710	1.709	1.710	1.732	1.731	1.732
25.32	4.191	4.191	3.942	4.273	4.273	4.016
62.60	9.355	9.355	8.000	9.677	9.677	8.244
78.51	11.348	11.348	9.439	11.800	11.800	9.766

Table 5-6(b): Rain attenuation with bins removal at *f* = 19.5, 35 and 40 GHz for gamma and lognormal DSD models for Durban, South Africa.

19.5 GHz						
Gamma model				**Lognormal model**		
Rain rate	All bins	Bins removed	Bins removed	All bins	Bins removed	Bins removed
	B1-B20	B1-B4	B17-B20	B1-B20	B1-B4	B17-B20
1.67	0.094	0.089	0.094	0.093	0.088	0.093
3.49	0.206	0.205	0.182	0.204	0.203	0.180
8.45	0.527	0.523	0.362	0.521	0.517	0.358
19.50	1.281	1.281	0.985	1.267	1.267	0.974
47.57	3.295	3.295	2.560	3.267	3.266	2.530
117.15	8.439	8.439	6.204	8.397	8.397	6.163
			35 GHz			
Gamma model				**Lognormal model**		
Rain rate	All bins	Bins removed	Bins removed	All bins	Bins removed	Bins removed
(mm/h)	B1-B20	B1-B4	B17-B20	B1-B20	B1-B4	B17-B20
1.67	0.290	0.276	0.290	0.294	0.280	0.294
3.49	0.587	0.586	0.526	0.593	0.592	0.531
8.45	1.371	1.363	0.978	1.379	1.371	0.985
19.50	3.058	3.058	2.412	3.070	3.069	2.422
47.57	7.182	7.181	5.715	7.206	7.205	5.734
117.15	16.855	16.855	12.742	16.927	16.927	12.790
			40 GHz			
Gamma model					**Lognormal model**	
Rain rate	All bins	Bins removed	Bins removed	All bins	Bins removed	Bins removed
(mm/h)	B1-B20	B1-B4	B17-B20	B1-B20	B1-B4	B17-B20
1.67	0.365	0.348	0.365	0.371	0.354	0.371
3.49	0.723	0.722	0.650	0.732	0.731	0.658
8.45	1.646	1.636	1.186	1.658	1.648	1.196
19.50	3.581	3.580	2.845	3.598	3.598	2.860
47.57	8.192	8.191	6.564	8.227	8.226	6.593
117.15	18.748	18.748	14.288	18.838	18.838	14.351

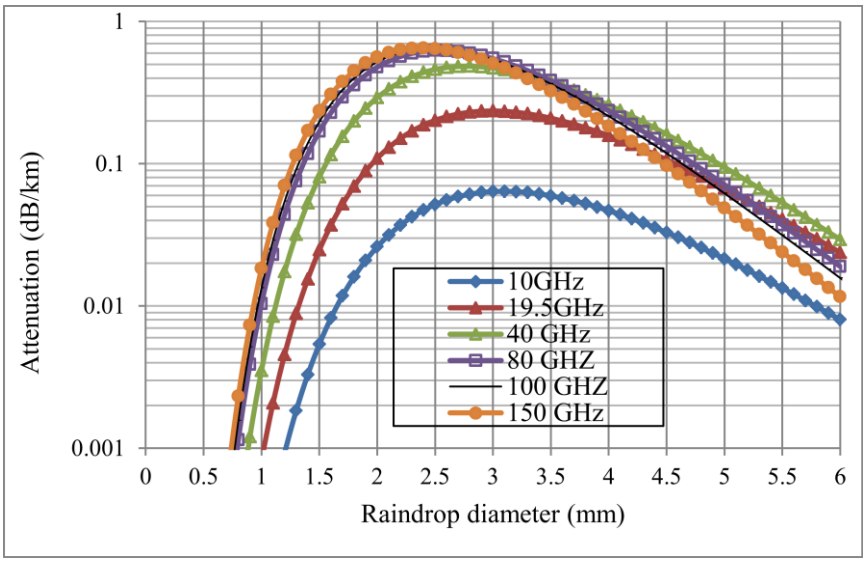

(a)

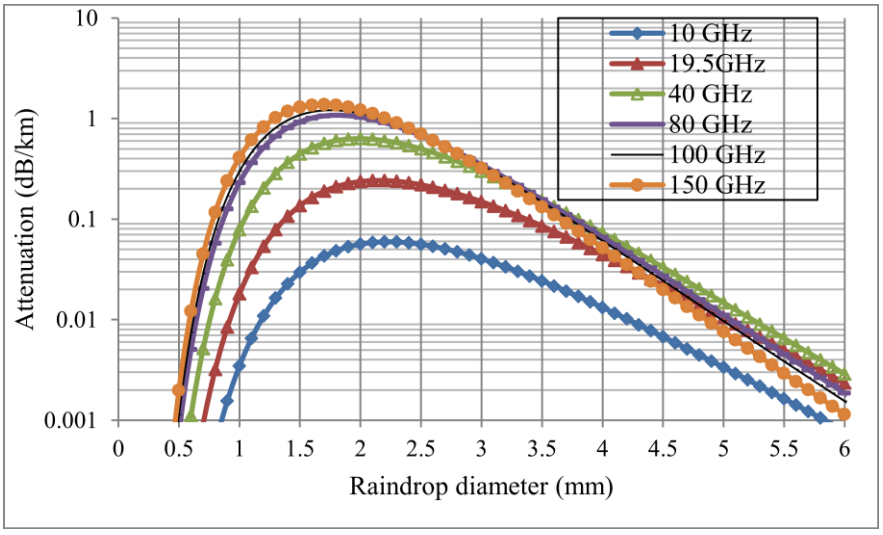

(b)

Figure 5-7: Contributions of individual drop diameters to attenuation at various frequencies for (a) Butare (b) Durban.

By using the estimated $R_{0.01}$ values for Rwanda and South Africa in section 5.1, the contribution of the individual raindrop diameters to the total attenuation at these locations are also compared and

shown in Figures 5-7(a) and (b). As observed, the highest contribution to the rain attenuation occurs

Table 5-7: Percentage (%) fraction of the specific attenuation formed by diameter range (mm) to the overall attenuation at f = 10-150 *G*Hz at Butare ($R_{0.01}$ = 73.88 mm/h)

f (GHz)	$0.1 \leq D \leq 2.0$	$0.5 \leq D \leq 2.5$	$1.0 \leq D \leq 3.0$	$1.5 \leq D \leq 3.5$	$4.0 \leq D \leq 7.0$
10	5.66	18.16	36.14	54.29	32.54
19.5	6.92	20.96	39.97	58.08	29.05
40	10.47	28.02	48.82	66.03	21.96
60	13.69	33.67	55.18	71.06	17.56
80	16.32	37.86	59.56	74.15	14.85
100	18.36	40.93	62.59	76.11	13.09
150	21.50	45.34	66.73	78.50	10.87

Table 5-8: Percentage (%) fraction of the specific attenuation formed by diameter range (mm) to the overall attenuation at f = 10-150 *G*Hz at Durban ($R_{0.01}$ = 66.25 mm/h)

f (GHz)	$0.1 \leq D \leq 2.0$	$0.5 \leq D \leq 2.5$	$1.0 \leq D \leq 3.0$	$1.5 \leq D \leq 3.5$	$4.0 \leq D \leq 7.0$
10	27.84	52.46	72.20	79.98	8.58
19.5	31.52	56.67	75.56	81.04	7.04
40	40.33	65.70	82.00	81.65	4.39
60	46.92	71.63	85.64	80.62	3.05
80	51.59	75.45	87.68	79.19	2.33
100	54.88	77.98	88.89	77.84	1.91
150	59.46	81.28	90.22	75.49	1.43

for the raindrop diameters not exceeding 2 mm. Tables 5-7 and 5-8 show the percentage contribution of the drop diameters to specific attenuation at different frequencies. The largest contribution to the total attenuation is observed at the diameter range $1.5 \leq D \leq 3.5$ mm at Butare and for Durban at frequencies below 40 GHz. At frequencies above 40 GHz, the maximum contribution to the rain attenuation is observed in the diameter range $1.0 \leq D \leq 3.0$ mm in Durban. A minimal percentage contribution is observed at larger diameters as the frequency increases.

5.7 Chapter Summary

Raindrop size distribution measurements obtained from Butare, Rwanda and Durban, South Africa has been analyzed in this chapter. The proposed three-parameter lognormal and gamma models are adequate for the modeling of the drop size distributions at these locations. The modeled distributions are also compared with those of some countries in the tropical, subtropical and equatorial regions. Results reveal that the removal of larger diameters of the bins affects the specific rain attenuation at these locations especially at high rain rates. The removal of raindrop bins 1 to 4 does

not have any significant effect on the total attenuation and overall measured rain rate. The major contribution to the overall measured rain rate was observed at diameter $D \geq 0.771$mm. This is in agreement with the results by *Lee et al* [2007 and *Kumar et al* [2010] in Singapore, and *Fiser* [2002] in the Czech Republic. Similarly, using the $R_{0.01}$ values estimated for these locations, the largest contributions to the total rain attenuation is associated with drop diameters in the range $1.5 \leq D \leq 3.5$mm and $1.0 \leq D \leq 3.0$ mm for Butare and Durban respectively. The amount of rain attenuation produced with the removal of the larger diameters is however significant at both sites. This shows that the smaller bins can be discarded while estimating the rain rate and specific attenuation, since they do not alter the estimated values significantly. Adequate knowledge of this estimated attenuation characteristics will be necessary for predicting the accurate fade margin, required to achieve the expected quality of service on radio communication systems operating in these locations for link budget designs on satellite and terrestrial links.

CHAPTER SIX

COMPUTATION OF CROSS-POLARISATION DUE TO RAIN OVER DURBAN IN SOUTH AFRICA

6.1 Introduction

Depolarization due to raindrops and ice crystals is caused by the differential attenuation and the differential phase shift between the major (horizontal) and the minor (vertical) axes of the hydrometeors. While the rain effects are predominant in C-band **(**6/4 GHz), the ice effects become more considerable in Ku-band (14/11 GHz) and sometimes quite significant in Ka-band (30/20 GHz) [*Brussaard*, 1974; *Chu*, 1974]. The computation of the cross polarisation caused by rain (XPD) at frequency band 10-35 *GHz* over Durban (29^{o}52'S, 30^{o} 58'E) is carried out in this chapter. Two elevation angles of 23^{o} and 55^{o} are assumed for wave propagation along the coastal region. The globally accepted lognormal drop size distribution model for tropical region has been used to compute the raindrop sizes assumed to be spherical at 20^{o}C. The power law relationship between attenuation and rainfall rate based on the measured complimentary cumulative distribution function (CCDF) of rain rates in Durban is used to estimate the total attenuation. The ITU-R procedure in recommendation 618-9 [*ITU-R P*. 2007] is employed for the estimation of the cross polarisation discrimination due to rain on earth-satellite path. The variation of the estimated values of XPD with co-polar attenuation (CPA), frequencies and rain rates at these elevation angles is also discussed. The circular polarisation for earth-satellite propagation paths is assumed for the purpose of analysis.

6.2 Depolarisation of Radio Waves by Rain

The orientation of the lines of the electric flux in an electromagnetic (EM) field is generally referred to as wave polarisation. The use of orthogonal polarisations allows two independent information channels using the same frequency band to transmit signals over a single link. This method is useful in satellite communication systems to effectively increase the available spectrum. However, some degrees of interference between these channels are inevitable due to depolarizing effects caused by scattering and absorption of the hydrometeor (rain, ice, etc.) along the propagation path. This depolarisation is due to the non-spherical symmetry of the raindrops (the top and bottom are flattened), along with their tendency to have a preferred orientation. Depolarisation results in cross talk between two orthogonal polarized channels, transmitted on the same path and frequency band [*Barclay*, 2003; *Van de Kamp*, 2001; *Ajewole*, 1997; *Brussaard and Watson*, 1997; *Oguchi*, 1983]. As

a result of this, radiowaves propagating through them suffers differential attenuation and phase shift. This also may constitute a problem in communication systems using polarisation orthogonality to maintain isolation between channels. Differential attenuation and phase below 18 GHz increases with frequency for a given rain event; they however decrease for a given fade depth [*Barclay*, 2003]. This is partly because less deformed smaller drops make a greater relative contribution to the total attenuation as frequency is increased. Polarisation can be linear or circular (elliptical).The most general case of polarisation is the elliptical or circular polarisation. The electric field vector **E** (*t*), is expressed by *Brussaard and Watson*, [1997] by equation (6.2) composed of two sinusoidal components, having different amplitudes $|E_x|$ and $|E_y|$ and a phase difference $arg\left(\frac{E_y}{E_x}\right)$:

$$\boldsymbol{E}(t) = \mathrm{R_e E} e^{jwt} = \mathrm{R_e}\left[\left(u_x E_x + u_y E_y\right) e^{jwt}\right] \tag{6.1}$$

$$= u_x|E_x|\cos(wt) + u_y|E_y|\cos(wt + \phi) \tag{6.2}$$

where u_x, and u_y are the units vectors in the x- and y-directions respectively; ω is the angular frequency and *t* is the time. The phase is taken relative to the phase of E_x. As observed in equation (6.1), the polarisation may be frequency dependent and time varying as the hydrometeor changes. Oftentimes, EM waves transmitted along the principal planes arrive unchanged (in magnitude) but, experience differential attenuation and phase shifts. Consequently, any transmitted polarisation that is not one of the link's principal planes will be cross polarized on reception [*Barclay*, 2003; *Brussaard and Watson*, 1997]. It is important to mention that the relative contribution of differential attenuation and phase shift is different at different frequencies. Differential phase shift appears to be the dominant factor in rain induced depolarisation at frequencies below 10 GHz while differential attenuation becomes increasingly significant at higher frequencies. Linearly polarized waves have an infinite axial ratio (the ratio of the maximum to the minimum magnitude of the electric field vector) while circularly polarized waves have an axial ratio that lies between +1 and -1, corresponding to either left-hand circular polarisation (LHCP) or right-hand circular polarisation (RHCP) [*Brussaard and Watson*, 1997].

A reliable estimate of the depolarizing properties of tropical rainfall for terrestrial and earth space links therefore requires among other parameters; the investigation of the differential attenuation, differential phase shift, cross polarisation discrimination (*XPD*) in the orthogonal channels and the co-polar attenuation (*CPA*). The aim of this paper is to estimate the cross polarisation of millimeter waves in the Ku and Ka band frequencies caused by rainfall over Durban (29°52'S, 30° 58'E) at two elevation angles of 23° and 55° at frequency range 10-35 GHz. The elevation angles 23° and 55° are

for links above the Indian Ocean Region (IOR) and over the Atlantic Ocean Region (AOR) respectively. The ITU-R recommendation [*ITU-R P.618-9,* 2007] for propagation data and prediction methods required for the design of Earth-space telecommunications systems is adopted for the purpose of computation. An attempt is made to determine the variation of the XPD with co-polar attenuation (CPA), rainfall rate and frequency. The raindrop sizes are assumed spherical at 20^{o}C and the circular polarisation for Earth-satellite propagation paths is also assumed for the purpose of computation.

6.3 Related Studies on Cross Polarisation due to Rain

A good number of researchers have determined the propagation effects of cross polarisation caused by rain. Experimental results have shown the existence of a relationship between attenuation and depolarisation especially when rain depolarisation is dominant. This has been extensively discussed by *Nowland et al,* [1977]; *Dissanayake et al.* [1980] and *Chu* [1982]. In their separate studies, *Ajewole* [1997] and *Oguchi* [1983] showed that rain induced cross polarisation of radio waves has its roots in the differential attenuation and differential phase shift produced between the two polarisation states and in the slight tilt of the axis of symmetry (canting angle) of the raindrop away from the vertical due to wind effects. By assuming a constant canting angle of raindrops along a propagation path, *Oguchi and Hosoya* [1974] estimated the cross polarisation due to different rainfall rates. Similarly, *Ajewole et al.* [1999a] computed XPD due to rain for four tropical types of rain by adopting the method earlier proposed by *Oguchi* [1973].The effects of varying the canting angles of the raindrops was also investigated by *Ajewole et al*. [1999b] using different types of rain and raindrop sizes on cross polarisation discrimination and established that XPD improves by about 4-7 *dB* over those models having equal orientation. Recently, the dependence of XPD on co-polar attenuation, frequency and rainfall was estimated by *Ojo* [2012] over some stations in Nigeria at various elevation angles and frequencies. In this chapter, the computation of XPD at frequency range 10-35 GHz and at elevation angles of 23^{o} and 55^{o} is carried out over the eastern coast of South Africa assuming a spherical raindrop sizes at 20^{o}C. The variation of the estimated values of XPD with other parameters such as co-polar attenuation, rain rate and frequency is also discussed.

6.4 Experimental Setup

In this chapter, the rainfall rate data measured over a period of one year (January - December, 2009) using a Joss-Waldvogel (JW) RD-80 disdrometer measuring system has been utilized to estimate the cross polarisation caused by rain over Durban. Figure 6-1 and Table 6-1 show the complementary cumulative distribution function (CCDF) of the rainfall rate for the one year data in Durban and the specific relationship between the percentages of time the rain rate is exceeded.

Table 6-1: Rain rate distribution at various percentages of exceedence in Durban

Percentage of time rainfall rate is exceeded (%)	Rainfall rate (mm/h)
2	6.62
1	10.53
0.5	16.21
0.3	20.96
0.2	24.26
0.1	32.33
0.05	47.57
0.03	51.67
0.02	57.35
0.01	66.25

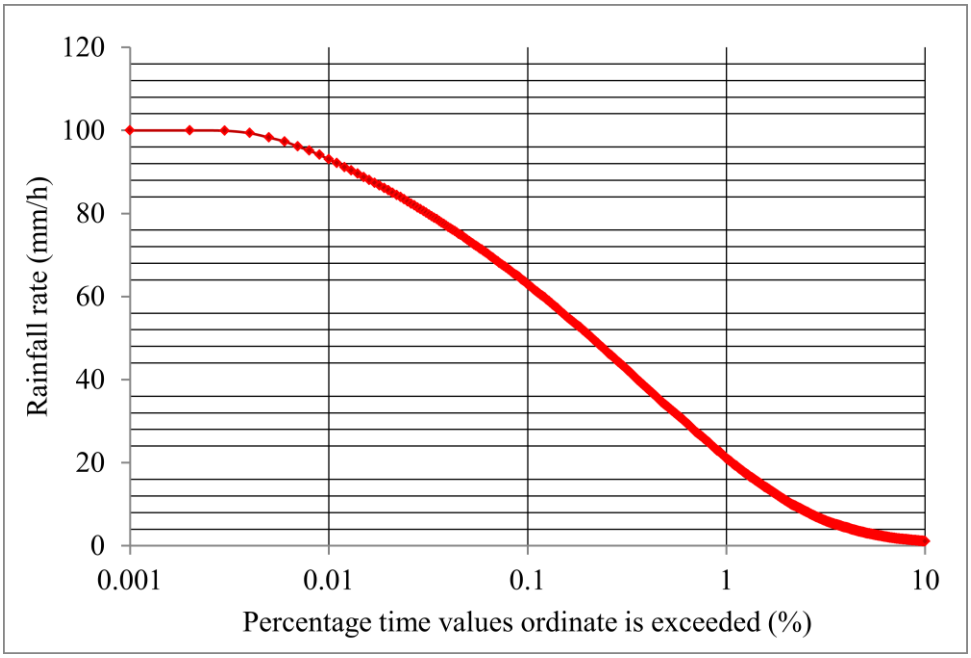

Figure 6-1: Rainfall rate complementary cumulative distribution function (CDDF) for Durban

Rainfall rate values of 32.33 mm/h, 66.25 mm/h and 101.56 mm/h were estimated at 0.1 %, 0.01 % and 0.001 % of time exceeded respectively.

6.5 Computational Procedures

The ratio (in dB) of the power in the co-polarised wave to the power in the cross-polarised wave that was transmitted in the same state is termed the cross polarisation discrimination due to rain (XPD_{rain}). In other words, it is the appearance in the course of propagation of a radio wave through the atmosphere, of a polarisation component which is orthogonal to the desired polarisation. It can be expressed mathematically as [see *Oguchi*, 1983; *Brussaard and Watson* 1995; *Ajewole and Afolayan*, 2008]:

$$XPD_{rain} = 20\log_{10}\left|\frac{E_{xx}}{E_{xy}}\right| \quad \text{(dB)} \tag{6.3}$$

where E_{xx} and E_{xy} are the co-polarized and cross polarised waves transmitted in the same polarisation states respectively. The ITU-R step-by step methods to compute the XPD_{rain} statistics are stated as follows (Appendix F-1):

Step 1: Calculate the frequency-dependent term:

$$C_f = 30\log f \text{ for } 8 \leq f \leq 35\ GHz \tag{6.4}$$

where f is the frequency in GHz.

Step 2: Calculate the rain attenuation dependent term:

$$C_A = V(f)\log A_p \tag{6.5}$$

where A_p is the estimated rainfall attenuation (in dB) exceeded for the required percentages of time. The estimated rainfall attenuation may also be computed from [*Van de Kamp*, 2001]:

$$V(f) = 12.8 * f^{0.19} \qquad \text{for } 8 \leq f \leq 20\ GHz \tag{6.5a}$$

$$V(f) = 22.6 \qquad \text{for } 20 < f \leq 35\ GHz \tag{6.5b}$$

Step 3: Calculate the polarisation improvement factor:

$$C_\tau = -10\log[1 - 0.484(1 + \cos 4\tau)] \quad (6.6)$$

where C_τ= 0 for τ = 45° and reaches the maximum value of 15 dB for τ = 0° or 90°.

Step 4: Calculate the elevation angle dependent term:

$$C_\theta = -40\log(\cos\theta) \qquad \text{for } \theta \leq 60^o \quad (6.7)$$

Step 5: Calculate the canting angle dependent term:

$$C_\sigma = 0.0052\sigma^2 \quad (6.8)$$

where σ is the effective standard deviation of the raindrop canting angle distribution (in degrees). It takes the value 0°, 5°, 10° and 15° for 1%, 0.1%, 0.01% and 0.001% of the time respectively. In this study, the value of 10° is used. The canting angle is chosen because the percentage of time rain rate is exceeded, $R_{0.01}$ used in this study is at 0.01 %.

Step 6: Calculate rain *XPD* not exceeded for *p %* of the time:

$$XPD_{rain} = C_f - C_A + C_\tau + C_\theta + C_\sigma \quad \text{(dB)} \quad (6.9)$$

6.6 Results and Discussions

The variation of XPD at various elevation angles and frequencies 12, 15, 20 and 35 GHz are shown in Figures 6-2 to 6-5. In general and at all frequencies, XPD decreases as frequency increases for all the elevation angles. As the elevation angle increases for a given frequency, the XPD increases. A larger value of XPD is observed as the percentage of time also increases. A difference of about 8-9 dB is observed between 0.1 % and 0.01% of time while a difference of about 5-6 dB is noticed between 0.01 % and 0.001% of time. A low value of XPD implies an increased interference (cross-talk) at the satellite receiver station. The following sub-sections further explain the variation of XPD with co-polar attenuation, rainfall rate and operating frequencies for different elevation angles.

6.6.1 XPD-CPA Relations in Durban

Figures 6-6 and 6-7 show the variations of the XPD and the rain attenuation exceeded for the required period of time, often called the co-polar attenuation (CPA) over the elevation angles at *f* =

15 GHz and 35 GHz respectively. It is observed that the CPA increases with decreasing angle of elevation. The cross polarisation discrimination degrades with increasing CPA. This shows an agreement with *Ajewole et al.* [1999a] and confirms the inverse relation between the CPA and XPD. This implies that signal degradation as a result of XPD is enhanced more by CPA for a given fade depth than due to XPD as the frequency decreases.

6.6.2 Variation of XPD with Frequency

It is important to mention that the relative contribution of differential attenuation and phase shift is different at different frequencies. Differential phase shift appears to be the dominant factor in rain induced depolarisation at frequencies below 10 GHz and differential attenuation becomes increasingly significant at higher frequencies. The dependence of XPD on frequency at the elevation angles for different rain events is shown in Tables 6-2 and 6-3. In general and for all the elevation angles, XPD decreases as the frequency of operation increases. However, at higher frequencies above 30 GHz, a sharp change in XPD values is observed. Cross-polar interference being higher at low frequencies signifies that low frequency systems are not subjected to serious degree of randomness in the polarization of the transmitted signal compared to the high frequency links which will require good level of polarisation isolation [*Ajewole and Afolayan*, 2008; *Ajewole et al.,* 1999]. The presence of ice crystals in the upper layer of rain clouds may also produce a greater contribution to depolarisation. Similarly, less deformed smaller drops make a greater relative contribution to the total attenuation as frequency is increased. The contributions of the differential attenuation and phase shift to cross polarisation at varying frequencies and the complex dielectric property of water which depends on frequency are also probable factors that may be responsible for the sudden change in the XPD as the frequency increases. The differential propagation reduces with frequency for a given fade depth.

6.6.3 XPD versus Rainfall Rate

The variation of XPD with rain rate at f = 15 GHz and 30 GHz is given in Figures 6-8 and 6-9. This is also illustrated in Table 6-4 at 12 and 30 GHz at the two elevation angles. An inverse relation is also observed between the XPD and rainfall rate at all angles of elevation. As the rainfall rate increases, XPD decreases. Table 6-5 shows the XPD-rain rate relation at different elevation angles operating at f = 12 and 30 GHz. At a given rain rate, the cross polarisation discrimination increases with increase in elevation angles. The cross polarization discrimination becomes poorer as the rain rate and frequency are raised. This results in poor interference level in the orthogonal channels.

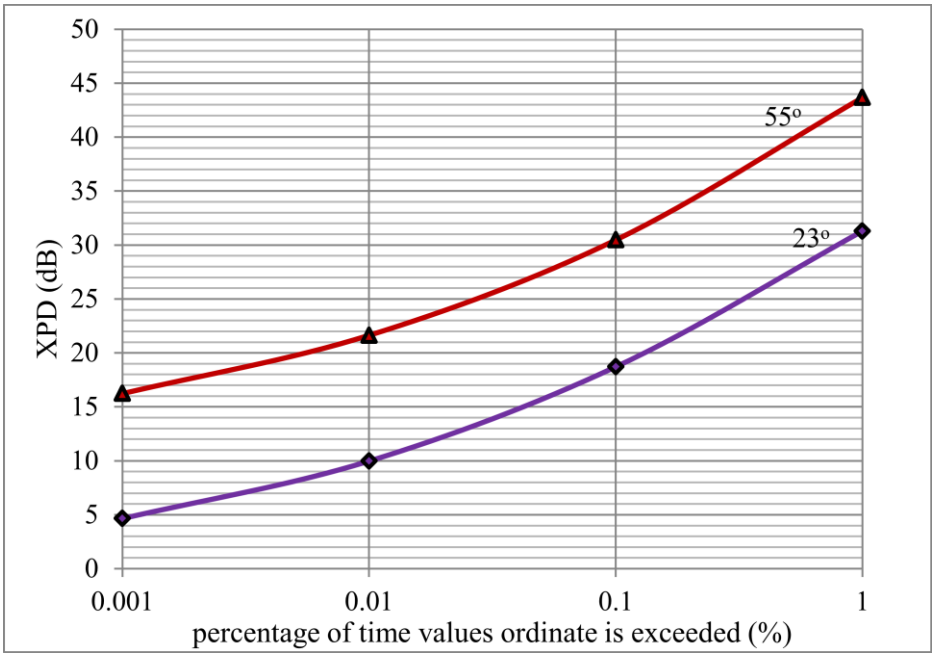

Figure 6-2: Cross polarisation discrimination (XPD) over different elevation angles at 12 GHz in Durban ($R_{0.01}$ = 66.25 mm/h).

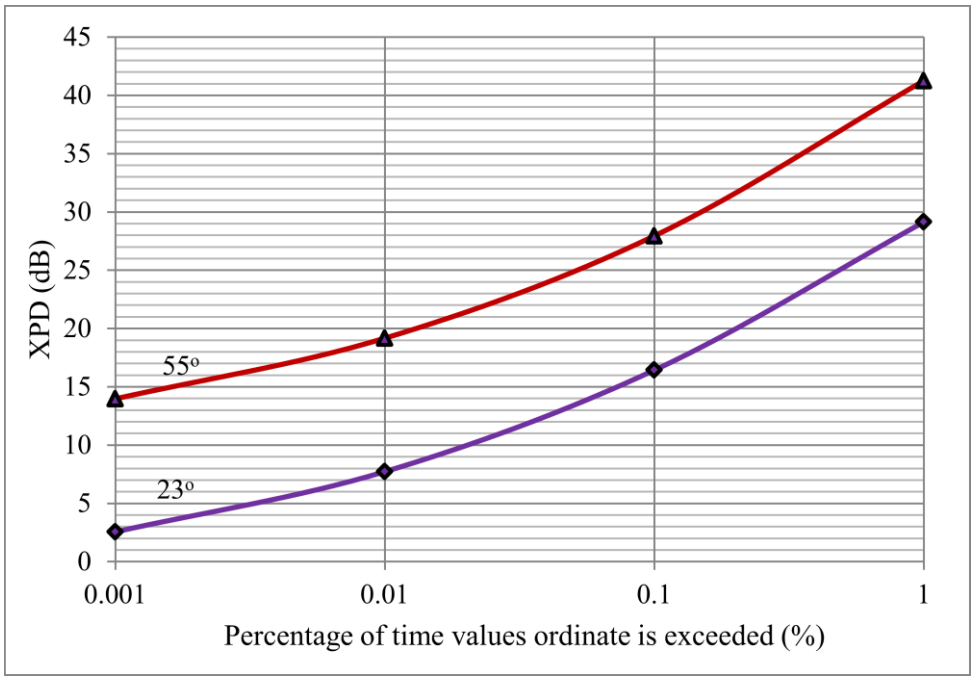

Figure 6-3: Cross polarisation discrimination (XPD) over different elevation angles at 15 GHz in Durban ($R_{0.01}$ = 66.25 mm/h).

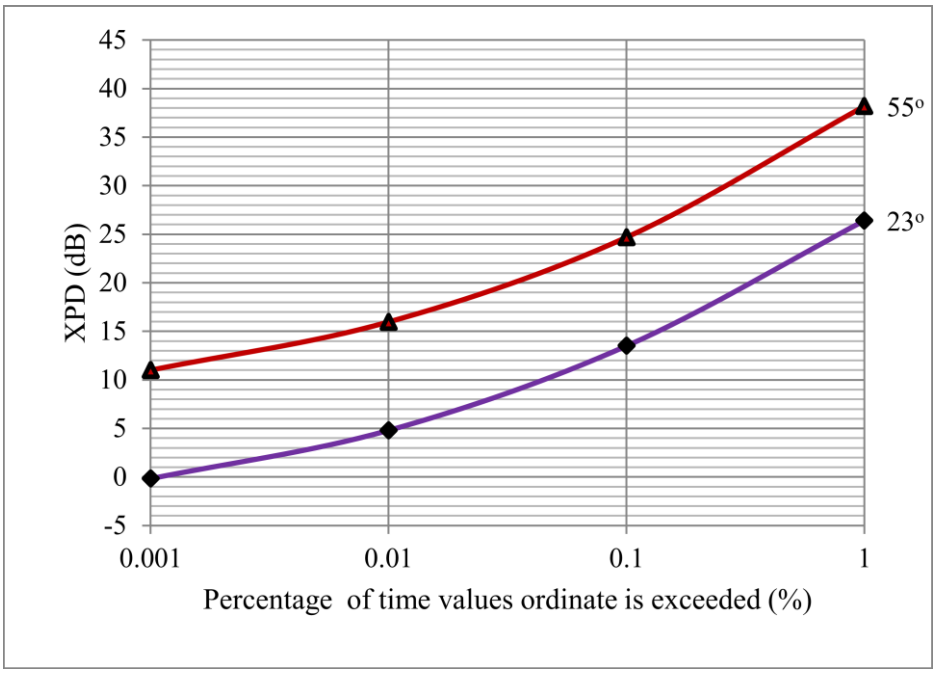

Figure 6-4: Cross polarisation discrimination (XPD) over different elevation angles at 20 GHz in Durban ($R_{0.01}$ = 66.25 mm/h).

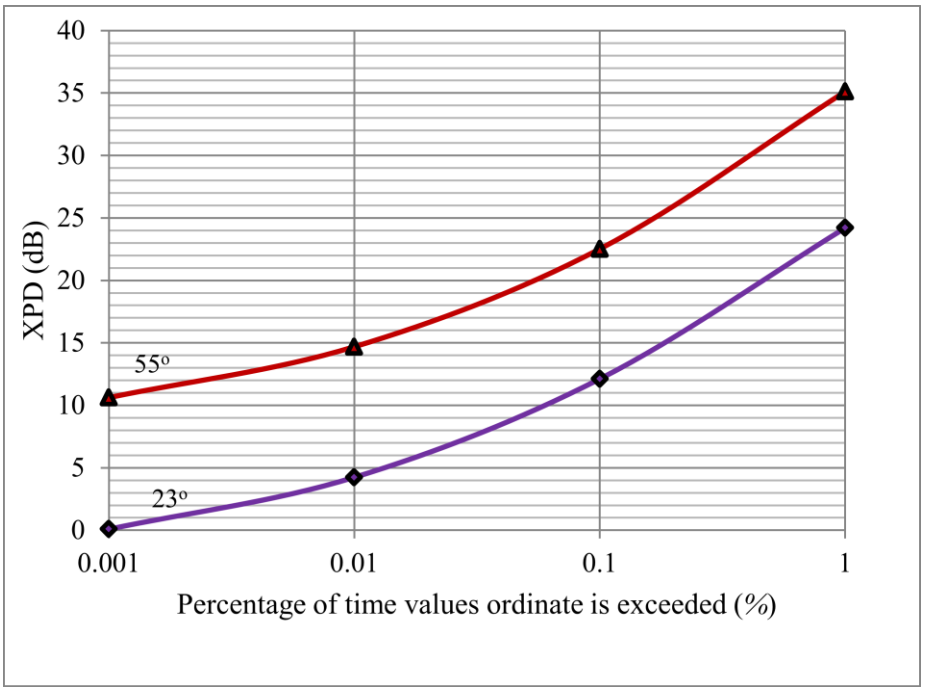

Figure 6-5: Cross polarisation discrimination (XPD) over different elevation angles at 35 GHz in Durban ($R_{0.01}$ = 66.25 mm/h).

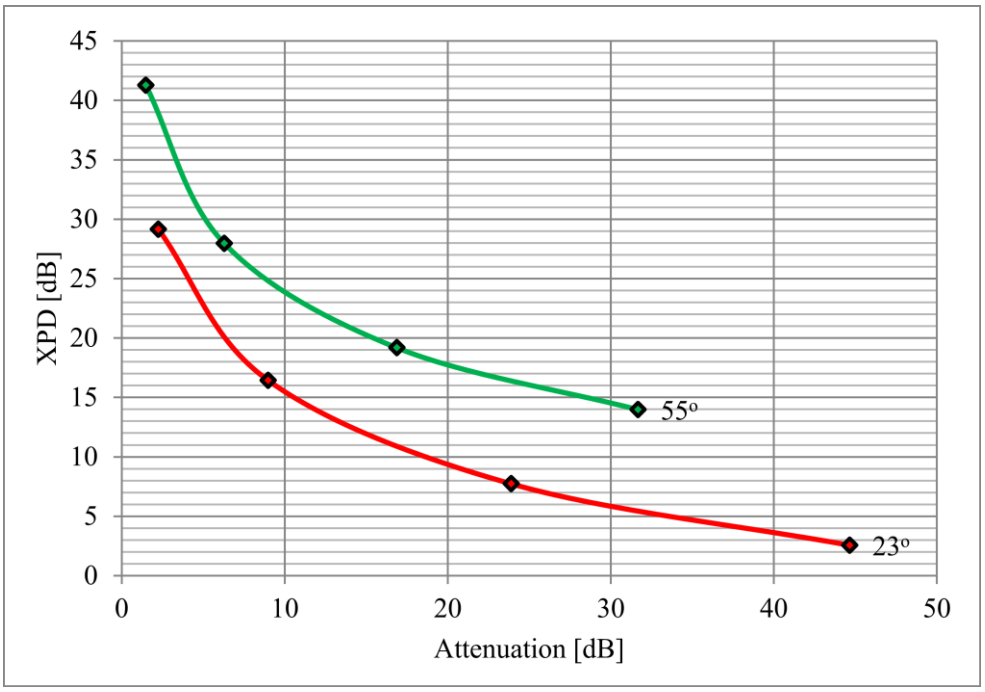

Figure 6-6: XPD versus Co-polar attenuation at 15 GHz

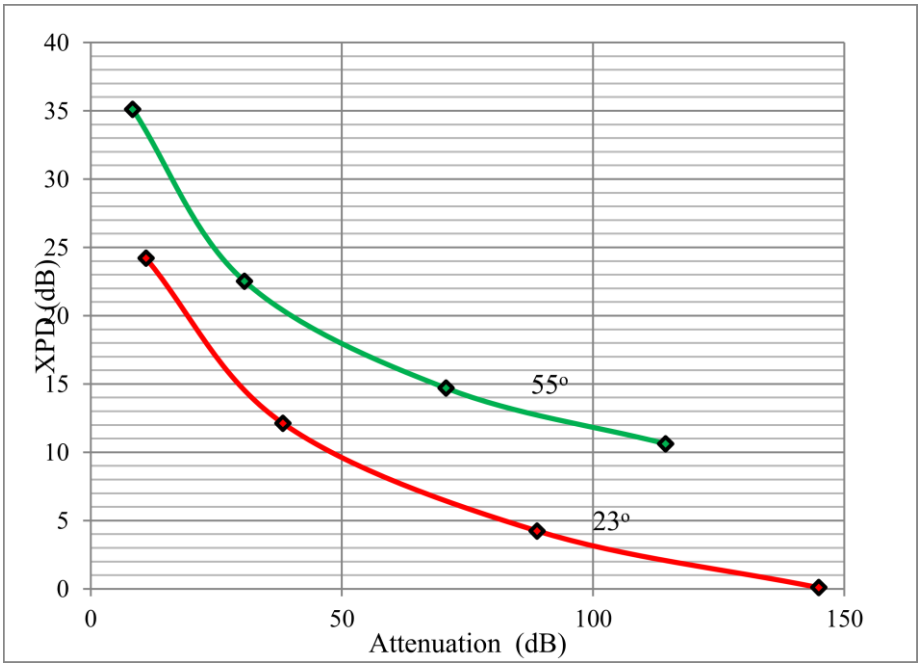

Figure 6-7: XPD versus Co-polar attenuation at 35 GHz

Table 6-2: Variation of XPD with frequency for different elevation angles at $R_{0.01}$

Frequency (GHz)	12	15	20	30	35
23°	31.297	29.139	26.407	24.497	24.202
	18.714	16.431	13.497	12.214	12.117
	9.978	7.726	4.801	4.142	4.242
	4.648	2.562	-0.170	-0.207	0.091
55°	43.667	41.259	38.188	35.609	35.119
	30.469	27.948	24.688	22.795	22.518
	21.636	19.176	15.969	14.757	14.695
	16.234	13.975	11.007	10.474	10.627

Table 6-3: Variation of XPD with frequency for different elevation angles at $R_{0.1}$

Frequency (GHz)	12	15	20	30	35
23°	36.249	34.169	31.567	29.319	28.869
	23.240	21.028	18.214	16.622	16.383
	14.079	11.892	9.075	8.136	8.108
	8.324	6.296	3.661	3.373	3.556
55°	48.806	46.502	43.610	40.749	40.121
	35.168	32.739	29.645	27.494	27.092
	25.892	23.518	20.461	19.015	18.839
	20.049	17.867	15.033	14.291	14.342

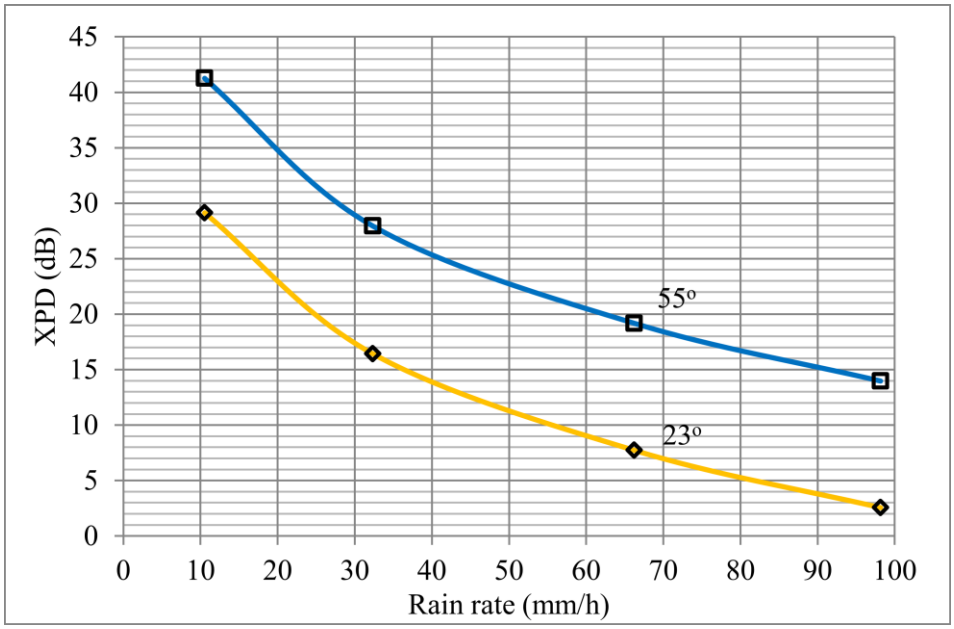

Figure 6-8: XPD versus rainfall rate at *f* = 15GHz

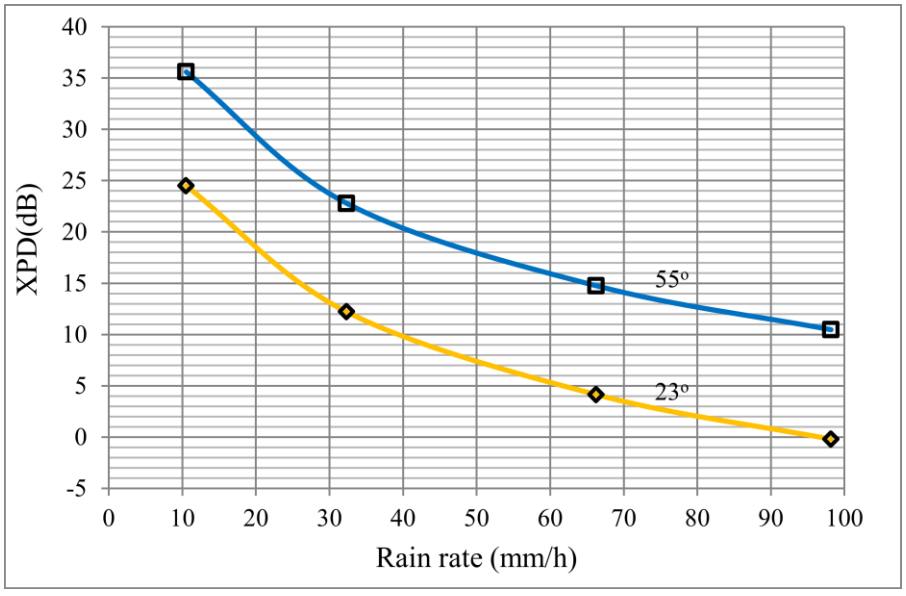

Figure 6-9: XPD versus rainfall rate at *f* = 30 GHz

12 GHz					
$R_{0.01}$(mm/h)		10.53	32.33	66.25	98.16
Elevation angle	23^o	31.297	18.714	9.978	4.648
	55^o	43.667	30.469	21.636	16.234
30 GHz					
Elevation angle	23^o	24.497	12.214	4.142	-0.207
	55^o	35.609	22.795	14.757	10.474

Table 6-4: Computed XPD values and rainfall rates at operating frequencies 12 an

6.7 Chapter Summary

The reliability of a transmission link is mostly determined from the quantities measured at one time or the other on the link. The computation of cross polarisation discrimination and its relationship to co-polar attenuation and other quantities along the Earth-space propagation paths at elevation angles of 23^o and 55^o and frequency band 10-35 GHz has been carried out in this chapter. From the results obtained, a linear difference of about 9 dB between 0.1 and 0.01percent of time is observed at all frequencies over the elevation angles. The XPD observed at 0.1% of time is higher than that of 0.01% at the same elevation angle and frequency. A lower value of XPD results in higher cross-talk or higher interference between the two orthogonal channels at the satellite receiver station. The results also show that cross polarisation discrimination degrades with increasing co-polar attenuation and decreases sharply as the elevation angle decreases due to the larger attenuation as a result of longer distance the signal travels at low elevation angles.

CHAPTER SEVEN

CONCLUSION AND SUGGESTIONS FOR FUTURE WORK

A brief summary of findings is presented in this chapter. Suggestions for future work are also highlighted.

7.1 Conclusion

In this study, an effort has been made to analyze and present the characteristics of the raindrop size distributions with the aid of the Joss-Waldvogel RD-80 impact disdrometer measurements obtained over a period of three years in Durban, a coastal region in South Africa. The study has been carried out to examine the appropriateness of various drop size distribution models, namely: lognormal, Weibull modified gamma and negative exponential, to the observed DSD spectra at different rain rate and rainfall regimes in Durban. Two methods of parameters estimation are compared; and the method of moments (MoM) was found to give better estimates when compared to the maximum likelihood estimation (MLE) method. A comparison of the DSD parameters with the disdrometer data showed a good correlation with the lognormal model as best fit for the region. The investigation showed that the DSD is influenced to a large extent by the intensity of rainfall.

By employing the Mie scattering technique at an ambient temperature of 20^{o}C for spherical rain droplets, the extinction cross sections at frequency of 1 to 500 GHz was computed for all the disdrometer bins using Liebe's refractive index functions. Mätzler's MATLAB codes were used to determine the scattering coefficients (Appendix D). This was required to investigate the variability of the DSD with the rainfall attenuation. A comparison of the specific attenuation values of the DSD models shows that the lognormal and the modified gamma models are suitable and adequate for the modeling of DSD in Durban. The lognormal model however gives a lower error value which makes it more suitable for the Southern Africa region. The proposed lognormal DSD model was also compared with other raindrop size distributions, namely: Rwanda, Nigeria, Malaysia, Singapore and India. The South Africa model shows a wider range of raindrop size distribution for the rain rates considered. The study also showed that specific rain attenuation varies with seasons, with the autumn season shows the highest attenuation compared to other seasons in Durban. Hence, seasonal effects must not be overlooked when analyzing the rain attenuation in specific seasons. In general, the raindrop size distribution has been found to influence to a large extent the variability of the attenuation characteristics with increasing rain rate frequency. This may result in significant problems in consistent availability of communication links.

Further investigation of the influence of the raindrop diameters (channels) on attenuation was also carried out in this study. Two critical diameters have been defined: the peak and the critical raindrop diameters. The peak diameter is the diameter at which the specific rain attenuation is maximum while the critical diameters are the range of diameters producing the highest attenuation for a given rain event. Seasonal, annual and regimes analysis were carried out. With the lognormal DSD, the peak diameter D_p , has been found in this study to be $D_p = exp[\sigma^2(\alpha - 1) + \mu]$. The peak attenuation for the drizzle and widespread occurs between $0.7 \leq D \leq 1.5$ mm, whereas for the shower and thunderstorm rainfall, the specific rain attenuation peaks between $1.3 \leq D \leq 2.7$ mm at all frequencies. The critical diameters are range of diameters over which the specific rainfall attenuation is most dominant. The maximum (peak) value of the rain attenuation is found to be in the range 0.5 mm $\leq D \leq$ 2.5 mm and 1.0 mm $\leq D \leq$ 3.0 mm for both the seasonal and overall values of $R_{0.01}$ in Durban. A comparative analysis of the DSD and the influence of the raindrop diameters on attenuation were carried out between Durban, a subtropical region and Butare, an equatorial region in Africa. The Butare data was analyzed using the estimated $R_{0.01}$ value, the critical range of diameters that produced maximum attenuation was found to be $1.5 \leq D \leq 3.5$mm. This range of diameters is critical to the overall determination of rain attenuation in these locations. However, at larger diameters in the range 4.0 mm $\leq D \leq$ 7.0 mm, the percentage contribution to rainfall attenuation was observably small. In general, the critical diameters are seen to coalesce around the peak diameter, D_p at which the maximum attenuation occurs. It should be noted that the peak diameter D_p is frequency dependent, since α is dependent on frequency. The parameters, μ and σ in Table 4-1 are region-dependent.

Lastly, cross polarisation due to rain over Durban has been estimated and the variations of the cross polarisation discrimination (XPD) with respect to operating frequency, rain rate and the elevation angles discussed. A linear difference of about 9 dB between 0.1 and 0.01 percent of time is observed at all frequencies over the elevation angles. The XPD observed at 0.1% of time is higher than that of 0.01% of the time at the same elevation angle and frequency. A lower value of XPD results in higher cross-talk or high interference between two orthogonal channels at the satellite receiver station. In conclusion, adequate knowledge of the estimated attenuation statistics and cross polarisation due to rain characteristics is required to properly design a line-of-sight terrestrial or earth-space communication link, with adequate fade margin levels, to achieve the expected quality of service at these locations. The results obtained in this work will thus be immensely beneficial in the design of terrestrial and Earth-space links in southern Africa.

7.2 Suggestions for Future Work

Due to some assumptions made in this study, the estimation of the specific attenuation may not be the same as the measured raindrop shape; it will be necessary to compare the results with

experimental attenuation measurements performed in the same region or attenuation data from satellite communications links in some future works. However, due to inadequate experimental data, it will be of interest to further investigate and validate this work in the future and to estimate the same for other regions across South Africa. It will also be interested as future work to investigate the actual path loss with data taken over a long period of time for different conditions (say from 3^{o}C to 30^{o}C as an example) and possibly use other sensors rather than the disdrometer.

Since the spherical raindrop shapes assumed in this study may not give an accurate prediction or estimation of the attenuation as the size of the raindrop increases, their shape departs from spherical and is similar to that of oblate spheroids as the operating frequency increases. As a result of this, it is hereby suggested that the Pruppacher-Pitter [*Pruppacher and Pitter*, 1971] drop shape be used for future work in the region to handle the effects caused by the large raindrop diameters.

Generally, the disdrometer used in this study measures the raindrop sizes in every 60 seconds. As a suggestion for accurate prediction and estimation of attenuation based on this work, another disdrometer could be installed in a location within the KwaZulu-Natal Province (preferably, at the Westville campus or Pietermaritzburg campus of the University of KwaZulu-Natal), having similar or higher sampling period. This can assist to capture more drops per time. Different DSDs can then therefore be investigated and compared to ascertain the best model at different sampling times that represent the DSD in the region.

The investigation of the peak and critical diameters influencing the rainfall attenuation was investigated in this work. This has been limited to Durban in South Africa and Butare in Rwanda. Future work should investigate other regions based on the input parameters for the DSD in those regions. Although the cross polarisation due to rain in Durban was computed in this study, the effects of rain drop size distribution, rain rate, frequency, elevation angles and different polarisation in other parts of southern Africa could be investigated as future work.

REFERENCES

A.Y. Abdulrahamn, T.A. Rahman, S.K.A. Rahim and M.R. Ul Islam, "Empirically derived path reduction factor for terrestrial microwave links operating at 15 GHz in Peninsulla Malaysia," *Journal of electromagnetic waves and application,* 25:1, 23-27, DOI: 10.1163/156939311793898369, 2011.

O. Adetan and T. J. Afullo, "Comparison of two methods to evaluate the lognormal raindrop size distribution model in Durban," in *The Southern Africa Telecommunication Networks and Applications Conference (SATNAC),* pp. 2-5, 2012a.

O. Adetan and T. J. Afullo, "Three- parameter raindrop size distribution modeling for microwave propagation in South Africa," in *Proceedings of The International Association of Science and Technology for Development (IASTED), International Conference on Modelling and Simulation (Africa MS 2012),* pp. 155-160, 2012b.

I. Adimula and G. Ajayi, "Variations in raindrop size distribution and specific attenuation due to rain in Nigeria," in *Annales des télécommunications*, pp. 87-93, 1996.

T. J. O. Afullo, "Raindrop size distribution modeling for radio link design along the eastern coast of South Africa," *Progress In Electromagnetics Research B,* vol. 34, pp. 345-366, 2011.

G. Ajayi, *Handbook on radio propagation related to satellite communications in tropical and subtropical countries*: International Centre for Theoretical Physics, 1996.

G.O. Ajayi, and R.L. Olsen, Modeling of a tropical raindrop size distribution for microwave and millimeter wave applications, *Radio Sci*. vol. 20, no 2, pp.193-202, 1985.

G. O. Ajayi, "Some aspects of tropical rainfall and their effect on microwave propagation," *International Journal of Satellite Communications,* vol. 8, pp. 163-172, 1990.

G.O. Ajayi, S. Feng, S.M. Radicella, and B.M Reddy (Eds.), *Handbook on radio propagation related to satellite communications in tropical and subtropical countries,* pp. 2-14, ICTP Press, Trieste, 1996.

M. O. Ajewole, "Scattering and attenuation of centimeter and millimeter radio signals by tropical rainfall," Federal University of Technology, 1997.

M.O. Ajewole, L.B. Kolawole, and G.O. Ajayi, "Theoretical study of the effect of different types of tropical rainfall on microwave and millimeter-wave propagation," *Radio Science,* vol. 34, No 5, pp. 1103-1124, 1999a.

M.O. Ajewole, L.B. Kolawole and G.O. Ajayi, “Cross polarisation of line-of-sight links in a tropical location: effects of the variation in canting angle and drop size distribution,” *IEEE Trans on Ant. Propag.*47 (8): pp.1-6, 1999b.

M.O. Ajewole, and B.O. Afolayan, “Rain induced depolarisation scaling parameters for linearly polarized SHF waves communication on earth-space paths in Nigeria,” *Global journal of pure and applied sciences,* Vol. 14, No.2, pp. 235-240, 2008.

P. O. Akuon and T. J. O. Afullo, "Rain Cell Size Mapping for Microwave Link Design Systems in South Africa," *Progress In Electromagnetics Research B,* vol. 35, pp. 263-285, 2011.

A. Alonge and T. J. O. Afullo, "Seasonal analysis and prediction of rainfall effects in Eastern South Africa at microwave frequencies," *Progress In Electromagnetics Research B,* vol. 40, pp. 279-303, 2012.

D. Atlas and C. Ulbrich, "The physical basis for attenuation-rainfall relationships and the measurement of rainfall parameters by combined attenuation and radar methods," *J. Rech. Atmos,* vol. 8, pp. 275-298, 1974.

D. Atlas, C. W. Ulbrich, F. D. Marks, E. Amitai, and C. R. Williams, "Systematic variation of drop size and radar-rainfall relations," *Journal of Geophysical Research: Atmospheres* (1984–2012), vol. 104, pp. 6155-6169, 1999.

E. Baltas and M. Mimikou, "The use of Joss-type disdrometer for the derivation of ZR relationships," in *Proc. ERAD*, pp. 291-294, 2002.

L. Barclay*: Propagation of Radio Waves, The Institution of Electrical Engineers* 2nd Edition, 2003.

M. Bartholomew, "Disdrometer and tipping bucket rain gauge handbook," DOE/SC-ARM/TR-079, ARM Climate Research Facility, 2009.

L. J. Battan, "Some observations of vertical velocities and precipitation sizes in a thunderstorm," *Journal of Applied Meteorology,* vol.3, pp. 415-420, 1964.

W.A. Bentley, “Studies of raindrops and raindrop phenomena,” Mon. Wea. Rev. 32:450-456, 1904

S. Bernard, “*Digital communications- fundamentals and applications.* 2nd Edition, Prentice Hall New Jersey, USA, 2001.

C. F. Bohren and D. R. Huffman, *Absorption and scattering of light by small particles*: Wiley-Vch, 2008.

C. Bostian, W. Stutzman, P. Wiley, and R. Marshall, "The influence of polarization on millimeter wave propagation through rain," Final report, 1 Jan. 1972-31 Dec. 1973 Virginia Polytechnic Inst. and State Univ., Blacksburg. Dept. of Electrical Engineering. vol. 1, 1974.

S. Bradley and C. Stow, "The Measurement of charge and size of raindrops: Part II. Results and analysis at ground level," *Journal of Applied Meteorology,* vol. 13, pp. 131-147, 1974.

D. Brawn and G, Upton, "Estimation of an atmospheric gamma drop size distribution using disdrometer data," *Atmospheric research,* vol. 87, pp. 66-79, 2008.

G. Brussaard and P.A. Watson, "*Atmospheric modelling and millilitre wave propagation*," Chapman and Hall, London SE1 8HN, 1st edition, United Kingdom, 1995.

C. Caracciolo, , F. Prodi, A. Battaglia and F. Porcu, "Analysis of the moments and parameters of gamma DSD to infer precipitation properties: A convective stratiform discrimination algorithm," *Atm. Research.* 80, pp.165-186, 2006.

C.E. Carter, J.D. Greer, H.J. Braund and J.M Floyd, "Raindrop characteristics in South Central United States," Transactions of the ASAE 6:1033-1037, 1974.

T. Chu, "Rain-induced cross-polarization at centimeter and millimeter wavelengths," *AT T Technical Journal,* vol. 53, pp. 1557-1579, 1974.

T.S.A. Chu, "A Semi-empirical formula for microwave depolarisation versus raindrop attenuation on Earth-space paths," *IEEE Trans. Commun*., COM-30, no. 12, 2550, 1982.

A. C. Cohen and B. J. Whitten, "Estimation in the three-parameter lognormal distribution," *Journal of the American Statistical Association,* vol. 75, pp. 399-404, 1980.

R. Crane, "Prediction of attenuation by rain," *Communications, IEEE Transactions on,* vol. 28, pp. 1717-1733, 1980.

R.K. Crane, "A two component rain model for the prediction of attenuation statistics," *Radio Science*, vol. 17 No.6, pp.1371-1387, 1982

R. K. Crane, *Electromagnetic wave propagation through rain*: Wiley New York, 1996.

R.K. Crane, "Rain attenuation models: Attenuation by clouds and rain," *Propagation Handbook for Wireless Communication System,* 225-280, CRC Press, U.S.A, July, 2003.

R.K. Crane, and H.C. Shieh, "A two component rain attenuation model for prediction of site diversity improvement performance", Radio. Sci., 24(5), 641-665, 1989

P. E. Cruvinel, E. R. Minatel, M. L. Mucheroni, S. R. Vieira, and S. Crestana, "An automatic method based on image processing for measurements of drop size distribution from agricultural sprinklers." *Anais do IX SIBIGRAPI,* outubro de, 1996.

A.L. Cullen, and A. Kumar, "The absolute determination of extinction cross sections by the use of an open resonator," *Proc. Roy.Sec*. Lond.,315, pp.217-230, 1970.

S. Das, A. Maitra and A.K. Shukla, “Rain attenuation modeling in the 10-100 GHz frequency using drop size distributions for different climatic zones in tropical India,” *Progress in Electromagnetics Research*, vol. 25, pp. 211-224, 2010.

R. Dennis, *Satellite Communications*, Third Edition, McGraw-Hill, USA, 2001.

D. Deirmendjian, R. Clasen, and W. Viezee, "Mie scattering with complex index of refraction," *JOSA*, vol. 51, pp. 620-633, 1961.

A.W. Dissanayake, D.P. Haworth and P.A. Watson, “Analytical models for cross polarisation on Earth-space radio paths for frequency range 9-30*GHz*,” *Antenna Telecomm.,* vol.35 no 16, pp. 398-404, 1980.

B. I. Edelson, J. N. Pelton, C. W. Bostian, W. T. Brandon, V. W. Chan, E. P. Hager, *et al.*, "Satellite communications systems and technology. Volume 2: Site reports,” 1993.

J.D. Eigel, and I.D. Moore, “A simplified technique for measuring raindrop size and distribution,” Transactions of the ASAE 26:1079-1084, 1983.

A. A. Evans, "Maximum likelihood estimation," *Advanced Biometry Spring*, 2008.

M. Fashuyi, P. Owolawi, and T. Afullo, "Rainfall rate modelling for LOS radio systems in South Africa," *South African Institute of Electrical Engineer Journal*, vol. 97, pp. 74-81, 2006.

O. Fiser, "A simple generator of forward scattering functions on spherical dielectrics," *Radio engineering*, vol. 2, pp. 21-22, 1993.

O. Fiser, "The role of particular rain drop size classes on specific rain attenuation at various frequencies with Czech data example," in *Proceedings of ERAD*, 2002.

R. A. Fisher, "On the mathematical foundations of theoretical statistics," Philosophical Transactions of the Royal Society of London. Series A, vol. 222, pp. 309-368, 1922.

N. Fuchs, and I. Petrjanoff, “Microscopic examination of fog-, cloud-, and rain-droplets,” Nature 139:111-112, 1937.

T. Gillespie, “The spreading of low vapour pressure liquids in paper,” J. Colloid Soc.12:32-50, 1958.

H.E. Green, “Propagation impairment on Ka-band SATCOM links in tropical and equatorial regions,” *IEEE Antennas Propag. Mag 46(2),* pp. 31- 44, 2004.

R. Gunn and G. D. Kinzer, "The terminal velocity of fall for water droplets in stagnant air," *Journal of Meteorology*, vol. 6, pp. 243-248, 1949.

M.J. Hall, “Use of the stain method in determining the drop-size distribution of coarse liquid sprays,” Transactions of the ASAE, 13(1): 33-37, 1970.

K. Hardy, "The development of raindrop-size distributions and implications related to the physics of precipitation," *Journal of Atmospheric Sciences,* vol. 20, pp. 299-312, 1963.

R. Harikumar, S. Sampath, and V. Sasi Kumar, "An empirical model for the variation of rain drop size distribution with rain rate at a few locations in southern India," *Advances in Space Research,* vol. 43, pp. 837-844, 2009.

R.A. Houze Jr., "Observed structure of mesoscale convective systems and implications for large-scale heating," *Quart.J. Roy. Meteor. Soc* vol. 115, pp. 425-461, 1989.

R. A. Houze Jr, *Cloud dynamics* vol. 53: Academic press, 1994.

R. A. Houze Jr, "Stratiform precipitation in regions of convection: A meteorological paradox?" *Bulletin of the American Meteorological Society,* vol. 78, pp. 2179-2196, 1997.

L.J. Ippolito, Kaul, R. and Wallace, R. *Propagation Effects Handbook for Satellite Systems Design,* National Aeronautics and Space Administration, Chap.4, 1981.

A. Ishimaru, "Wave propagation and scattering in random media," Ed: IEEE Press (New York and Oxford and New York), 1997.

ITU-R: "Characteristics of precipitation for propagation modeling," Int. Telecommunications Union, Geneva, *ITU-R 837-1, 2, 3, 4,* 2008.

ITU-R: Specific Rain Attenuation Model for Rain for use in Prediction Models, *Recommend. 838-3, ITU-R P Ser,* Int. Telecommunications Union, Geneva, 2005.

ITU-R: Propagation data and prediction methods required for the design of terrestrial line-of-sight systems," *Recommed.530-12 ITU-R P Ser.,* Int. Telecommun. Union, Geneva, 2007.

ITU-R P.618-9: Propagation data and prediction methods required for the design of Earth-space telecommunications systems, Recommendation P, ITU-R Ser., *Inter. Telecomm Union*, Geneva, Switzerland, 2007.

G. Ivanovs, and D. Serdega, "Rain intensity influence on microwave line payback terms," *Electronics and Electrical Engineering,* no.6 (70), pp.60-64, ISSN 1392-1215, 2006.

H. Jiang, M. Sano and M. Sekine, "Weibull raindrop size distribution and its application to rain attenuation," *IEE Proc. Microw. Antennas propag.,* 144(3), June 1997.

J. Joss and A. Waldvogel, "Raindrop size distribution and sampling size errors," *J. Atmos. Sci,* vol. 26, pp. 566-569, 1969.

J. Joss, J.C. Thams and A. Waldvogel, "The Variation of Raindrop-Size Distribution at Locarno," *Proceedings of International Conference on Cloud Physics,* pp. 369-373, 1968.

J.D. Kanellopoulos, Koukoulas, S.G, Kolliopoulos, N.J, Capsalis, C.N and Ventouras, S.G., "Rain attenuation problems affecting the performance of microwave communication systems," *Ann. of Telecommun.,-annales des télécomm* vol. 45, no. 7-8,pp. 437-451, DOI:10.1007/BF03000944, 1990.

N. H. H. Khamis, J. Din, and T. A. Rahman, "Analysis of rain cell size distribution from meteorological radar data for rain attenuation studies," in *Applied Electromagnetics,* 2005. *APACE 2005. Asia-Pacific Conference on*, 2005,

P.I.A. Kinnell, "Some observations of the Joss-Waldvogel rainfall disdrometer," J. App. Met. 15:499-502, 1976.

R.A. Kohl, "Drop size distribution from medium –sized agricultural sprinklers," Transactions of the ASAE, 17(4): 690-693, 1974

L. S. Kumar, Y. H. Lee, and J. T. Ong, "Truncated gamma drop size distribution models for rain attenuation in Singapore," *Antennas and Propagation, IEEE Transactions on,* vol. 58, pp. 1325-1335, 2010.

A. Kültegin, and S.E.A. Daisley, "Relationships between rainfall rate and 35-*GHz* rainfall attenuation and differential attenuation: Modeling the effects of raindrop size distribution, canting, and oscillation," *IEEE Transactions on geoscience and remote sensing,* vol. 40, no.11, November 2011.

S. Lakshmi, Y. Lee, and J. Ong, "The role of particular rain drop size on rain attenuation at 11 GHz," in *Information, Communications & Signal Processing,* 2007 *6th International Conference on*, pp. 1-4, 2007.

H. Lam, J. Din, L. Luini, A. Panagopoulos, and C. Capsoni, "Analysis of raindrop size distribution characteristics in Malaysia for rain attenuation prediction," in *General Assembly and Scientific Symposium,* 2011 *XXXth URSI*, 2011, pp. 1-4, 2011.

J. O. Laws and D. A. Parsons, "The relation of raindrop-size to intensity," *Transactions, American Geophysical Union*, vol. 24, pp. 452-460, 1943.

Y. Lee, S. Lakshmi, and J. Ong, "Rain drop size distribution modelling in Singapore-Critical diameters," in *Antennas and Propagation, 2007. EuCAP 2007. The Second European Conference on*, pp. 1-5, 2007.

L. Li, T. Yeo, P. Kooi and M. Leong "An efficient calculation approach to evaluation of microwave specific attenuation," *IEEE Trans. Antennas*, 48(8), pp. 1220-1229, 2000.

H.J. Liebe, G.A. Hufford and T. Manabe, “A model for the complex permittivity of water at frequencies below 1THz” *International J. of Infrared and Millimeter Waves,* vol. 12, no. 7, 1991.

A. Maitra, "Rain attenuation modeling from measurements of rain drop size distribution in the Indian region," *Antennas and Wireless Propagation Letters, IEEE,* vol. 3, pp. 180-181, 2004.

J.S. Mandeep, N.Y. Yann and S.I.S. Hassan, “Case study of rain attenuation at Ka band,” *Journal of Electromagnetic Waves and Application,* vol. 22, no. 11-12, pp. 1517-1525, 2008.

M. Marcus and B. Pattan, “Millimeter Wave Propagation: Spectrum Management and Implications,” *IEEE Microwave Magazine,* vol.6, no.2, pp. 54-62, Jun. 2005.

J. S. Marshall and W. M. K. Palmer, "The distribution of raindrops with size," *Journal of Meteorology,* vol. 5, pp. 165-166, 1948.

M. Marzuki, T. Kozu, T. Shimomai, W. Randeu, H. Hashiguchi, and Y. Shibagaki, "Diurnal variation of rain attenuation obtained from measurement of raindrop size distribution in equatorial Indonesia," *Antennas and Propagation, IEEE Transactions on,* vol. 57, pp. 1191-1196, 2009.

M. Marzuki, , W.L. Randeau, M. Schonhuber, V.N. Bringi, T. Kozu and T. Shimomai , “Raindrop size distribution parameters of disdrometer data with different bin sizes,” *IEEE Trans., Geosci., Remote Sens.,* vol. 48, pp. 3075-3080, 2010.

P. A. Matthews, *Radio wave propagation: VHF and above*: Chapman and Hall, 1965.

E. Matricciani, and A. Pawlina-Bonati, Statistical characterization of rainfall structure and occurrence for convective and stratiform rain inferred from long –term point rain rate data, *AP-2000 Millenium Conference Antennas Propag.* Davos, Switzerland, June 2000.

C. Mätzler,: “MATLAB functions for Mie scattering and absorption,” *IAP Res. Rep.* 2002-8, Univ of Bern, Bern, June 2002.

C. Mätzler, “Advanced model of extinction by rain and measurements at 38 GHZ and 94 GHz and in the visible range,” ,” *IAP Res. Rep.* 2003-18, Univ of Bern, Bern, June 2003.

K.R. May, “The Cascade Impactor: an instrument for sampling coarse aerosols,” J. Sci Instr. 22(10), 187-195, 1945.

F. Moupfouma and J. Tiffon, "Raindrop size distribution from microwave scattering measurements in equatorial and tropical climates," *Electronics Letters,* vol. 18, pp. 1012-1014, 1982.

F. Moupfouma, “Improvement of a rain attenuation prediction method for terrestrial microwave links,” *IEEE Trans. Antennas Propag.,* vol. 32, no. 12 pp. 1368-1372, 1984.

F. Moupfouma, “Electromagnetic waves attenuation due to rain: A prediction model for terrestrial or L.O.S. SHF and EHF radio communication links, *J. Infra. Milli., Tetrahertz waves,* 30(6), pp. 622-632, 2009.

C. Mulangu and T. Afullo, "Variability of the propagation coefficients due to rain for microwave links in southern Africa," *Radio Science,* vol. 44, 2009.

D.N. Murthy, M. Xie, and R. Jiang., *Weibull Models,* John Wiley and Sons Inc., New York, pp. 50-58, 68-74, 2004.

J. Nader., “Modeling and performance of microwave radio links in rain,” MSc. Thesis, McGill Uni., Montreal, Canada, August 1998.

H. Neuberger; “Notes on measurements of raindrop sizes,” Bull Amer. Met. Soc. 23:274-276, 1942.

W.L. Nowland, R.L. Olsen and I.P. Sharkofsky, “Theoretical relationship between rain depolarisation and attenuation,” *Electronic letters,* No. 13, pp. 676-678, 1977.

M. Odedina and T. Afullo, "Determination of rain attenuation from electromagnetic scattering by spherical raindrops: Theory and experiment," *Radio Science,* vol. 45, 2010.

M. O. Odedina and T. Afullo, "Characteristics of seasonal attenuation and fading for line-of-sight links in South Africa," in *Proc. of SATNAC,* pp. 203-208, 2008.

T. Oguchi, "Attenuation of electromagnetic wave due to rain with distorted raindrops," Journal of *the Radio* Research Laboratories, vol. 7, no. 33, pp. 467-485, Sep.1960.

T. Oguchi., “Scattering properties of oblate raindrops and cross polarization of radio waves due to rain: Calculations at 19.3 and 34.8 GHz,” *J. Radio Research Lab.,* vol. 20, no.102, pp. 79-118, September, 1973.

T. Oguchi, "Scattering properties of Pruppacher-and-Pitter form raindrops and cross polarization due to rain: Calculations at 11, 13, 19.3, and 34.8 GHz," *Radio Science,* vol. 12, pp. 41-51, 1977.

T. Oguchi, "Electromagnetic wave propagation and scattering in rain and other hydrometeors," *Proceedings of the IEEE,* vol. 71, pp. 1029-1078, 1983.

T. Oguchi and Y. Hosoya, "Scattering properties of oblate raindrops and cross polarization of radio waves due to rain. II-Calculations at microwave and millimeter wave regions," *Radio Research Laboratory, Journal,* vol. 21, pp. 191-259, 1974.

J.S. Ojo, “Estimation of cross-polarisation due to rain over some stations in Nigeria,” *Ann. Telecomm* DOI 10.1007/s12243-011-0269-4, 67:241-245, 2012.

J. S. Ojo, M. O. Ajewole, and S. K. Sarkar, "Rain rate and rain attenuation prediction for satellite communication in Ku and Ka bands over Nigeria," *Progress In Electromagnetics Research B,* vol. 5, pp. 207-223, 2008.

R. L. Olsen, D. V. Rogers. and D. B. Hodge, 'The aR^b relation in the calculation of rain attenuation," IEEE Transactions on Antennas and Propagation, vol. 26, no. 2,pp. 3 18-329, Mar. 1978.

P. Owolawi, "Rainfall rate and rain drop size distribution models for line-of-sight millimetric systems in South Africa," M. Sc. thesis submitted to the University of KwaZulu-Natal, Durban, 2006.

P. A. Owolawi, "Rainfall rate probability density evaluation and mapping for the estimation of rain attenuation in South Africa and surrounding islands," *Progress In Electromagnetics Research,* vol. 112, pp. 155-181, 2011.

P. A. Owolawi and T. J. Afullo, "Rainfall rate modeling and worst month statistics for millimetric line-of-sight radio links in South Africa," *Radio Science,* vol. 42, 2007.

A. Paraboni, C. Oestges, and A. Martellucci, "Experimental assessment of atmospheric depolarization at Ka and V band based on Olympus and Italsat propagation campaigns," in *The European Conference on Antennas and Propagation: EuCAP* 2006, pp. 354, 2006.

K. Pearson, ""Skew Variation in homogeneous material," *Philosophical Trans., of the Royal Soc,, of London*, 186, series A, pp.414-895, 1895.

M.S. Pontes, da Silva Mello, L, de Souza, R.S.L and Miranda, E.C.B, "Review of rain attenuation studies in tropical and equatorial regions of Brazil," *IEEE, 5th International conference on Information, Communications and Signal Processing,* DOI: 10. 1109/ICICS.2005.1689223, pp. 1097-1101, Bangkok, 2005.

J. G. Proakis, M. Salehi, N. Zhou, and X. Li, *Communication systems engineering* vol. 2, Prentice-Hall Englewood Cliffs, 1994.

H. Pruppacher and R. Pitter, "A semi-empirical determination of the shape of cloud and rain drops," *Journal of the atmospheric sciences,* vol. 28, pp. 86-94, 1971.

R. F. Rincon and R. H. Lang, "Microwave link dual-wavelength measurements of path-average attenuation for the estimation of drop size distributions and rainfall," *Geoscience and Remote Sensing, IEEE Transactions on,* vol. 40, pp. 760-770, 2002.

A. Rocha and R. Teixeira, "Earth-satellite ice depolarization revisited: New data," in *Antennas and Propagation, 2006. EuCAP 2006. First European Conference on*, 2006, pp. 1-5.

D. Roddy, *Satellite communications*: McGraw-hill New York, 2001.

D. Rosenfeld, E. Amitai, and D. B. Wolff, "Classification of rain regimes by the three-dimensional properties of reflectivity fields," *J. Appl Meteor,* vol. 34, pp. 198-211, 1995.

A. Safaai-Jazi, H. Ajaz and W.L. Stutzman: "Empirical models for rain fade time on Ku- and Ka-band satellite links," *IEEE Trans. on Antennas and Propagation,* vol. 43, no.12, pp.1411-1415, December 1995.

M. Sekine and G. Lind, "Rain attenuation of centimeter, millimeter and Sub-millimeter radio Waves," in *Microwave Conference,* 1982. *12th European*, 1982, pp. 584-589.

M. Sekine, and C. D. Chen, "Rain attenuation in terrestrial and satellite communications links," *Proc. 15th European Microwave Conf, Paris, France,* pp.985-990, Sept. 1985.

B. Sheppard and P. Joe, "Comparison of raindrop size distribution measurements by a Joss-Waldvogel disdrometer, a PMS 2DG spectrometer, and a POSS Doppler radar," *Journal of Atmospheric and Oceanic Technology,* vol. 11, pp. 874-887, 1994.

J. Simpson, R.F. Adler, and G. North, "A proposed tropical rainfall Measuring Mission (TRMM) satellite," *Bull. Ame. Met. Soc.*, vol. 69, pp. 278-295, 1988.

South Africa year book, 1991

M. Tamošiūnaitė, M. Žilinskas, and M. T. and Stasys Tamošiūnas, "Atmospheric attenuation due to humidity," Electromagnetic waves (Ed.), InTech, ISBN: 978-953-307—304-0, June 2011.

M. Thurai and V.N. Bringi, "Drop axis ratios from 2D video disdrometer," *J. Atmos. Ocean. Technol.* 22, 966–978, 2005.

M. Thurai, Szakáll M., Bringi V.N., Beard K.V., Mitra S.K., Borrmann S., Drop shapes and axis ratio distributions: Comparison between 2D video disdrometer and wind-tunnel measurements. *J. Atmos. Ocean. Technol*. 26, 1427–1432, 2009.

M. Thurai, V. N. Bringi, and T. Shimomai, "20 GHz Specific attenuation calculations using drop size distributions and drop shape measurements from 2D video disdrometer data in different rain climates," in *Information, Communications & Signal Processing, 2007 6th International Conference on*, pp. 1-4, 2007.

K. Timothy and S. Sarkar, "Generalized mathematical model for raindrop size distribution (RSD) for application in radiowave propagation and meteorological studies," *Electronics Letters,* vol. 33, pp. 895-897, 1997.

K. I. Timothy, J. T. Ong, and E. B. Choo, "Raindrop size distribution using method of moments for terrestrial and satellite communication applications in Singapore," *Antennas and Propagation, IEEE Transactions on,* vol. 50, pp. 1420-1424, 2002.

A. Tokay and D. A. Short, "Evidence from tropical raindrop spectra of the origin of rain from stratiform versus convective clouds," *Journal of applied meteorology,* vol. 35, pp. 355-371, 1996.

A. Tokay, A. Kruger, and W. F. Krajewski, "Comparison of drop size distribution measurements by impact and optical disdrometer," *Journal of Applied Meteorology,* vol. 40, pp. 2083-2097, 2001.

W. Tomasi, *Electronic communications systems: fundamentals through advanced*: Prentice Hall PTR, 1987.

A.J. Townsend, "A study of raindrop size distribution and its effects on microwave," University of Bath, 2011.

P. D. Tyson, R. Preston-Whyte, and R. Schulze, *The climate of the Drakensberg* vol. 15: Town and Regional Planning Commission, 1976.

P. D. Tyson, "Climatic change and variability in southern Africa," 1986.

C. W. Ulbrich, "Natural variations in the analytical form of the raindrop size distribution," *Journal of Climate and Applied Meteorology,* vol. 22, pp. 1764-1775, 1983.

H.C. Van de Hurst, *Light scattering by small particles* John Wiley and Sons, Inc, New York, 1957.

M.M.J.L. Van de Kamp, "Depolarisation due to rain: the XPD-CPA relation," *Int. J. Satell. Commun.* 19; 285-301, DOI: 10.1002/sat.672, 2001.

A. Waldvogel, "The No jump of raindrop spectra," *Journal of the Atmospheric Sciences,* vol. 31, pp. 1067-1078, 1974.

Y. Xie, X.-l. Zhou, and Z.-d. Yang, "Error analysis of non-spherical raindrops on precipitation measurement," *Journal of Shanghai University (English Edition),* vol. 15, pp. 92-95, 2011.

T. Yesufu, "On the Applicability of Rain Gauge Measurements," *CLIMPARA'98,* pp. 66-69, 1998.

Internet Websites/URL

http://www.biztradeshows.com/southafrica/durban/durban.html.

http://www.ceroi.net/reports/durban/drivers/Climate/index.htm.

http://ww.southafrica.info/plantrip/traveltips/questions/climate.html

http://www.southafrica.info/travel/advice/climate.html

http://www.biztradeshows.com/southafrica/durban/durban.html

Appendices

Appendix A-1: ITU-R Rainfall Attenuation Model (*ITU-R. P. 530-13*, 2009)

The following simple method is used to compute the specific rain attenuation at R0.01 exceeded for 0.01% of time:

First, obtain the rain rate $R_{0.01}$ exceeded for 0.01% of the time (with an integration time of 1 min). If this information is not available from local sources of long-term measurements, an estimate can be obtained from the information given in Recommendation ITU-R P.837.

Secondly, compute the specific attenuation, γ_R (dB/km) for the frequency, polarization and rain rate of interest using Recommendation ITU-R P.838.

Thirdly, compute the effective path length, d_{eff}, of the link by multiplying the actual path length d by a distance factor r. An estimate of this factor is given by:

$$r = \frac{1}{1 + {}^{d}/_{d_0}} \qquad (A.1)$$

where, for $R_{0.01} \leq 100$ *mm/h*:

$$d_0 = 35e^{-0.015R_{0.01}} \qquad (A.2)$$

For $R_{0.01} > 100$ mm/h, use the value of 100 *mm/h* is used in place of $R_{0.01}$.

Fourthly, an estimate of the path attenuation exceeded for 0.01% of the time is given by:

$$A_{0.01} = \gamma_R \times d_{eff} = \gamma_R d_r \ \ (dB) \qquad (A.3)$$

Appendix B-1: ITU-R Frequency-Dependent Parameters for the Estimation of Specific Attenuation at Horizontal and Vertical Polarization

[*ITU-R 383-3*, 2005]

According to the ITU-R recommendation P. 838-3, the specific attenuation from the knowledge of rainfall rate can be calculated using the power-law relationship:

$$\gamma_R = \kappa R^{\alpha} \qquad (A.4)$$

The parameters κ and α depend on frequency and wave polarization. The numerical values of κ and α at 1 to 1000 GHz for the computation of specific attenuation due to rain in any locality of region are given below:

Frequency (GHz)	κ_H	α_H	κ_v	α_v
1	0.000259	0.9691	0.0000308	0.8592
1.5	0.000443	1.0185	0.0000574	0.8957
2	0.0000847	1.0664	0.0000998	0.9490
2.5	0.0001321	1.1209	0.0001464	1.0085
3	0.0001390	1.2322	0.0001942	1.0688
3.5	0.0001155	1.4189	0.0002346	1.1387
4	0.0001071	1.6009	0.0002461	1.2476
4.5	0.0001340	1.6948	0.0002347	1.3987
5	0.0002162	1.6969	0.0002428	1.5317
5.5	0.0003909	1.6499	0.0003115	1.5882
6	0.0007056	1.5900	0.0004878	1.5728
7	0.001915	1.4810	0.001425	1.4745
8	0.004115	1.3905	0.003450	1.3797
9	0.007535	1.3155	0.006691	1.2895
10	0.01217	1.2571	0.1129	1.2156
11	0.01772	1.2140	0.01731	1.1617
12	0.02386	1.1825	0.02455	1.1216
13	0.03041	1.1586	0.03266	1.0901

Frequency (GHz)	κ_H	α_H	κ_v	α_v
14	0.03738	1.1396	0.04126	1.0646
15	0.04481	1.1233	0.05008	1.0440
16	0.05282	1.1086	0.05899	1.0273
17	0.06146	1.0949	0.06797	1.0137
18	0.07078	1.0818	0.07708	1.0025
19	0.08084	1.0691	0.08642	0.9930
20	0.09164	1.0568	0.09611	0.9847
21	0.1032	1.0447	0.1063	0.9771
22	0.1155	1.0329	0.1170	0.9700
23	0.1286	1.0214	0.1284	0.9630
24	0.1425	1.0101	0.1404	0.9561
25	0.1571	0.9991	0.1533	0.9491
26	0.1724	0.9884	0.1669	0.9421
27	0.1884	0.9780	0.1813	0.9349
28	0.2051	0.9679	0.1964	0.9277
29	0.2224	0.9580	0.2124	0.9203
30	0.2403	0.9485	0.2291	0.9219
31	0.2588	0.9392	0.2465	0.9055
32	0.2778	0.9302	0.2646	0.8981
33	0.2972	0.9214	0.2833	0.8907
34	0.3171	0.9129	0.3026	0.8834
35	0.3374	0.9047	0.3224	0.8761
36	0.3580	0.8967	0.3427	0.8690
37	0.3789	0.8890	0.3633	0.8621
38	0.4001	0.8816	0.3844	0.8552
39	0.4215	0.8743	0.4058	0.8486
40	0.4431	0.8673	0.4274	0.8421
41	0.4647	0.8605	0.4492	0.8357
42	0.4865	0.8539	0.4712	0.8296
43	0.5084	0.8476	0.4932	0.8236
44	0.5302	0.8414	0.5153	0.8179
45	0.5521	0.8355	0.5375	0.8123
46	0.5738	0.8297	0.5596	0.8069

47	0.5956	0.8241	0.5817	0.8017
48	0.6172	0.8187	0.6037	0.7967
49	0.6386	0.8134	0.6255	0.7918
50	0.6600	0.8084	0.6472	0.7871
51	0.6811	0.8034	0.6687	0.7826
52	0.7020	0.7987	0.6901	0.7783
53	0.7228	0.7941	0.7112	0.7741
54	0.7433	0.7896	0.7321	0.7700
55	0.7635	0.7853	0.7527	0.7661
56	0.7835	0.7811	0.7730	0.7623
57	0.8032	0.7771	0.7931	0.7587
58	0.8226	0.7731	0.8129	0.7552
59	0.8418	0.7693	0.8324	0.7518
60	0.8606	0.7656	0.8515	0.7486
61	0.8791	0.7621	0.8704	0.7454
62	0.8974	0.7586	0.8889	0.7424
63	0.9153	0.7552	0.9071	0.7395
64	0.9328	0.7520	0.9250	0.7366
65	0.9501	0.7488	0.9425	0.7339
66	0.9670	0.7458	0.9598	0.7313
67	0.9836	0.7428	0.9767	0.7287
68	0.9999	0.7400	0.9932	0.7262
69	1.0159	0.7372	1.0094	0.7238
70	1.0315	0.7345	1.0253	0.7215
71	1.0468	0.7318	1.0409	0.7193
72	1.0618	0.7293	1.0561	0.7171
73	1.0764	0.7268	1.0711	0.7150
74	1.0908	0.7244	1.0857	0.7130
75	1.1048	0.7221	1.1000	0.7110
76	1.1185	0.7199	1.1139	0.7091
77	1.1320	0.7177	1.1276	0.7073
78	1.1451	0.7156	1.1410	0.7055
79	1.1579	0.7135	1.1541	0.7038
80	1.1704	0.7115	1.1668	0.7021
81	1.1827	0.7096	1.1793	0.7004

Frequency (GHz)	κ_H	α_H	κ_v	α_v
82	1.1946	0.7077	1.1915	0.6988
83	1.2063	0.7058	1.2034	0.6973
84	1.2177	0.7040	1.2151	0.6958
85	1.2289	0.7023	1.2265	0.6943
86	1.2398	0.7006	1.2376	0.6929
87	1.2504	0.6990	1.2484	0.6915
88	1.2607	0.6974	1.2590	0.6902
89	1.2708	0.6959	1.2694	0.6889
90	1.2807	0.6944	1.2795	0.6876
91	1.2903	0.6929	1.2893	0.6864
92	1.2997	0.6915	1.2989	0.6852
93	1.3089	0.6901	1.3083	0.6840
94	1.3179	0.6888	1.3175	0.6828
95	1.3266	0.6875	1.3265	0.6817
96	1.3351	0.6862	1.3352	0.6806
97	1.3434	0.6850	1.3437	0.6796
98	1.3515	0.6838	1.3520	0.6785
99	1.3594	0.6826	1.3601	0.6775
100	1.3671	0.6815	1.3680	0.6765
120	1.4866	0.6640	1.4911	0.6609
150	1.5823	0.6494	1.5896	0.6466
200	1.6378	0.6382	1.6443	0.6343
300	1.6286	0.6296	1.6286	0.6262
400	1.5860	0.6262	1.5820	0.6256
500	1.5418	0.6253	1.5366	0.6272
600	1.5013	0.6262	1.4967	0.6923
700	1.4654	0.6284	1.4622	0.6315
800	1.4335	0.6315	1.4321	0.6334
900	1.4050	0.6353	1.4056	0.6351
1000	1.3795	0.6396	1.3822	0.6365

Appendix C-1: Drop size classes of RD-80 disdrometer [*Bartholomew, 2005;* www.disdromet.com]

Drop size Class in DISDRODATA program	Lower threshold of drop diameter (mm)	Average diameter of drops in class i D_i (mm)	Fall velocity of a drop with diameter D_i $v(D_i)$ (m/s)	Diameter interval of drop size class i, ΔD_i (mm)
1	0.313	0.359	1.435	0.092
2	0.405	0.455	1.862	0.100
3	0.505	0.551	2.267	0.091
4	0.596	0.656	2.692	0.119
5	0.715	0.771	3.154	0.112
6	0.827	0.913	3.717	0.172
7	0.999	1.116	4.382	0.233
8	1.232	1.331	4.986	0.197
9	1.429	1.506	5.423	0.153
10	1.582	1.665	5.793	0.166
11	1.748	1.912	6.315	0.329
12	2.077	2.259	7.009	0.364
13	2.441	2.584	7.546	0.286
14	2.727	2.869	7.903	0.284
15	3.011	3.198	8.258	0.374
16	3.385	3.544	8.556	0.319
17	3.704	3.916	8.784	0.423
18	4.127	4.350	8.965	0.446
19	4.573	4.859	9.076	0.572
20	5.145	5.373	9.137	0.455

Appendix D: Computation of the Scattering parameters at Selected Frequencies

D-1: Scattering amplitudes and extinction cross sections at 10 GHz (m = 8.0649 + j2.0188)

Radius (mm)	Size	Scattering amplitude		Q_{ext} (mm^2)
		Real part	Imaginary part	
0.1795	0.037594	1.11972E-06	-5.13371E-05	0.000321
0.2275	0.047647	2.3907E-06	-0.000104759	0.000685
0.2755	0.057701	4.49674E-06	-0.000186583	0.001288
0.328	0.068696	8.16455E-06	-0.000316081	0.002339
0.3855	0.080739	1.45196E-05	-0.000515734	0.00416
0.4565	0.095609	2.73512E-05	-0.000862718	0.007836
0.558	0.116867	6.11056E-05	-0.001595932	0.017505
0.6655	0.139382	0.000131065	-0.002752791	0.037547
0.753	0.157708	0.000232685	-0.004051534	0.066659
0.8325	0.174358	0.000381362	-0.005565035	0.109252
0.956	0.200224	0.000790146	-0.008672441	0.22636
1.1295	0.236562	0.002077579	-0.014965855	0.595183
1.292	0.270596	0.004915829	-0.023311933	1.408281
1.4345	0.300441	0.010009151	-0.032384097	2.867411
1.599	0.334894	0.020313749	-0.0426023	5.81946
1.772	0.371127	0.033231596	-0.048776691	9.520151
1.958	0.410083	0.041752076	-0.053771274	11.96109
2.175	0.455531	0.048476316	-0.068358117	13.88744
2.4295	0.508833	0.063814741	-0.09575442	18.28158
2.6865	0.562659	0.087980428	-0.127796804	25.20454

D-2: Scattering amplitudes and extinction cross sections at 19.5 GHz (m = 6.7332 + j2.7509)

Radius (mm)	Size	Scattering amplitude		Q_{ext} (mm^2)
		Real part	Imaginary part	
0.1795	0.073309065	1.77485E-05	-0.000381976	0.001337
0.2275	0.092912603	4.00413E-05	-0.000782467	0.003017
0.2755	0.112516141	8.02043E-05	-0.001400111	0.006043
0.328	0.133957511	0.000156957	-0.002385875	0.011825
0.3855	0.157440916	0.000304341	-0.003921291	0.022929
0.4565	0.186437816	0.000639379	-0.006623141	0.048171
0.558	0.227891131	0.001663796	-0.012412392	0.12535
0.6655	0.271794888	0.00412198	-0.021551301	0.310548
0.753	0.307530505	0.007991013	-0.031445014	0.60204
0.8325	0.339998865	0.013611902	-0.042031253	1.025515
0.956	0.390437135	0.026541148	-0.059937879	1.9996
1.1295	0.461295757	0.049373505	-0.087442268	3.719781
1.292	0.527661902	0.075858318	-0.122110684	5.715137
1.4345	0.585859906	0.109461918	-0.160787988	8.246819
1.599	0.653042865	0.164629835	-0.210637569	12.40315
1.772	0.723697284	0.243704302	-0.264169626	18.36059
1.958	0.799660994	0.354520997	-0.314645783	26.70948
2.175	0.888285323	0.510398004	-0.349115328	38.45319
2.4295	0.992224916	0.701418215	-0.34805593	52.84458
2.6865	1.097185526	0.877063656	-0.321484699	66.07764

D- 3: Scattering amplitudes and extinction cross sections at 35 GHz (m = 5.2500 + j2.8072)

Radius (mm)	Size	Scattering amplitude		Q_{ext} (mm^2)
		Real part	Imaginary part	
0.1795	0.13158	0.000198568	-0.002214434	0.004644
0.2275	0.166766	0.000471701	-0.004562943	0.011031
0.2755	0.201952	0.00099899	-0.008215404	0.023362
0.328	0.240437	0.002077764	-0.014084372	0.048591
0.3855	0.282586	0.004279288	-0.02323436	0.100076
0.4565	0.334632	0.009484376	-0.039076794	0.221802
0.558	0.409035	0.02477496	-0.070710951	0.579388
0.6655	0.487837	0.05453523	-0.113938887	1.275363
0.753	0.551978	0.090548029	-0.155948527	2.117559
0.828	0.606956	0.132475847	-0.196938519	3.098084
0.956	0.700785	0.235935241	-0.269937427	5.517589
1.1295	0.827967	0.436754252	-0.341093749	10.21395
1.292	0.947085	0.653775044	-0.356814932	15.2892
1.4345	1.051543	0.837969887	-0.337942251	19.59679
1.599	1.172128	1.02903087	-0.30652129	24.06495
1.772	1.298944	1.216794563	-0.293308901	28.456
1.958	1.435289	1.436211561	-0.314895371	33.58729
2.175	1.594358	1.753798492	-0.365629312	41.01439
2.4295	1.780917	2.21339985	-0.397901337	51.76264
2.6865	1.969307	2.710827783	-0.372282413	63.39551

D-4: Scattering amplitudes and extinction cross sections at 50 GHz (m = 4.4428 + j2.5752)

Radius (mm)	Size	Scattering amplitude		Q_{ext} (mm^2)
		Real part	Imaginary part	
0.1795	0.187972	0.000857636	-0.006458536	0.009828
0.2275	0.238237	0.002112384	-0.013383232	0.024206
0.2755	0.288503	0.004640155	-0.024202647	0.053172
0.328	0.343481	0.009986142	-0.041534421	0.114433
0.3855	0.403695	0.021021853	-0.068024078	0.240893
0.4565	0.478046	0.046294451	-0.111561903	0.530495
0.558	0.584336	0.114052367	-0.190331897	1.306944
0.6655	0.69691	0.240570647	-0.281862828	2.756737
0.753	0.78854	0.389456011	-0.338596378	4.462837
0.8325	0.871792	0.544627151	-0.359517559	6.240967
0.956	1.001121	0.78031277	-0.343374108	8.941726
1.1295	1.18281	1.068800649	-0.298092456	12.24755
1.292	1.352979	1.329775356	-0.29704415	15.2381
1.4345	1.502205	1.601255966	-0.335772035	18.34904
1.599	1.674469	1.996438722	-0.382143339	22.8775
1.772	1.855634	2.473453326	-0.379519147	28.34369
1.958	2.050413	2.988626886	-0.335622052	34.24714
2.175	2.277655	3.59684321	-0.31412457	41.21679
2.4295	2.544166	4.423054503	-0.334709054	50.68447
2.6865	2.813296	5.378845261	-0.303829449	61.63703

D-5: Scattering amplitudes and extinction cross sections at 100 GHz (m = 3.3061 + j1.8778)

Radius (mm)	Size	Scattering amplitude		Q_{ext} (mm^2)
		Real part	Imaginary part	
0.1795	0.375944	0.01502127	-0.051128529	0.043033
0.2275	0.476475	0.041790007	-0.106325795	0.11972
0.2755	0.577006	0.100933899	-0.186253351	0.289154
0.328	0.686962	0.224951807	-0.286852864	0.644439
0.3855	0.807389	0.439413732	-0.367476573	1.258828
0.4565	0.956091	0.748165945	-0.363703478	2.143338
0.558	1.168672	1.099901485	-0.276783711	3.150986
0.6655	1.39382	1.456400639	-0.282527713	4.17228
0.753	1.57708	1.847466582	-0.327244327	5.292602
0.8325	1.743584	2.275194537	-0.332586103	6.517952
0.956	2.002242	2.96785922	-0.268757079	8.50229
1.1295	2.365619	3.997064492	-0.228041088	11.45075
1.292	2.705958	5.172070558	-0.185402703	14.81689
1.4345	3.00441	6.275759531	-0.092783508	17.97873
1.599	3.348938	7.663463005	-0.02694762	21.9542
1.772	3.711268	9.307028131	0.081098655	26.66267
1.958	4.100826	11.19378798	0.21430088	32.06784
2.175	4.555309	13.64305292	0.369642915	39.08447
2.4295	5.088333	16.77627788	0.591457949	48.0605
2.6865	5.626592	20.2796083	0.836283694	58.0968

Appendix E

E-1: Contributions (dB/km) of raindrop diameters to specific attenuation for Overall $R_{0.01}$ at f = 10-100 GHz using the lognormal DSD

Diameter (mm)	10GHz	19.5GHz	40GHz	60GHz	80GHz	100GHz
0.1	2.14712E-18	2.3252E-17	5.088E-16	3.17699E-15	1.04979E-14	2.39134E-14
0.2	1.44943E-11	1.2602E-10	1.6943E-09	7.48951E-09	1.94534E-08	3.73532E-08
0.3	2.04218E-08	1.5615E-07	1.5789E-06	5.70267E-06	1.28666E-05	2.23558E-05
0.4	1.46404E-06	1.0219E-05	8.4419E-05	0.000264183	0.000539383	0.000873025
0.5	2.44494E-05	0.00015901	0.00112294	0.003144345	0.005941097	0.009101391
0.6	0.00017656	0.0010838	0.0067338	0.01721787	0.030536303	0.044723871
0.7	0.000748777	0.00437749	0.02440411	0.05778582	0.0971421	0.136970812
0.8	0.002212681	0.01239995	0.06293711	0.139433676	0.223775884	0.305308441
0.9	0.005055563	0.02729388	0.12752855	0.266427495	0.410449163	0.543971075
1	0.009552573	0.04987928	0.21642554	0.4290216	0.63718848	0.822820544
1.1	0.015623754	0.07915384	0.32119864	0.607181281	0.872431727	1.100437459
1.2	0.022841084	0.1125724	0.42971408	0.777847067	1.084384568	1.338758874
1.3	0.030552254	0.14680668	0.52974415	0.921422568	1.249323979	1.512255771
1.4	0.038045815	0.178572	0.61167049	1.025351032	1.354911917	1.610377571
1.5	0.044693481	0.20523825	0.66974166	1.084755054	1.399471134	1.635289547
1.6	0.050037856	0.22512997	0.70207989	1.101144192	1.389127405	1.597584045
1.7	0.053822885	0.23755303	0.709925	1.080315021	1.334456007	1.511944374
1.8	0.055980712	0.24264308	0.69658845	1.030254747	1.247605384	1.393765721
1.9	0.056593332	0.24113261	0.66644472	0.959471014	1.140274704	1.256996125
2	0.055845165	0.23410953	0.62412799	0.875872843	1.022544224	1.113051905
2.1	0.053977629	0.22280994	0.57398349	0.786154982	0.902381466	0.970510686
2.2	0.051251721	0.2084629	0.51975263	0.695565643	0.785603631	0.835282731
2.3	0.047920732	0.19218872	0.4644405	0.607927442	0.676102322	0.711023127
2.4	0.044212751	0.17494295	0.41030834	0.52580139	0.576186558	0.599622971
2.5	0.040321344	0.15749524	0.35894122	0.450713399	0.486950326	0.501683318
2.6	0.03640237	0.14043195	0.3113526	0.383391012	0.408611363	0.416923832
2.7	0.032574969	0.12417318	0.2681	0.323980518	0.340796415	0.344509387
2.8	0.028925071	0.10899701	0.22939555	0.272230505	0.282766243	0.283295919
2.9	0.025510185	0.09506611	0.19520324	0.227637987	0.233583773	0.232005764
3	0.022364563	0.08245333	0.16531926	0.189559075	0.192233523	0.189345918
3.1	0.019504202	0.0711647	0.13943542	0.157288951	0.157701948	0.154082604
3.2	0.016931345	0.06115891	0.11718694	0.130116877	0.129027951	0.125083937
3.3	0.01463833	0.0523632	0.09818717	0.107361827	0.105331619	0.101340323
3.4	0.012610758	0.04468569	0.08205151	0.088393697	0.085827691	0.081970028
3.5	0.010830001	0.03802486	0.06841311	0.072644183	0.06982883	0.06621543
3.6	0.009275135	0.03227628	0.05693221	0.05961055	0.056742443	0.053433876
3.7	0.007924367	0.02733746	0.04730109	0.048854755	0.046063734	0.043085846

3.8	0.00675606	0.02311096	0.03924572	0.039999705	0.037366868	0.034722202
3.9	0.00574943	0.01950632	0.0325254	0.032723952	0.030295475	0.027971615
4	0.004884991	0.0164411	0.02693095	0.026755673	0.024553263	0.02252883
4.1	0.004144811	0.01384123	0.02228228	0.021866545	0.019895236	0.018144085
4.2	0.00351263	0.01164091	0.01842544	0.017865838	0.016119726	0.014613826
4.3	0.002973875	0.00978227	0.01522965	0.014594968	0.013061358	0.011772686
4.4	0.002515617	0.00821483	0.0125844	0.011922595	0.010584941	0.009486687
4.5	0.002126469	0.00689479	0.01039674	0.009740292	0.008580251	0.007647515
4.6	0.00179648	0.00578443	0.00858873	0.007958796	0.006957614	0.006167764
4.7	0.001516997	0.00485136	0.00709527	0.006504791	0.005644201	0.004976999
4.8	0.001280535	0.00406793	0.00586211	0.005318169	0.004580953	0.004018529
4.9	0.001080646	0.00341059	0.00484414	0.004349734	0.003720029	0.00324676
5	0.000911798	0.00285933	0.00400393	0.003559268	0.003022715	0.002625054
5.1	0.000769255	0.00239724	0.00331048	0.002913929	0.002457698	0.002123977
5.2	0.000648977	0.00201001	0.00273812	0.00238692	0.001999672	0.001719892
5.3	0.000547524	0.00168559	0.00226564	0.001956391	0.001628184	0.00139382
5.4	0.000461973	0.00141382	0.00187555	0.001604532	0.001326712	0.001130522
5.5	0.000389847	0.00118617	0.0015534	0.001316832	0.00108191	0.000917759
5.6	0.000329045	0.00099547	0.00128726	0.001081469	0.000882992	0.000745703
5.7	0.000277791	0.00083571	0.00106731	0.000888813	0.000721247	0.000606454
5.8	0.000234586	0.00070186	0.00088547	0.000731021	0.000589631	0.000493665
5.9	0.000198162	0.00058968	0.00073506	0.000601701	0.00048245	0.00040223
6	0.000167452	0.00049565	0.00061059	0.000495645	0.0003951	0.000328043
6.1	0.000141553	0.0004168	0.00050753	0.000408607	0.000323854	0.000267795
6.2	0.000119709	0.00035067	0.00042215	0.000337126	0.000265695	0.000218824
6.3	0.000101278	0.00029518	0.00035138	0.000278377	0.000218178	0.000178983
6.4	8.5723E-05	0.0002486	0.00029267	0.000230057	0.000179324	0.000146539
6.5	7.2591E-05	0.00020948	0.00024395	0.000190284	0.000147525	0.000120094
6.6	6.15005E-05	0.00017662	0.00020349	0.000157519	0.000121477	9.85177E-05
6.7	5.21305E-05	0.000149	0.00016986	0.000130507	0.000100121	8.08978E-05
6.8	4.42108E-05	0.00012577	0.0001419	0.000108219	8.25969E-05	6.64947E-05
6.9	3.75141E-05	0.00010623	0.00011862	8.98148E-05	6.82031E-05	5.47098E-05
7	3.18489E-05	8.9777E-05	9.9244E-05	7.46042E-05	5.63702E-05	4.50578E-05

E-2: Contributions (dB/km) of raindrop diameters to specific attenuation for Overall $R_{0.01}$ at f = 10-100 GHz using the gamma DSD

Diameter (mm)	10 GHz	19.5 GHz	40 GHz	60 GHz	80 GHz	100 GHz
0.1	6.48894E-08	7.02706E-07	1.53766E-05	9.60135E-05	0.000317264	0.0007227
0.2	4.35583E-06	3.78708E-05	0.000509166	0.002250746	0.005846116	0.011225373
0.3	4.47165E-05	0.000341913	0.003457253	0.012486834	0.028173246	0.048951241
0.4	0.000212805	0.001485422	0.012270738	0.038400319	0.078402183	0.126898819
0.5	0.000664581	0.004322293	0.030523641	0.085469317	0.1614904	0.247393232
0.6	0.00158999	0.009760584	0.060639732	0.155051207	0.274986884	0.402749405
0.7	0.003165073	0.018503613	0.103155999	0.244260242	0.410618952	0.578974631
0.8	0.005507103	0.030862003	0.156643046	0.347033999	0.556951822	0.759876753
0.9	0.008646101	0.046678417	0.218101298	0.455648404	0.701956478	0.930307708
1	0.012517079	0.065358612	0.283590164	0.562162419	0.834930961	1.078171325
1.1	0.016970542	0.08597701	0.348886399	0.659521122	0.947636513	1.195296645
1.2	0.021795337	0.107418429	0.410040239	0.742234451	1.034737571	1.277465713
1.3	0.02674713	0.128522678	0.463767289	0.806664206	1.09372721	1.323912223
1.4	0.031576751	0.148208771	0.507665998	0.851006979	1.124531465	1.336559393
1.5	0.036054359	0.16556628	0.540282505	0.875074998	1.128957357	1.319192745
1.6	0.039987223	0.17991023	0.561059717	0.879967731	1.110106468	1.276692387
1.7	0.043230462	0.190802246	0.570210706	0.867707427	1.071833091	1.214391484
1.8	0.04569122	0.198044256	0.568552537	0.840889554	1.018290222	1.137585669
1.9	0.047327433	0.201652509	0.557329224	0.802378978	0.953580086	1.05119097
2	0.04814263	0.201819597	0.538044131	0.755066663	0.881508157	0.95953242
2.1	0.048178246	0.198871129	0.512314424	0.701690107	0.805429161	0.866238545
2.2	0.047504736	0.193222293	0.481753807	0.644713225	0.728168585	0.774215673
2.3	0.046212547	0.185337948	0.447885024	0.586257222	0.652001936	0.685677952
2.4	0.044403701	0.175698509	0.412080418	0.528072268	0.578675044	0.602212677
2.5	0.042184486	0.164772675	0.375526933	0.471539663	0.509451002	0.524864766
2.6	0.039659493	0.15299718	0.339211053	0.417695139	0.445172096	0.454228328
2.7	0.036927088	0.140763109	0.303919015	0.367265349	0.386327903	0.390536941
2.8	0.034076249	0.128407961	0.270247909	0.32071121	0.333123225	0.333747229
2.9	0.031184622	0.11621244	0.238623872	0.278273346	0.285541701	0.283612683
3	0.028317604	0.104400918	0.209324254	0.240016267	0.243402605	0.239746372
3.1	0.025528252	0.093144566	0.182501316	0.205869076	0.20640963	0.20167242
3.2	0.022857796	0.08256627	0.158205697	0.175661477	0.174191396	0.168866865
3.3	0.020336583	0.072746583	0.136408424	0.149154493	0.146333987	0.140789002
3.4	0.017985287	0.063730111	0.117020724	0.126065857	0.122406255	0.11690451
3.5	0.015816249	0.055531905	0.099911229	0.106090339	0.101978768	0.09670172
3.6	0.013834856	0.048143518	0.084920472	0.088915506	0.084637418	0.079702336
3.7	0.012040863	0.041538532	0.071872728	0.074233486	0.069992605	0.065467784
3.8	0.010429637	0.035677432	0.060585402	0.061749362	0.057684932	0.05360224
3.9	0.008993257	0.030511781	0.050876215	0.051186796	0.047388173	0.043753193
4	0.007721478	0.02598769	0.042568511	0.042291453	0.038810205	0.035610277

4.1	0.006602549	0.022048627	0.035494959	0.034832699	0.031692467	0.028902941
4.2	0.00562388	0.01863762	0.029499967	0.028604019	0.025808415	0.023397399
4.3	0.004772577	0.015698926	0.024441058	0.023422504	0.020961313	0.018893209
4.4	0.004035862	0.013179239	0.02018945	0.019127696	0.016981666	0.015219712
4.5	0.00340138	0.011028519	0.016630033	0.015580019	0.013724484	0.012232532
4.6	0.002857417	0.009200509	0.01366093	0.012658979	0.011066534	0.009810227
4.7	0.002393053	0.007652997	0.011192747	0.010261267	0.008903692	0.007851185
4.8	0.001998239	0.006347898	0.009147661	0.008298856	0.00714845	0.006270803
4.9	0.001663841	0.005251187	0.007458389	0.006697165	0.005727626	0.004998947
5	0.001381641	0.004332728	0.006067134	0.005393336	0.0045803	0.003977728
5.1	0.001144313	0.003566041	0.004924534	0.004334645	0.003655975	0.003159543
5.2	0.000945375	0.00292802	0.003988658	0.003477067	0.002912955	0.002505395
5.3	0.000779139	0.002398635	0.003224065	0.002783991	0.002316944	0.001983439
5.4	0.000640643	0.001960622	0.002600933	0.002225092	0.001839824	0.001567756
5.5	0.000525588	0.001599184	0.002094276	0.001775341	0.001458622	0.001237316
5.6	0.000430266	0.001301701	0.001683247	0.001414153	0.001154621	0.000975098
5.7	0.0003515	0.00105746	0.001350514	0.00112465	0.000912622	0.00076737
5.8	0.000286576	0.000857406	0.001081718	0.000893035	0.000720309	0.000603074
5.9	0.000233192	0.000693916	0.000865003	0.000708064	0.000567733	0.000473333
6	0.000189396	0.000560599	0.000690612	0.000560598	0.000446878	0.000371032
6.1	0.000153547	0.000452115	0.000550536	0.000443227	0.000351294	0.000290485
6.2	0.000124265	0.000364016	0.000438223	0.000349959	0.000275809	0.000227154
6.3	0.000100397	0.00029261	0.000348322	0.000275957	0.000216281	0.000177426
6.4	8.098E-05	0.000234844	0.000276481	0.000217328	0.000169402	0.000138431
6.5	6.52142E-05	0.000188196	0.000219162	0.000170947	0.000132533	0.000107889
6.6	5.24367E-05	0.000150593	0.0001735	0.000134305	0.000103574	8.39985E-05
6.7	4.20996E-05	0.000120331	0.000137178	0.000105395	8.08563E-05	6.53316E-05
6.8	3.37512E-05	9.60175E-05	0.000108326	8.26164E-05	6.30557E-05	5.07631E-05
6.9	2.70201E-05	7.65138E-05	8.54415E-05	6.46906E-05	4.91244E-05	3.94056E-05
7	2.16018E-05	6.08923E-05	6.73133E-05	5.0601E-05	3.82336E-05	3.05609E-05

E-3: Contributions (dB/km) of raindrop diameters to specific attenuation for different rainfall regimes at f = 10-100 GHz using the lognormal DSD

R = 4 mm/h (Drizzle)						
Diameter (mm)	**10GHz**	**19.5GHz**	**25GHz**	**40GHz**	**60GHz**	**100GHz**
0.1	1.242E-17	1.345E-16	3.631E-16	2.94E-15	3.06E-18	1.38E-13
0.2	1.439E-10	1.251E-09	2.957E-09	1.68E-08	1.68E-10	3.71E-07
0.3	1.652E-07	1.263E-06	2.761E-06	1.28E-05	4.77E-07	0.000181
0.4	8.104E-06	5.657E-05	0.000117	0.000467	4.46E-05	0.004833
0.5	8.827E-05	0.0005741	0.0011379	0.004054	0.000802	0.032858
0.6	0.0004123	0.0025308	0.0048442	0.015723	0.005635	0.104429
0.7	0.0011383	0.0066548	0.0123666	0.0371	0.02198	0.208227
0.8	0.0022175	0.0124268	0.0225088	0.063073	0.057757	0.305968
0.9	0.0033887	0.0182949	0.0323976	0.085481	0.114929	0.36462
1	0.0043469	0.0226978	0.0393904	0.098485	0.186696	0.374428
1.1	0.0048975	0.0248118	0.042279	0.100684	0.260432	0.344946
1.2	0.005001	0.0246474	0.0413038	0.094085	0.323201	0.293117
1.3	0.0047339	0.0227469	0.0375383	0.082081	0.366057	0.234316
1.4	0.0042233	0.0198223	0.0322503	0.067898	0.385577	0.17876
1.5	0.0035953	0.0165099	0.0265079	0.053876	0.383131	0.131547
1.6	0.0029483	0.0132651	0.0210362	0.041368	0.36309	0.094133
1.7	0.0023463	0.0103555	0.0162323	0.030947	0.331	0.06591
1.8	0.0018224	0.0078991	0.0122467	0.022677	0.292234	0.045373
1.9	0.0013879	0.0059137	0.009074	0.016344	0.251235	0.030827
2	0.0010403	0.004361	0.006626	0.011626	0.211246	0.020734
2.1	0.0007696	0.0031769	0.004782	0.008184	0.174347	0.013838
2.2	0.0005634	0.0022917	0.0034189	0.005714	0.141659	0.009182
2.3	0.0004089	0.0016401	0.0024261	0.003963	0.113592	0.006068
2.4	0.0002948	0.0011664	0.0017114	0.002736	0.090078	0.003998
2.5	0.0002113	0.0008255	0.0012017	0.001881	0.070763	0.002629
2.6	0.0001508	0.0005819	0.0008408	0.00129	0.05515	0.001728
2.7	0.0001073	0.000409	0.0005867	0.000883	0.042695	0.001135
2.8	7.614E-05	0.0002869	0.0004087	0.000604	0.032868	0.000746
2.9	5.393E-05	0.000201	0.0002843	0.000413	0.025183	0.00049
3	3.814E-05	0.0001406	0.0001977	0.000282	0.019219	0.000323
3.1	2.696E-05	9.837E-05	0.0001374	0.000193	0.01462	0.000213
3.2	1.905E-05	6.881E-05	9.554E-05	0.000132	0.011092	0.000141
3.3	1.346E-05	4.815E-05	6.645E-05	9.03E-05	0.008397	9.32E-05
3.4	9.514E-06	3.371E-05	4.626E-05	6.19E-05	0.006346	6.18E-05
3.5	6.728E-06	2.362E-05	3.224E-05	4.25E-05	0.004789	4.11E-05
3.6	4.763E-06	1.657E-05	2.25E-05	2.92E-05	0.003611	2.74E-05
3.7	3.375E-06	1.164E-05	1.572E-05	2.01E-05	0.002721	1.83E-05
3.8	2.394E-06	8.189E-06	1.1E-05	1.39E-05	0.002049	1.23E-05
3.9	1.701E-06	5.769E-06	7.712E-06	9.62E-06	0.001543	8.27E-06

4	1.21E-06	4.072E-06	5.416E-06	6.67E-06	0.001162	5.58E-06
4.1	8.62E-07	2.878E-06	3.811E-06	4.63E-06	0.000875	3.77E-06
4.2	6.152E-07	2.039E-06	2.687E-06	3.23E-06	0.000659	2.56E-06
4.3	4.398E-07	1.447E-06	1.898E-06	2.25E-06	0.000497	1.74E-06
4.4	3.15E-07	1.029E-06	1.343E-06	1.58E-06	0.000374	1.19E-06
4.5	2.26E-07	7.328E-07	9.53E-07	1.1E-06	0.000283	8.13E-07
4.6	1.625E-07	5.231E-07	6.775E-07	7.77E-07	0.000213	5.58E-07
4.7	1.17E-07	3.742E-07	4.826E-07	5.47E-07	0.000161	3.84E-07
4.8	8.444E-08	2.682E-07	3.446E-07	3.87E-07	0.000122	2.65E-07
4.9	6.106E-08	1.927E-07	2.465E-07	2.74E-07	9.24E-05	1.83E-07
5	4.423E-08	1.387E-07	1.768E-07	1.94E-07	7E-05	1.27E-07
5.1	3.211E-08	1.001E-07	1.271E-07	1.38E-07	5.31E-05	8.87E-08
5.2	2.336E-08	7.234E-08	9.151E-08	9.85E-08	4.04E-05	6.19E-08
5.3	1.702E-08	5.241E-08	6.605E-08	7.04E-08	3.07E-05	4.33E-08
5.4	1.243E-08	3.805E-08	4.778E-08	5.05E-08	2.34E-05	3.04E-08
5.5	9.098E-09	2.768E-08	3.464E-08	3.63E-08	1.78E-05	2.14E-08
5.6	6.671E-09	2.018E-08	2.517E-08	2.61E-08	1.36E-05	1.51E-08
5.7	4.901E-09	1.474E-08	1.832E-08	1.88E-08	1.04E-05	1.07E-08
5.8	3.608E-09	1.079E-08	1.337E-08	1.36E-08	7.97E-06	7.59E-09
5.9	2.661E-09	7.919E-09	9.777E-09	9.87E-09	6.1E-06	5.4E-09
6	1.967E-09	5.821E-09	7.164E-09	7.17E-09	4.69E-06	3.85E-09
6.1	1.456E-09	4.288E-09	5.26E-09	5.22E-09	3.6E-06	2.75E-09
6.2	1.08E-09	3.165E-09	3.871E-09	3.81E-09	2.77E-06	1.97E-09
6.3	8.031E-10	2.341E-09	2.854E-09	2.79E-09	2.13E-06	1.42E-09
6.4	5.981E-10	1.734E-09	2.108E-09	2.04E-09	1.65E-06	1.02E-09
6.5	4.463E-10	1.288E-09	1.561E-09	1.5E-09	1.27E-06	7.38E-10
6.6	3.336E-10	9.58E-10	1.158E-09	1.1E-09	9.84E-07	5.34E-10
6.7	2.498E-10	7.141E-10	8.604E-10	8.14E-10	7.62E-07	3.88E-10
6.8	1.875E-10	5.333E-10	6.407E-10	6.02E-10	5.91E-07	2.82E-10
6.9	1.409E-10	3.99E-10	4.781E-10	4.46E-10	4.59E-07	2.05E-10
7	1.061E-10	2.991E-10	3.574E-10	3.31E-10	3.57E-07	1.5E-10

R = 9mm/h (Widespread)						
Diameter (mm)	**10GHz**	**19.5GHz**	**25GHz**	**40GHz**	**60GHz**	**100GHz**
0.1	1.92E-23	2.08E-22	5.63E-22	4.5615E-21	2E-19	2.1439E-19
0.2	3.65E-14	3.17E-13	7.5E-13	4.2675E-12	7E-11	9.4084E-11
0.3	5.34E-10	4.08E-09	8.93E-09	4.129E-08	5E-07	5.8462E-07
0.4	1.31E-07	9.16E-07	1.89E-06	7.5639E-06	6E-05	7.8223E-05
0.5	4.46E-06	2.9E-05	5.74E-05	0.00020466	0.001	0.00165877
0.6	4.9E-05	0.000301	0.000576	0.00187004	0.01	0.01242023
0.7	0.000266	0.001552	0.002885	0.00865481	0.038	0.0485761
0.8	0.000893	0.005004	0.009064	0.02539918	0.097	0.12321162

0.9	0.002146	0.011583	0.020512	0.05412183	0.182	0.23085584
1	0.004032	0.021051	0.036533	0.09134014	0.273	0.34726281
1.1	0.006296	0.031899	0.054356	0.1294437	0.349	0.44347852
1.2	0.008529	0.042036	0.070443	0.16046079	0.393	0.49990987
1.3	0.010334	0.049657	0.081947	0.17918464	0.403	0.51151674
1.4	0.011458	0.053778	0.087496	0.18420956	0.382	0.48497834
1.5	0.011827	0.054309	0.087198	0.17722374	0.341	0.43272227
1.6	0.011516	0.051814	0.082168	0.16158419	0.289	0.36768511
1.7	0.01069	0.04718	0.073955	0.14099717	0.236	0.30028507
1.8	0.009537	0.041336	0.064087	0.11866747	0.187	0.23743526
1.9	0.008231	0.035072	0.053814	0.09693135	0.144	0.18282436
2	0.00691	0.028969	0.044016	0.07723126	0.108	0.13773201
2.1	0.005668	0.023396	0.035216	0.06027013	0.08	0.10190678
2.2	0.004558	0.018539	0.027658	0.04622317	0.058	0.07428421
2.3	0.003605	0.014457	0.021385	0.03493684	0.042	0.05348564
2.4	0.002811	0.011122	0.016318	0.02608498	0.03	0.03812048
2.5	0.002165	0.008458	0.012313	0.01927677	0.021	0.02694267
2.6	0.001651	0.00637	0.009204	0.0141233	0.015	0.01891212
2.7	0.001248	0.004758	0.006825	0.01027325	0.01	0.01320116
2.8	0.000937	0.003529	0.005027	0.00742799	0.007	0.00917332
2.9	0.000698	0.002603	0.003682	0.00534408	0.005	0.00635162
3	0.000518	0.00191	0.002685	0.00382909	0.003	0.00438559
3.1	0.000382	0.001396	0.00195	0.00273445	0.002	0.0030217
3.2	0.000281	0.001016	0.001411	0.00194752	0.002	0.00207876
3.3	0.000206	0.000738	0.001019	0.00138414	0.001	0.00142859
3.4	0.000151	0.000535	0.000734	0.00098215	8E-04	0.00098117
3.5	0.00011	0.000387	0.000528	0.00069608	5E-04	0.00067372
3.6	8.03E-05	0.000279	0.000379	0.00049294	4E-04	0.00046265
3.7	5.85E-05	0.000202	0.000272	0.00034892	3E-04	0.00031782
3.8	4.25E-05	0.000145	0.000195	0.00024693	2E-04	0.00021846
3.9	3.09E-05	0.000105	0.00014	0.00017476	1E-04	0.00015029
4	2.24E-05	7.55E-05	0.0001	0.00012372	8E-05	0.00010349
4.1	1.63E-05	5.44E-05	7.21E-05	8.7625E-05	6E-05	7.1351E-05
4.2	1.18E-05	3.92E-05	5.17E-05	6.2102E-05	4E-05	4.9255E-05
4.3	8.6E-06	2.83E-05	3.71E-05	4.4048E-05	3E-05	3.4049E-05
4.4	6.25E-06	2.04E-05	2.67E-05	3.1271E-05	2E-05	2.3574E-05
4.5	4.55E-06	1.47E-05	1.92E-05	2.2223E-05	1E-05	1.6347E-05
4.6	3.31E-06	1.06E-05	1.38E-05	1.5811E-05	9E-06	1.1355E-05
4.7	2.41E-06	7.7E-06	9.93E-06	1.1263E-05	6E-06	7.9006E-06
4.8	1.75E-06	5.57E-06	7.16E-06	8.0337E-06	4E-06	5.5072E-06
4.9	1.28E-06	4.04E-06	5.17E-06	5.738E-06	3E-06	3.8459E-06
5	9.35E-07	2.93E-06	3.74E-06	4.1041E-06	2E-06	2.6908E-06
5.1	6.83E-07	2.13E-06	2.7E-06	2.9398E-06	1E-06	1.8862E-06
5.2	5E-07	1.55E-06	1.96E-06	2.109E-06	1E-06	1.3247E-06

5.3	3.66E-07	1.13E-06	1.42E-06	1.5153E-06	7E-07	9.3222E-07
5.4	2.69E-07	8.22E-07	1.03E-06	1.0905E-06	5E-07	6.573E-07
5.5	1.97E-07	6E-07	7.51E-07	7.86E-07	4E-07	4.6437E-07
5.6	1.45E-07	4.39E-07	5.47E-07	5.6746E-07	3E-07	3.2873E-07
5.7	1.07E-07	3.21E-07	3.99E-07	4.1036E-07	2E-07	2.3317E-07
5.8	7.87E-08	2.36E-07	2.92E-07	2.9724E-07	1E-07	1.6572E-07
5.9	5.81E-08	1.73E-07	2.14E-07	2.1566E-07	9E-08	1.1801E-07
6	4.3E-08	1.27E-07	1.57E-07	1.5674E-07	7E-08	8.4208E-08
6.1	3.18E-08	9.37E-08	1.15E-07	1.141E-07	5E-08	6.0206E-08
6.2	2.36E-08	6.91E-08	8.45E-08	8.3207E-08	3E-08	4.3131E-08
6.3	1.75E-08	5.11E-08	6.23E-08	6.0778E-08	2E-08	3.0959E-08
6.4	1.3E-08	3.78E-08	4.59E-08	4.447E-08	2E-08	2.2266E-08
6.5	9.7E-09	2.8E-08	3.39E-08	3.2593E-08	1E-08	1.6045E-08
6.6	7.23E-09	2.08E-08	2.51E-08	2.3928E-08	9E-09	1.1585E-08
6.7	5.4E-09	1.54E-08	1.86E-08	1.7596E-08	7E-09	8.3802E-09
6.8	4.04E-09	1.15E-08	1.38E-08	1.2961E-08	5E-09	6.0738E-09
6.9	3.02E-09	8.56E-09	1.03E-08	9.5632E-09	3E-09	4.4106E-09
7	2.27E-09	6.39E-09	7.64E-09	7.0677E-09	3E-09	3.2088E-09

25 mm/h (Shower)						
Diameter (mm)	**10GHz**	**19.5GHz**	**25GHz**	**40GHz**	**60GHz**	**100GHz**
0.1	4.34E-36	4.7E-35	1.27E-34	1.03E-33	6.42E-33	4.83E-32
0.2	3.78E-22	3.29E-21	7.76E-21	4.42E-20	1.95E-19	9.74E-19
0.3	1.06E-15	8.13E-15	1.78E-14	8.22E-14	2.97E-13	1.16E-12
0.4	6.9E-12	4.82E-11	9.97E-11	3.98E-10	1.25E-09	4.12E-09
0.5	2.29E-09	1.49E-08	2.95E-08	1.05E-07	2.95E-07	8.53E-07
0.6	1.37E-07	8.41E-07	1.61E-06	5.22E-06	1.34E-05	3.47E-05
0.7	2.76E-06	1.61E-05	2.99E-05	8.98E-05	0.000213	0.000504
0.8	2.65E-05	0.000148	0.000269	0.000753	0.001667	0.003651
0.9	0.00015	0.000809	0.001433	0.00378	0.007897	0.016123
1	0.000574	0.003	0.005206	0.013016	0.025802	0.049485
1.1	0.001637	0.008294	0.014132	0.033654	0.063619	0.115301
1.2	0.003703	0.018248	0.03058	0.069657	0.126089	0.217013
1.3	0.006972	0.033502	0.055287	0.120891	0.210275	0.345107
1.4	0.011328	0.053167	0.086501	0.182115	0.305282	0.479464
1.5	0.016314	0.074916	0.120283	0.244468	0.395955	0.59691
1.6	0.02127	0.095697	0.151759	0.298437	0.468069	0.679093
1.7	0.025523	0.11265	0.176579	0.336654	0.512297	0.71698
1.8	0.028564	0.123807	0.191951	0.355429	0.52568	0.711158
1.9	0.030132	0.128386	0.196997	0.354836	0.510852	0.669263
2	0.030225	0.126706	0.192516	0.337794	0.474045	0.602412

2.1	0.029036	0.119857	0.180413	0.308765	0.422899	0.52207
2.2	0.026876	0.109315	0.163083	0.272551	0.364744	0.43801
2.3	0.024087	0.096604	0.142896	0.233451	0.305575	0.357396
2.4	0.020993	0.083065	0.121871	0.194819	0.249657	0.284708
2.5	0.017855	0.069741	0.101525	0.158945	0.199583	0.222153
2.6	0.014866	0.057349	0.082859	0.127148	0.156567	0.170261
2.7	0.012148	0.046307	0.066423	0.09998	0.120819	0.128475
2.8	0.009765	0.036798	0.052417	0.077446	0.091908	0.095643
2.9	0.007738	0.028835	0.040798	0.059208	0.069046	0.07037
3	0.006053	0.022317	0.031372	0.044746	0.051307	0.05125
3.1	0.004683	0.017086	0.023868	0.033478	0.037764	0.036994
3.2	0.003587	0.012957	0.017989	0.024826	0.027565	0.026499
3.3	0.002724	0.009742	0.013447	0.018268	0.019975	0.018855
3.4	0.002052	0.007271	0.009979	0.013352	0.014384	0.013338
3.5	0.001536	0.005392	0.007358	0.0097	0.0103	0.009389
3.6	0.001142	0.003975	0.005395	0.007011	0.007341	0.00658
3.7	0.000845	0.002915	0.003937	0.005044	0.00521	0.004595
3.8	0.000622	0.002129	0.00286	0.003615	0.003685	0.003199
3.9	0.000456	0.001549	0.00207	0.002582	0.002598	0.002221
4	0.000334	0.001123	0.001493	0.001839	0.001827	0.001538
4.1	0.000243	0.000811	0.001074	0.001306	0.001282	0.001064
4.2	0.000177	0.000585	0.000771	0.000926	0.000898	0.000734
4.3	0.000128	0.000421	0.000552	0.000655	0.000628	0.000507
4.4	9.26E-05	0.000302	0.000395	0.000463	0.000439	0.000349
4.5	6.68E-05	0.000217	0.000282	0.000327	0.000306	0.00024
4.6	4.82E-05	0.000155	0.000201	0.00023	0.000213	0.000165
4.7	3.47E-05	0.000111	0.000143	0.000162	0.000149	0.000114
4.8	2.5E-05	7.93E-05	0.000102	0.000114	0.000104	7.84E-05
4.9	1.79E-05	5.66E-05	7.25E-05	8.05E-05	7.22E-05	5.39E-05
5	1.29E-05	4.04E-05	5.15E-05	5.66E-05	5.03E-05	3.71E-05
5.1	9.26E-06	2.89E-05	3.66E-05	3.99E-05	3.51E-05	2.56E-05
5.2	6.65E-06	2.06E-05	2.6E-05	2.81E-05	2.45E-05	1.76E-05
5.3	4.77E-06	1.47E-05	1.85E-05	1.97E-05	1.71E-05	1.22E-05
5.4	3.43E-06	1.05E-05	1.32E-05	1.39E-05	1.19E-05	8.38E-06
5.5	2.46E-06	7.48E-06	9.36E-06	9.8E-06	8.31E-06	5.79E-06
5.6	1.77E-06	5.34E-06	6.66E-06	6.91E-06	5.8E-06	4E-06
5.7	1.27E-06	3.82E-06	4.74E-06	4.87E-06	4.06E-06	2.77E-06
5.8	9.11E-07	2.73E-06	3.38E-06	3.44E-06	2.84E-06	1.92E-06
5.9	6.55E-07	1.95E-06	2.41E-06	2.43E-06	1.99E-06	1.33E-06
6	4.71E-07	1.39E-06	1.72E-06	1.72E-06	1.39E-06	9.23E-07
6.1	3.39E-07	9.98E-07	1.22E-06	1.22E-06	9.79E-07	6.41E-07
6.2	2.44E-07	7.15E-07	8.75E-07	8.61E-07	6.88E-07	4.46E-07
6.3	1.76E-07	5.13E-07	6.25E-07	6.1E-07	4.84E-07	3.11E-07
6.4	1.27E-07	3.68E-07	4.47E-07	4.33E-07	3.41E-07	2.17E-07

6.5	9.16E-08	2.64E-07	3.2E-07	3.08E-07	2.4E-07	1.52E-07
6.6	6.62E-08	1.9E-07	2.3E-07	2.19E-07	1.69E-07	1.06E-07
6.7	4.78E-08	1.37E-07	1.65E-07	1.56E-07	1.2E-07	7.42E-08
6.8	3.46E-08	9.85E-08	1.18E-07	1.11E-07	8.47E-08	5.21E-08
6.9	2.51E-08	7.1E-08	8.5E-08	7.93E-08	6E-08	3.66E-08
7	1.82E-08	5.12E-08	6.12E-08	5.66E-08	4.26E-08	2.57E-08

R = 60 mm/h (Thunderstorm)						
Diameter (mm)	**10GHz**	**19.5GHz**	**25GHz**	**40GHz**	**60GHz**	**100GHz**
0.1	3.8203E-25	4.14E-24	1.11663E-23	9.05E-23	5.65E-22	4.25E-21
0.2	3.2466E-16	2.82E-15	6.66999E-15	3.79E-14	1.68E-13	8.37E-13
0.3	5.4517E-12	4.17E-11	9.11334E-11	4.22E-10	1.52E-09	5.97E-09
0.4	1.9384E-09	1.35E-08	2.7993E-08	1.12E-07	3.5E-07	1.16E-06
0.5	1.0249E-07	6.67E-07	1.32121E-06	4.71E-06	1.32E-05	3.82E-05
0.6	1.7905E-06	1.1E-05	2.10381E-05	6.83E-05	0.000175	0.000454
0.7	1.5385E-05	8.99E-05	0.000167141	0.000501	0.001187	0.002814
0.8	8.1318E-05	0.000456	0.000825435	0.002313	0.005124	0.01122
0.9	0.00030316	0.001637	0.002898337	0.007647	0.015976	0.032619
1	0.00087135	0.00455	0.00789587	0.019742	0.039134	0.075055
1.1	0.00205173	0.010395	0.017712229	0.04218	0.079736	0.14451
1.2	0.00413153	0.020362	0.03412288	0.077727	0.140698	0.242157
1.3	0.00734162	0.035277	0.058216604	0.127296	0.221415	0.363391
1.4	0.01178586	0.055318	0.090000905	0.189484	0.317634	0.498864
1.5	0.01740273	0.079916	0.128310925	0.260784	0.422381	0.636748
1.6	0.02396812	0.107837	0.171011306	0.336296	0.527448	0.765242
1.7	0.03113265	0.137407	0.215385316	0.41064	0.624884	0.874551
1.8	0.03847847	0.166781	0.258578587	0.478802	0.708148	0.958008
1.9	0.04557934	0.194204	0.297989018	0.536744	0.772742	1.012364
2	0.05205162	0.218207	0.331540597	0.581731	0.816375	1.037443
2.1	0.05758957	0.237719	0.357823977	0.612392	0.838761	1.035453
2.2	0.06198329	0.252113	0.376118571	0.628583	0.84121	1.010182
2.3	0.06512143	0.261173	0.386327361	0.631147	0.826137	0.966238
2.4	0.06698256	0.26504	0.38885945	0.621619	0.796592	0.908432
2.5	0.06761957	0.264122	0.38449123	0.60195	0.755854	0.841331
2.6	0.06714085	0.259014	0.374229268	0.574261	0.70713	0.768978
2.7	0.06569148	0.250411	0.359189599	0.540657	0.653347	0.694746
2.8	0.06343609	0.239043	0.340500825	0.503091	0.597034	0.621301
2.9	0.06054482	0.225626	0.319232968	0.463287	0.540267	0.550633
3	0.0571825	0.21082	0.296350466	0.422694	0.484671	0.484126
3.1	0.05350109	0.195209	0.272685711	0.382479	0.431452	0.422657

3.2	0.049635	0.17929	0.248928785	0.343539	0.381444	0.366689
3.3	0.0456988	0.163471	0.225629022	0.306526	0.335168	0.31637
3.4	0.04178662	0.148069	0.203204536	0.271883	0.292899	0.271613
3.5	0.03797294	0.133326	0.181956504	0.239875	0.25471	0.232169
3.6	0.0343142	0.119409	0.162085738	0.210626	0.220535	0.197683
3.7	0.03085086	0.106429	0.143709762	0.184151	0.1902	0.16774
3.8	0.02760972	0.094447	0.12687918	0.160384	0.163465	0.141898
3.9	0.0246062	0.083482	0.111592601	0.139201	0.140051	0.119712
4	0.02184658	0.073528	0.097809717	0.12044	0.119656	0.100753
4.1	0.01932995	0.064551	0.085462414	0.103917	0.101978	0.084618
4.2	0.01704999	0.056504	0.074463936	0.089435	0.086719	0.070934
4.3	0.01499647	0.049329	0.064716243	0.076799	0.073599	0.059367
4.4	0.01315645	0.042963	0.056115767	0.065815	0.062354	0.049615
4.5	0.01151533	0.037337	0.04855778	0.056301	0.052746	0.041413
4.6	0.01005765	0.032384	0.0419396	0.048084	0.044558	0.03453
4.7	0.00876769	0.028039	0.036162851	0.041008	0.037595	0.028765
4.8	0.00762994	0.024238	0.031134953	0.034929	0.031688	0.023944
4.9	0.00662943	0.020923	0.02677003	0.029717	0.026684	0.019918
5	0.00575197	0.018038	0.022989351	0.025258	0.022453	0.01656
5.1	0.00498428	0.015533	0.019721446	0.02145	0.01888	0.013762
5.2	0.0043141	0.013362	0.016901965	0.018202	0.015867	0.011433
5.3	0.00373019	0.011484	0.014473382	0.015435	0.013329	0.009496
5.4	0.00322233	0.009862	0.012384579	0.013082	0.011192	0.007886
5.5	0.00278134	0.008463	0.010590379	0.011083	0.009395	0.006548
5.6	0.00239894	0.007258	0.009051031	0.009385	0.007885	0.005437
5.7	0.00206779	0.006221	0.007731705	0.007945	0.006616	0.004514
5.8	0.00178135	0.00533	0.006601991	0.006724	0.005551	0.003749
5.9	0.00153382	0.004564	0.005635419	0.00569	0.004657	0.003113
6	0.00132013	0.003908	0.004809015	0.004814	0.003907	0.002586
6.1	0.0011358	0.003344	0.004102889	0.004072	0.003279	0.002149
6.2	0.00097691	0.002862	0.003499854	0.003445	0.002751	0.001786
6.3	0.00084003	0.002448	0.002985095	0.002914	0.002309	0.001485
6.4	0.00072219	0.002094	0.002545857	0.002466	0.001938	0.001235
6.5	0.00062078	0.001791	0.00217118	0.002086	0.001627	0.001027
6.6	0.00053355	0.001532	0.001851656	0.001765	0.001367	0.000855
6.7	0.00045854	0.001311	0.001579223	0.001494	0.001148	0.000712
6.8	0.00039406	0.001121	0.001346974	0.001265	0.000965	0.000593
6.9	0.00033865	0.000959	0.001149004	0.001071	0.000811	0.000494
7	0.00029104	0.00082	0.000980263	0.000907	0.000682	0.000412

Appendix F-1: Calculation of long-term statistics of hydrometeor-induced cross-polarization [*ITU-R P.618-9*, 2007]

To calculate long-term statistics of depolarization from rain attenuation statistics the following parameters are needed:

A_p : rain attenuation (dB) exceeded for the required percentage of time, p, for the path in question, commonly called co-polar attenuation (CPA)

τ : tilt angle of the linearly polarized electric field vector with respect to the horizontal (for circular polarization use $\tau = 45^o$)

f : frequency (GHz)

θ: path elevation angle (degrees).

The method described below to calculate cross-polarization discrimination (XPD) statistics from rain attenuation statistics for the same path is valid for $8 \leq f \leq 35$ GHz and $\theta \leq 60^o$.

Step 1: Calculate the frequency-dependent term:

$$C_f = 30 \log f \qquad \text{for } 8 \leq f \leq 35 \text{ GHz} \tag{A-5}$$

Step 2: Calculate the rain attenuation dependent term:

$$C_A = V(f) \log A_p \tag{A-6}$$

where:

$$V(f) = 12.8 f^{0.19} \qquad \text{for } 8 \leq f \leq 20 \text{ GHz}$$

$$V(f) = 22.6 \qquad \text{for } 20 \leq f \leq 35 \text{ GHz}$$

Step 3: Calculate the polarization improvement factor:

$$C_\tau = -10 \log [1 - 0.484 (1 + \cos 4\tau)] \tag{A-7}$$

The improvement factor $C_\tau = 0$ for $\tau = 45^o$ and reaches a maximum value of 15 dB for $\tau = 0^o$ or 90^o.

Step 4: Calculate the elevation angle-dependent term:

$$C_\theta = -40 \log(\cos\theta) \qquad for\ \theta \leq 60^o \tag{A-8}$$

Step 5: Calculate the canting angle-dependent term:

$$C_\sigma = 0.0052\sigma^2 \tag{A-9}$$

where σ is the effective standard deviation of the raindrop canting angle distribution, expressed in degree; σ takes the value of 0^o, 5^o, 10^o and 15^o for 1%, 0.1%, 0.01% and 0.001% of the time, respectively.

Step 6: Calculate rain XPD not exceeded for $p\%$ of the time:

$$XPD_{rain} = C_f - C_A + C_\tau + C_\theta + C_\sigma \qquad dB \qquad (A-10)$$

Appendix G-1: Derivation of the normalized deviation (%) for the drop size distribution

The normalized deviation (in %) as used in [*Kumar et al.* 2010] is adopted in this work (Figures 5-6 and 5-6). It is calculated using the true measured rain rate and the rain rate with some of the bins (channels) removed. The equation is given as:

$$N(D_j)[\%] = \frac{\left[R_{(true)} - R_{(jth\ bin\ removed)}\right]}{R_{(true)}} \times 100 \qquad (G-1)$$

where $R_{(true)}$ is obtained from equation (2.33) and $R_{(jth\ bin\ removed)}$ is also obtained from 2.33 but with some of the bins removed.

Appendix H-1 : The RD-80 Disdrometer

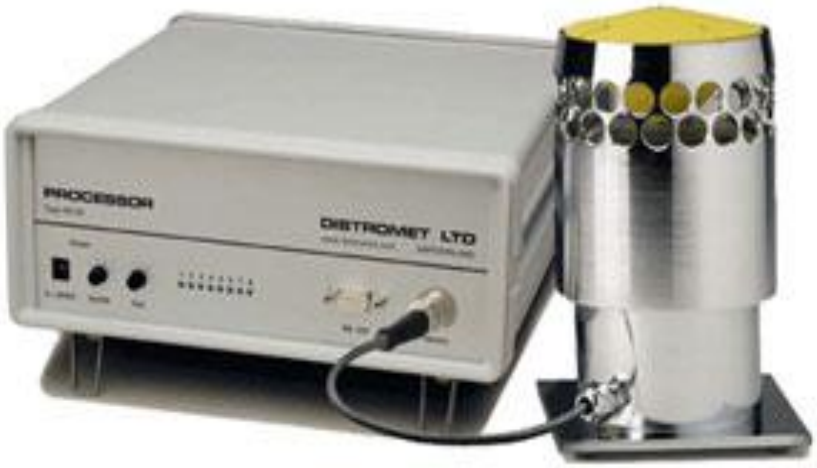

The RD-80 Disdrometer